Human brain dynamics during multitasking physical navigation

Tien-Thong Nguyen DO

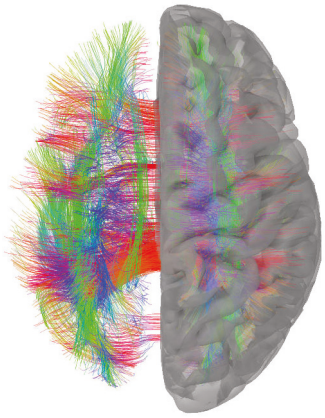

Thesis: Doctor of Philosophy
Faculty of Engineering and Information Technology
University of Technology Sydney, Sydney, Australia (October 2020)

UNIVERSITY OF TECHNOLOGY SYDNEY
Faculty of Engineering and Information Technology

Human brain dynamics during multitasking physical navigation

by

Tien-Thong Nguyen DO

Thesis Submitted
in Fulfillment of the
Requirements for the Degree of

Doctor of Philosophy

Supervisors: Prof. Chin-Teng Lin
Prof. Klaus Gramann
Dr. Tim-Chen

Sydney, Australia

2020

Certificate of Original Authorship

I, Tien-Thong Nguyen Do declare that this thesis, is submitted in fulfilment of the requirements for the award of Doctor of Philosophy, in the School of Computer Science, Faculty of Engineering and Information Technology at the University of Technology Sydney.

This thesis is wholly my own work unless otherwise referenced or acknowledged. In addition, I certify that all information sources and literature used are indicated in the thesis.

This document has not been submitted for qualifications at any other academic institution.

This research is supported by the Australian Government Research Training Program.

Production Note:
Signature: Signature removed prior to publication.

Date: 02 October 2020

ABSTRACT

Human brain dynamics during multitasking physical navigation

by

Tien-Thong Nguyen DO

Spatial navigation is an essential skill that helps one to keep track of their location and orientation and navigate efficiently through the environment. Investigating spatial cognitive processing can be beneficial by rendering a mechanism underlying diseases such as Alzheimer's disease, which might be diagnosed based on impairments in spatial tests long before established diagnostic criteria. Furthermore, navigation in real-life often involves multiple cognitive processes, such as landmark encoding, cognitive map anchoring, and goal-oriented planning, even in the simplest situation. Thus, investigating spatial navigation under multitasking situation might provide more insight of brain dynamics underlying navigation in our daily activities.

However, most studies on active physical navigation in 3D space are based on animal research, or the studies are confined to a specific patient population with limited movement ranges. These limitations hinder the generalization of findings in stationary laboratory set-ups to active navigation in healthy human participants.

In this work, we investigated human brain dynamics while multitasking in active navigation tasks in a more natural set-up that could be used with healthy populations. We performed simulated driving and physical spatial navigation task experiments, which mimic typical navigation tasks in our daily lives. Participants performed the tasks in a virtual environment, while their brain signal was measured simultaneously. We investigated brain dynamics of concurrent multitasking in the simulated driving experiment, where participants performed the driving task, and dynamic attention shifting task concurrently. We then further investigated brain dynamics in a physical spatial navigation experiment, where participants actively

ambulated from a location to several others.

We found an increase in the information flow of brain connectivity in the period of concurrent task response in the simulated driving experiment. Furthermore, in the same experiment, we observed an increase in frontal beta during the secondary task response. We then obtained a significant modulation of theta oscillations in the retrosplenial complex (RSC) during heading changes in the physical spatial navigation experiment; this is an essential mechanism for heading computation and generating the grid cell signal. Finally, we reported that local information processing in the RSC increases linearly with the navigation load level. The findings unpack the insight of brain dynamics and offer unprecedented benefits for estimating cognitive load in active navigation.

Dissertation directed by Professor Chin-Teng Lin
Australian Artificial Intelligence Institute (AAII)
School of Computer Science
University of Technology Sydney

To my loved ones

Acknowledgments

A Ph.D. journey is challenging; it is up and down. To go through this journey, one needs to be persistent. Of course, the task cannot be finished without help and support from others.

Foremost, I would like to express my gratitude to my supervisors, Prof. Chin-Teng Lin, Prof. Klaus Gramann, and Dr. Tim Chen, for their endless support and patience. It is my great honor to be supervised by Prof. Chin-Teng Lin. He has inspired me in everything from fundamental science to advanced machine learning and neuroscience knowledge. Prof. Lin has always shared the vision for my long-term research to motivate me. I also want to thank Prof. Klaus Gramann (Technical University of Berlin) for supervising my spatial navigation study. He tirelessly guided me in the navigation research field, which is a new insight for me since the beginning of my studies. And Dr. Tim Chen (University of Adelaide) continuously helped me in the research pathway to reach my end goal. I would also like to express my appreciation to Prof. Tzyy-Ping Jung, a collaborator from the University of California San Diego (UCSD) for his time and effort in discussions on active navigation experiments.

Through my Ph.D. journey, I am fortunate to have worked with excellent colleagues from the Computational Intelligence and Brain-Computer Interfaces (CIBCI) lab, UTS. I want to thank Carlos Tirado, Avinash Singh, Howe Zhu, Khuong Tran, Ashlesha Akella, Alka John, Fred Chang, Jia Liu, Yurui Ming, Dr. Yukai Wang, and Dr. Mukesh Prasad. I would also like to thank my friends Anna Wunderlich and Tung Huynh for sharing scientific knowledge during my Ph.D. study.

I would like to thank the Australian Research Council (ARC) for its financial support. In addition, I want to extend my gratitude to the Research Training

Program (RTP) scheme from the Department of Education and Training for funding my stipend.

Lastly, I appreciate my parents, Do Dinh Qua and Nguyen Thi Thuy Tam, and my sister Do Thi Anh Dao, for their love and mental support. I would especially like to thank my wife, Hanh Duong, for your love, spirit, and endless support, understanding my Ph.D. journey in hardship and good times. This thesis could not have been finished without tremendous support from all of you.

Tien-Thong Nguyen Do
Sydney, Australia, 2020.

List of Publications

Journal

J-1. C.-L. Lin, and **T.-T.N. Do**, "Direct-Sense Brain–Computer Interfaces and Wearable Computers". *IEEE Transactions on Systems, Man, and Cybernetics: Systems*, vol. 51, no. 1, pp. 298-312, 2021.

J-2. **T.-T.N. Do**, Y.-K. Wang, and C.-T. Lin, "Increase in brain effective connectivity when workload increases but not with high fatigue," *IEEE Transactions on Cognitive and Developmental Systems*, 2020.

J-3. **T.-T.N. Do**, C.-H. Chuang, S.-J. Hsiao, C.-T. Lin, and Y.-K. Wang, "Neural comodulation of independent brain processes related to multitasking," *IEEE Transactions on Neural Systems and Rehabilitation Engineering*, vol. 27, no. 6, pp. 1160-1169, 2019.

J-4. **T.-T.N. Do**, C.-T. Lin, and K. Gramann, 2020, "Human retrosplenial theta and alpha modulation in active spatial navigation". **(Under review)**

J-5. **T.-T.N. Do**, T.-P. Jung, and C.-T. Lin, "Retrosplenial segregation reflects the navigation load during ambulatory movement". **(Under review)**

J-6. C. Cortes, H.-T. Chen, **T.-T.N. Do**, C.-T. Lin, "EEG Signals and Body Kinematics During Different Levels of VR Sickness". **(Under review)**

J-7. N.H.-Shariati, T. N.-John, A.K. Singh, C. Cortes, **T.-T.N. Do**, A. Craig, J.W. Middleton, M.P. Jensen, Z. Trost, C.-T. Lin, and S.M. Gustin, "Evaluation of the effectiveness of a novel brain-computer interface neuromodulative intervention to relieve neuropathic pain following spinal cord injury: protocol for a single-case experimental design with multiple baselines", *JMIR Research Protocols*, vol. 9, no. 9, pp. e20979, 2020.

Conference

C-1. **T.-T.N. Do**, A.K. Singh, C. Cortes, and C.-T. Lin, "Estimating the cognitive load in physical spatial navigation" *IEEE Symposium Series on Computational Intelligence (SSCI)*, Canberra, Australia, pp. 568-575, Dec., 2020.

C-2. **T.-T.N. Do**, C.-T. Lin, and K. Gramann, "Human brain dynamics during physical spatial navigation" *4th International Conference on Mobile Brain/Body Imaging (MoBI)*, San Diego, USA, Jun., 2020 **(Accepted)** (rescheduled to 2021 due to COVID pandemic).

C-3. **T.-T.N. Do**, and T.T. Huynh, "Evaluate effects of multiple users in collaborative Brain-Computer Interfaces: A SSVEP study" *IEEE 8th International Conference on Communications and Electronics*, Phu Quoc, Vietnam, Jan., 2021 **(Accepted)** (rescheduled to 2021 due to COVID pandemic).

C-4. **T.-T.N. Do**, C.-T. Lin, C. Cortes, A.K. Singh, J. Liu, H.-T. Chen, and K. Gramann, "Human brain dynamics during navigation with natural walking under different workload conditions in Virtual Reality (VR)" *Society for Neuroscience (SfN)*, Chicago, USA, Oct., 2019.

C-5. J. Lu, A. Wunderlich, A.K. Singh, **T.-T.N. Do**, K. Gramann, and C.-T. Lin, "Investigating the impact of landmarks on spatial learning during active navigation" *Society for Neuroscience (SfN)*, Chicago, USA, Oct., 2019.

Contents

List of Figures

List of Tables

Abbreviation

EEG - Electroencephalography

MEG - Magnetoencephalogram

fMRI - functional Magnetic Resonance Imaging

ERSP - Event-Related Spectral Perturbation

ICA - Independent Component Analysis

AMICA - Adaptive Mixture Independent Component Analysis

PCA - Principle Component Analysis

sLORETA - standardized Low-Resolution Brain Electromagnetic Tomography

PLV - Phase Locking Value

MoBI - Mobile Brain/Body Imaging

RFP - Reference Frame Proclivity

HD - Head Direction

FMθ - Frontal Midline Theta

SAFTE - Sleep, Activity, Fatigue, and Task Effectiveness

Chapter 1

Introduction

1.1 Background

1.1.1 The evidence of cognitive map in navigation

Navigation is an essential skill of most of species. Tracking their orientation and location in 3D space helps people, as well as animals of all kinds, to navigate effectively. For efficient location in space, the brain has a mechanism to store spatial information and can encode and retrieve information about the surrounding environment. This capability is generally called a cognitive map.

The cognitive map was first proposed by Tolman (1948) to explain rodent behaviors in a navigational experiment. After learning a round about route to a goal, the rats would choose a new, direct path if one of the paths they knew was blocked. The results led Tolman (1948) to conclude that rats may obtain spatial knowledge from their surrounding environment, which can then be used to deal flexibly with a change in the environment.

O'Keefe and Dostrovsky (1971) continued developing the spatial map idea; they reported that neurons in the hippocampal formation fired when the rat located in the specific direction of testing platform. This report indicated that the hippocampus is an important brain region in maintaining the spatial map. Further, after hippocampal damage, the presence of cognitive-mapping deficits supports the notion that the hippocampus plays a crucial role in the spatial navigation task (O'Keefe and Nadel 1978). Moreover, O'Keefe and Nadel (1978) hypothesized that the spatial map has a strong affinity for the laws of Euclid (Euclidean coordinate system).

Although the global function of the hippocampus remains debated (Lisman et al. 2017), further research has identified other spatial navigation system components,

including (i) grid cells; (ii) place cells; (iii) head direction (HD) cells; and (iv) border cells (figure 1.1). Grid cells are reported that present in the para- and pre-subiculum (Boccara et al. 2010) and in the medial entorhinal cortex (mEC) (Hafting et al. 2005); these cells fire in multiple discrete and regular hexagon lattice locations. Place cells are found in rodent hippocampus (Muller et al. 1987), and they fire when rodents traverse at specific environment locations. Unlike grid cells and place cells, various brain areas present the evidence of HD cells (Taube 2007; Winter et al. 2015). These cells fire based on the head orientation of the animal. Boundary and border cells are reported in the entorhinal cortex and in the subiculum, respectively (Byrne et al. 2007).

All these cells contribute to a spatial navigation system, which may change in quality and properties based on navigation conditions in the real-world. However, there is uncertainty as to whether animal research can be applied to the human spatial navigation system. Investigating down to a single brain-cell level is one of the difficulties in studying the human spatial navigation system. Nevertheless, current brain imaging methodologies, such as functional magnetic resonance imaging (fMRI), has helped scientists overcome obstacles.

Most of the research aiming to understand the human brain navigation network has been carried out with fMRI. Visual stimulus is often used as input to engage memory and path planning in these studies (Maguire et al. 1998; Ghaem et al. 1997; Aguirre et al. 1996). Researchers have found that hippocampus activity is positively correlated with distance in the real-world (Nielson et al. 2015; Morgan et al. 2011). In addition, London taxi drivers have a larger right posterior hippocampus because of their prolong learning of the street maps (Woollett and Maguire 2011). Furthermore, in the virtual reality experiment, researchers found that hippocampus responds stronger when participant use cognitive-map in the navigation task (Suthana et al. 2009). Hence, it is believed that human hippocampus activity is related to cognitive map, and hippocampus size might indicate for the capacity of cognitive map. Furthermore, researchers have found evidence of grid-like human memory networks in the entorhinal cortex (Doeller et al. 2010), which is compara-

ble with the pattern found in rodent studies (McNaughton et al. 2006; Hafting et al. 2005). However, entorhinal cortex and hippocampus are not the only brain areas that link to long-term spatial memories (Maguire et al. 2006; Teng and Squire 1999). A person who has the medial temporal lobe damaged still could learn the cognitive map. Therefore, the question for future study is how these cortices interact with each other in the functioning of the spatial cognitive map.

Some early research has revealed a brain network that are highly actived in navigation than in passive control conditions (Vukovic and Shtyrov 2017a) (figure 1.2). For instance, the medial parietal and the retrosplenial and posterior parahippocampal cortex regions strongly respond when seeing cityscapes, rooms, landscapes, and buildings (Epstein and Kanwisher 1998), which represent the local visual environment. In another example, frontal lobe regions showed primarily respond during active navigation, which is inline with the assumpltion of their role in navigation plaining (Spiers and Gilbert 2015; Spiers and Maguire 2006). Also, the prefrontal activies are correlated to the error of path changing and re-formulates the route as a novel sub-goal (Spiers and Gilbert 2015). The hippocampus simulates the new path when a goal is blocked (Spiers and Gilbert 2015).

1.1.2 Mechanism of cognitive map

The grid- and map-like cells code the spatial environment in the human brain. There is also a mechanism to decode those cognitive maps in the real environment during navigational tasks. After perceiving the environment through the visual system, the brain needs to calibrate and anchor real-world coordinates with the cognitive map via discrete familiar objects such as houses, buildings or statues, or scattered entities, such as landscape topography or room shape. These object-based items and environmental properties are called landmarks (Epstein and Vass 2014), which help the cognitive maps to anchor to the real environment. It should be noted that navigation can be performed without landmarks as a reference to calibrating the position and head direction, which is called path integration. The place-, grid-, and HD cells systems are supported by the animal path integration task (McNaughton et al. 2006). In humans, it is believed that the medial prefrontal

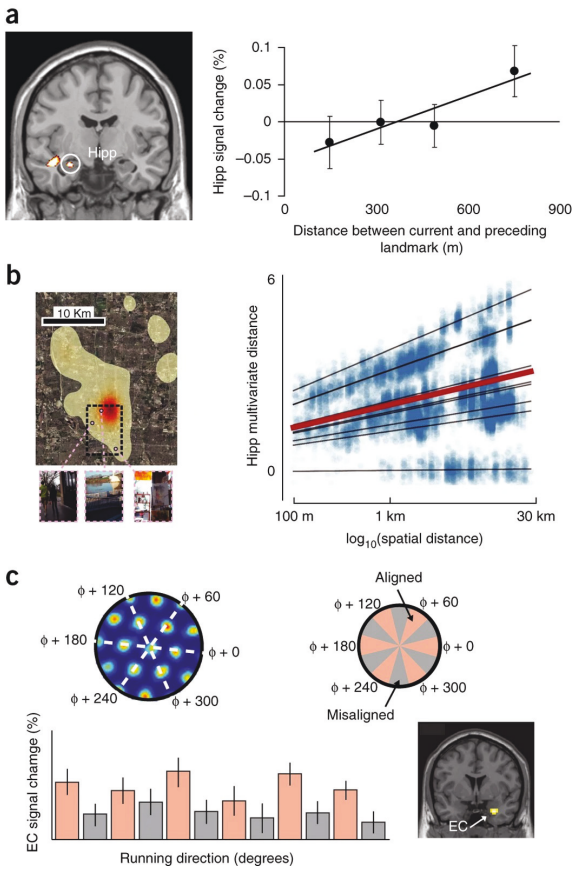

Figure 1.1 : Map- and grid-like coding of navigable space in humans. (a) Evidence from fMRI adaptation. When viewing images of landmarks from a familiar college campus, fMRI activity in the left hippocampus (Hipp) scales with the real-world distance between the landmark shown on each trial and the landmark shown on the immediately preceding trial. (b) Evidence from multi-voxel pattern analysis (MVPA). Voxelwise activity patterns in the hippocampus reflect distances between events intermittently logged by a camera worn by participants in the 30 days before the scan (aerial map of navigated territory shown on the left, as well as example pictures. (c) Evidence from an encoding model. Participants performed a navigation task in virtual reality. Grid cells in an individual rat all have the same orientation (Φ; top row), and thus it was predicted that movements aligned with the grid orientation should result in more fMRI activity than movements misaligned with the grid. The expected pattern of results was observed in the human entorhinal cortex (EC, bottom row). Reprinted by permission from Springer Nature, Nature Neuroscience, Epstein et al. (2017) ©.

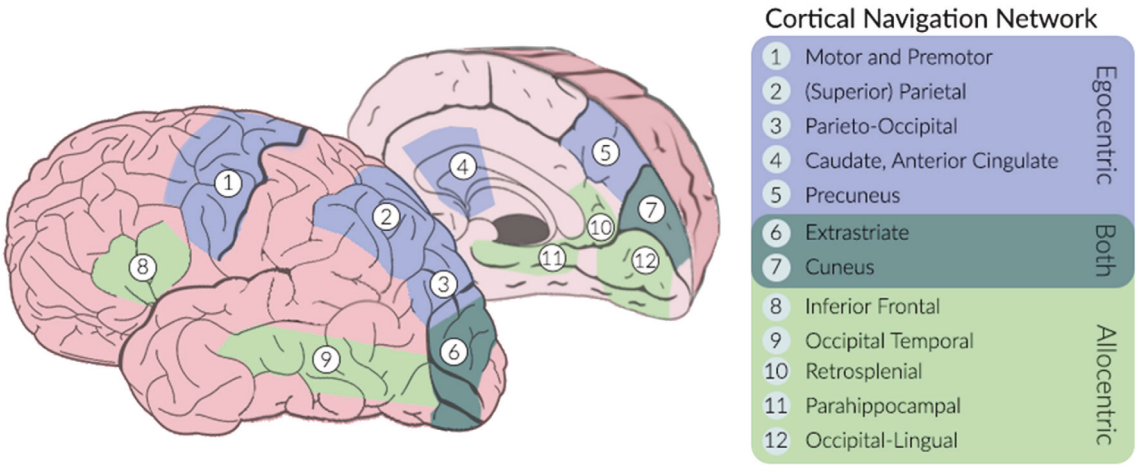

Figure 1.2 : Cortical areas involved in spatial reference frame processing/visual perspective-taking. Based on data from a meta-analytic study of Arora et al. (2015), and the studies of Burgess et al. (2001) and Committeri et al. (2004). Reprinted from NeuroImage, vol 161, Vukovic and Shtyrov, Cortical networks for reference-frame processing are shared by language and spatial navigation systems, pages 120-133, ©2020, with permission from Elsevier

cortex processes spatial working memory and the hippocampus process higher-level spatial information (Wolbers et al. 2007; Sherrill et al. 2013).

Landmark anchoring uses environmental cues to define the cognitive map's orientation and displacement, and the putative coordinate axes' angle and position. Previously, it was believed that the grid cell pattern representing the navigator's location is consistent and independent of the environment shape. However, another research showed that these cognitive maps are affected by the environment of the navigator (Krupic et al. 2015). The hexagonal grid symmetric pattern cannot be seen clearly in a highly polarized environment, such as trapezoids. These results have shown that most assumptions about the invariant of grid cell patterns are invalid, and the role of environmental boundaries should be taken into consideration (Krupic et al. 2015).

Environmental boundaries also control the displacement of the cognitive map. For example, the grid fields have been found to be distorted when these walls are

displaced (Barry et al. 2007). Therefore, boundary and border cells are believed to be important in mediating these effects. During a scene imagination experiment, the number of surrounding environment boundaries affected the hippocampal activity (Bird et al. 2010). In addition, the hippocampal activity is correlated with the capability of learning object locations in relationship with boundaries (Doeller et al. 2008). The displacemence of boundary can also affect human spatial memory when navigating to hidden locations (Hartley et al. 2004).

The landmarks are first processed by perceptual systems and can then be used for the cognitive map. There are three major regions involved in this process (Epstein 2008; Nasr et al. 2011): (i) the RSC, (ii) the occipital place area (OPA), and (iii) the parahippocampal place area (PPA). Among those regions, the RSC appears to be essential to anchor the cognitive map based on the environmental cues. A fMRI study showed that the RSC activity is increased when participants recover the location in the scene; that is, when they locate or orient themselves by using the scene (Epstein 2008; Maguire et al. 1998).

1.1.3 Navigation strategies - Spatial reference frame

In addition to the evidence on the human cognitive map, numerous studies have investigated on navigation strategies. The distinct coordination system in encoding spatial information can define the navigation strategies (Klatzky 1998). Allocentric strategy uses global coordination to code the spatial navigation, while the egocentric uses local coordination (within themself) to code the spatial navigation (Gramann et al. 2006; Gramann 2013). In order to classify the type of spatial reference frame proclivity (RFP), scientists often use simple tests to check their reference preference, such as the tunnel paradigm (Gramann et al. 2010) or the 3D space navigation paradigm (Goeke et al. 2015). In short, there are mainly two types of navigators which are turner who use an egocentric strategy, or non-turner who use an allocentric strategy and a third category of navigators can be described as changing their navigation strategy dependent on the environment. The underlying mechanism that determines the navigator's proclivity is believed to be influenced by gender, age, and cultural background. Males have been reported to perform better than females in

some navigation tasks (Newhouse et al. 2007; Moffat et al. 1998), such as the mental rotation task (Masters and Sanders 1993) and the Morris water maze (Woolley et al. 2010). Many studies have shown evidence that performance in spatial navigation tasks is negatively correlated with age (Salthouse et al. 1989; Perlmutter et al. 1981; Lord and Marsh 1975; Moffat et al. 2001). People from different cultures also show different scene perception behavior (Masuda and Nisbett 2001); Western people tend to pay attention to local objects while Easterners are more focusing on global information in a scene. Moreover, research on specific areas of the world has shown evidence of cultural differences in navigation tasks. For instance, Goeke et al. (2015) reported that reference-frame selection of the navigator is significantly influenced by cultural background; North Americans and Latin Americans tend to use an allocentric strategy, and an egocentric strategy, respectively, while Europeans and Asians are in between the egocentric and allocentric strategies.

To understand differences in navigator behavior in a spatial navigation task, scientists often look at the neural activities in various brain cortices and sub-cortices, which are believed to be central to manipulating navigator behavior. Gramann et al. (2010) showed that stronger alpha desynchronization near the right primary visual cortex during the tunnel turn in egocentric navigators. Furthermore, the occipitotemporal, bilateral inferior parietal, and retrosplenial show stronger alpha desynchronization in the allocentric group. The results in Gramann et al. (2010) reveal that activity in brain cortices and sub-cortices can be studied using high temporal resolution EEG. Consistent evidence has also been reported by (Lin et al. 2015) that the RSC plays essential role in translating between spatial informations. These studies indicate the important role of RSC in the spatial navigation task, and with other cognitive functions, including planning, imagination, and episodic memory(Vann et al. 2009) (figure 1.3).

1.1.4 Multiple resource theory

Individuals often handle multiple tasks simultaneously during daily activities. Examples include listening to music while walking or driving or taking notes while listening to a class lecture. Our capability in performing multitasking is limited

(Dux et al. 2009). The behavior performance deteriorates when we handle two or more than two tasks or the same task in shorter time allocation. The mechanism of multitasking might be explained through multiple resource theory (Wickens 2002). In this model, Wickens (2002) provided a 4-dimensional model that can explain the interference of multitasking in different working environments. Furthermore, the multitasking is closely related to the cognitive load or mental workload. For instance, given a limited time for handling two (or more than) tasks, the cognitive load can be identified as (Wickens 2002):

$$CL = \delta T/T$$

where CL indicates for cognitive load, δT indicates for time required (to perform tasks), T indicates for time available.

It has been demonstrated that the ability to handle multitasking can be improved via training (Ruthruff et al. 2001, 2003). In the neuroscience studies, Dux et al. (2009) revealed that the ability to perform multitasking, which is improved via training, is strongly correlated with the prefrontal cortex's information processing speed. Therefore, the human prefrontal cortex plays an essential role in multitasking processing. There is clear evidence that theta rhythm modulated by the cognitive load level in various experiments (Hsieh and Ranganath 2014; Jaeggi et al. 2003; Onton et al. 2005). In those studies, the frontal midline theta ($FM\theta$) spectral activities is strongly related to mental workload, working memory (Hsieh and Ranganath 2014; Jaeggi et al. 2003; Onton et al. 2005).

In our daily lives, people often navigate from one location to another. Being aware of where they are and avoiding getting lost in 3D space is quite critical. There are multiple tasks involved during navigation; even in a simple case, people need to track their orientation and location (Epstein et al. 2017) (figure 1.1). By doing so, we often remember landmarks in the surrounding environment, anchor that spatial information with our memory, and decide which direction to go in to reach our destination; this is a complex cognitive process. Like other conventional navigation studies, the investigation on multitasking in spatial navigation has been limited to stationary situations, where participants perform the cognitive task with

limited movement (Javadi et al. 2017).

1.1.5 Limitations of brain imaging in navigation studies

The human brain's essential function is to amend motor activities as a result of a dynamically changing environment (Makeig et al. 2009). Brain dynamics and cognitive function are coupled with our physical actions. To understand deeper neurocognitive processes in the natural world, participants need to interact naturally within a 3D environment. However, existing brain imaging paradigms do not support investigating active movement due to the limitation of devices or sensors. fMRI is a common methodology in studying human brain dynamics, but the fMRI device is bulky and not portable. Therefore, in most fMRI experiments, the participant usually has to keep their head in a consistent position. Moreover, the fMRI signal is of low temporal quality. Thus, it might not reflect the natural cognitive process in real-life. In contrast, electroencephalography (EEG) can provide a signal of high temporal quality with a portable ability that may help the researcher perform a complex assignment, closer to a real-life task such as active navigation. However, in a conventional EEG setup, the participant can move the body in a tiny scale-space but cannot make large movements due to the limitations of the methods for movement-related noise removal. To overcome these limitations, we can use an invasive method with implanted electrodes (Bohbot et al. 2017). However, while the invasive method can provide more direct activity from the brain cortices, the number of participants is limited, given the health effects on the participant. The study by Bohbot et al. (2017) involved patients with epilepsy, and interictal discharge might impact these oscillations (Blumenfeld et al. 2004). Another approach that has been subject to much attention recently is the Mobile Brain/Body Imaging (MoBI) approach, which was developed to investigate brain dynamics in more natual form of experimental cognition (Makeig et al. 2009; Gramann et al. 2014a). Many studies have examined brain activity at various levels, such as the channel level (Malcolm et al. 2015; De Sanctis et al. 2014) and the cortical and sub-cortical level (Luu et al. 2017; Artoni et al. 2017; Gramann et al. 2011; Jungnickel and Gramann 2016; Banaei et al. 2017).

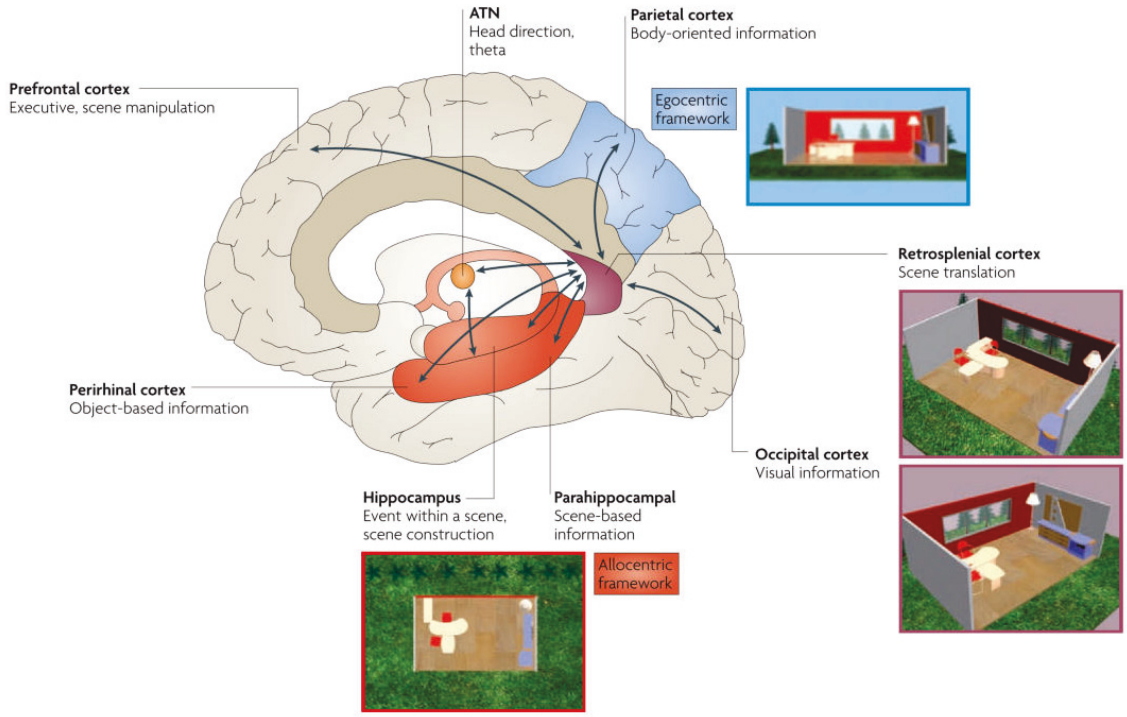

Figure 1.3 : The key anatomical and functional relationships of the retrosplenial cortex. Effective episodic memory, navigation and future thinking all require the ability to integrate and manipulate different frameworks of information, for example egocentric (self-centered) and allocentric (world-centered) frameworks. By virtue of its principal connections, the retrosplenial cortex is uniquely placed to enable translation within these domains: ATN, anterior thalamic nuclei. Reprinted by permission from Springer Nature, Nature Reviews Neuroscience, Vann et al. (2009) ©.

In summary, there is clear evidence of a cognitive map in the human brain, including a head direction cell network. However, most studies in humans have relied on specific patient populations or stationary experiments. Thus, there is still a gap in understanding whether the features identified can be generalized to a healthy population in a more natural navigation situation, which often involves physical movement and multitasking. Therefore, in this work, we investigate brain dynamics in active navigation with a more natural set-up in a healthy population.

To conduct this research, we modified the MoBI approach (Makeig et al. 2009; Gramann 2013) to allow far more natural movement than standard brain imaging

technology. All the time-series data streams were synchronized, allowing comprehensive investigation into brain dynamics and behavior changes in the different experimental conditions. In this work, we have investigated brain dynamics under different cognitive load conditions in active navigation. Two experiments were designed that mimicked our daily navigation tasks of driving and walking.

Due to the complexity of the experimental design and the sensitivity of the EEG data to external noise, we first investigated the brain dynamics in multitasking in the driving simulation with semi-physical movement (Chapters 3, and 4). Then, we explored cognitive brain function with full-body movement in the walking experiment (Chapters 5, and 6).

This research thesis aims to understand the underlying characteristics of human brain dynamics while multitasking in active navigation. The ultimate goal is to build an effective workload assessment tool that can be used to improve task performance. For instance, a system that can adapt the information presentation to reduce mental workload in a navigation task when the user's cognitive load is high.

1.2 Research Problems

1.2.1 Brain dynamics of concurrent multitasking

The frontal area is believed to relate to memory and executive function (Onton et al. 2005)—this question addresses how the frontal region and maybe other regions are modulated in concurrent multitasking. We designed an experiment where participants performed an additional task while handling a primary task such as driving. Then we investigated the spectral power as computed from activity in the fronto-medial cortex, as well as other brain areas. Examining brain dynamics in such conditions can reveal how different brain regions coordinate the information by distinct patterns in broadband frequency.

1.2.2 The effect of fatigue on brain connectivity in multitasking

The brain is a complex and dynamic system. Several brain cortices are involved in communicating and exchanging information mediated by brain connectivity in

performing a cognitive task. Thus, brain connectivity could be a useful indicator to characterize cognitive function when performing tasks (Fonseca et al. 2018). The brain network might be altered and re-configured based on the environment (external) and the participant's cognitive state (internal). We might find the brain pattern related to multitasking in invariance conditions, yet how this pattern changes in dynamic internal circumstances, such as with participant fatigue status, is still poorly understood. The research question explores the dynamic changes in multitasking brain connectivity. To this end, we might have more information to derive a human brain-like model, which demonstrated that out-performed conventional algorithm by applying brain-like architecture underlying in the cognitive state processing in object recognition (Kar et al. 2019; Kubilius et al. 2019), and navigation (Banino et al. 2018).

1.2.3 Heading computation in active navigation

The spatial reference frames play a crucial role in effective navigation for humans. There are two main strategies that human relies on when traveling including allocentric, referred as third-person perspective; and egocentric, referred as first-person perspective. Previous researches have shown that the RSC plays a central role in translation between spatial information reference frames in passive spatial navigation (Lin et al. 2015; Gramann et al. 2010). However, there is still missing information about the retrosplenial role in active spatial navigation. The research question's motivation is whether the reference-frame proclivity (RFP) observed in passive navigation can still be observed in active navigation and whether or not the biomarkers corresponding to a specific RFP will change with navigation modes (active/passive). We hypothesize that allocentric and egocentric users will exhibit different brain dynamics in active navigation. Egocentric participants will adjust their cognitive heading based on the visual stimulus. In contrast, allocentric participants will not update their cognitive heading based on visual flow information alone. As a consequence, the homing response of participants will indicate the use of a specific reference frame.

1.2.4 Local information processing in RSC under different navigation load conditions

The research question's motivation is how to find a reliable biomarker for spatial navigation in such a complicated situation. The capability of the human brain is still unknown; however, people believe that the brain has a limited capacity to manage many different tasks simultaneously, which may be because the brain has a mechanism to share a common network that reacts to changes in the surroundings. Recently, researchers (Vukovic and Shtyrov 2017b) have shown that some brain regions share common areas to control different tasks, but with a distinct region remaining active. Thus, there is a need to investigate the brain network in spatial navigation under different tasking conditions. We hypothesize that navigation conditions modulate the local information processed in the RSC due to its central role in navigation tasks; RSC activity could be a potential indicator of the participant's navigation cognitive status.

1.3 Thesis Organization

To address those research questions, the thesis presented the brain dynamic results in two experiments involving some common forms of navigation that humans use every day such as driving and walking. We disclosed the neural comodulation activity and information flow in the first driving experiment across the brain network. The results indicated that higher workload conditions might increase exchanged information flows. In the second experiment, we further explored how the retrosplenial complex governs spatial information in physical locomotion. We found the potential evidence of the heading computation in the RSC during the period required the head-direction estimation. Moreover, the thesis also demonstrated that the RSC segregation could be an essential indicator for the navigation load in the physical navigation.

The thesis is organized as follows:

- *Chapter 1*: Presents the introduction of spatial navigation.

- *Chapter 2*: Explains the research methodology and covers the key steps in extracting generic EEG features related to the experimental tasks. More detailed information is provided in Chapter 3, 4, 5, and 6.
- *Chapter 3 and Chapter 4*: Describe the results of the semi-active navigation simulated driving experiment. These chapters are heavily focused on understanding mental workload and brain dynamics in different domains:
  - Comodulation (Chapter 3)
  - Effective brain connectivity in channel-based analysis (Chapter 4)
- *Chapter 5 and Chapter 6*: Investigate spatial navigation in physical ambulatory tasks; the results reveal:
  - The human brain dynamics in heading computation (Chapter 5).
  - The effect of navigation loads in RSC activity (Chapter 6).
- And the *Chapter 7* concludes the thesis and sets out the future direction in researching physical spatial navigation.

Figure 1.4 shows the research map of the thesis:

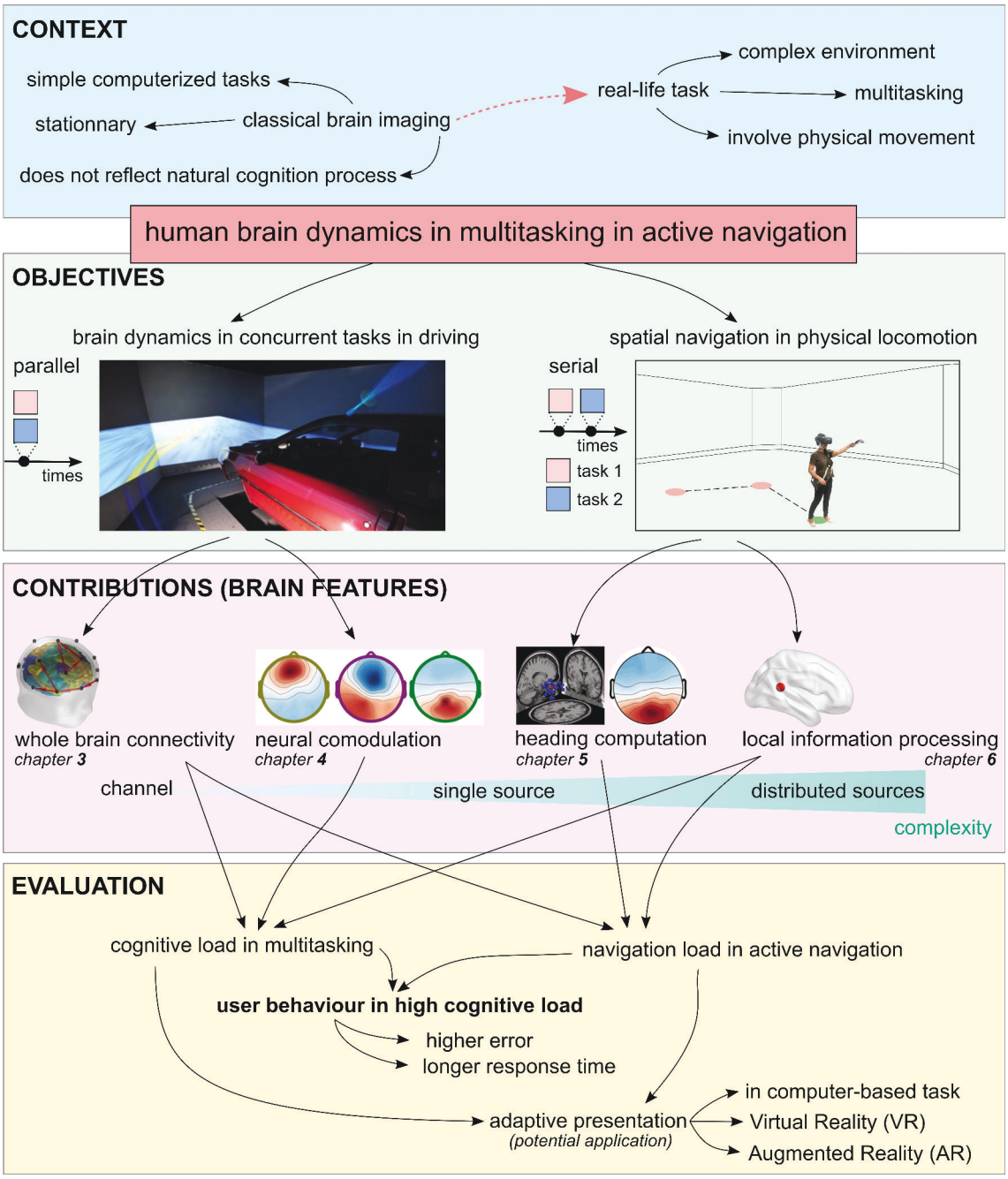

Figure 1.4 : Research map in this thesis.

Chapter 2

Techniques for Data Analysis

2.1 Background

EEG is commonly used, and there is a lot of useful material reviewing EEG methodologies in detail. This chapter does not set out to explain all the steps, which have already been described (Delorme et al. 2011; Michel and Brunet 2019; Delorme and Makeig 2004; Cohen 2014). This chapter reviews the key relevant steps in EEG data analysis that have been used in this thesis.

In brain imaging study, there are two principal methodologies for scanning brain activity during an experiment: invasive and non-invasive. The invasive method requires the sensor to be put inside the scalp, which is only suitable for a limited patient population. The non-invasive sensor can measure brain activity from the outside the scalp. For this reason, non-invasive techniques are quite popular in neuroscience studies. Among non-invasive brain imaging methods, EEG has unique advantages, including the lightweight sensor, high temporal resolution, and portability to measure neural activity in large populations. Although fMRI and Magnetoencephalogram (MEG) can provide excellent data quality with brain source localization of activation, fMRI and MEG systems are normally bulky, and they require participants to remain stationary during the experiment. Because a navigation task normally requires ambulatory movement, the EEG method is an excellent candidate for this study.

EEG measures brain electrical fields by placing electrode sensors on the head. The results of the electrochemical signal between neurons generate the electrical field. When large numbers of nearby neurons synchronously activate and are oriented in parallel, the electrical fields are big enough to be measured by the EEG system. It is estimated that when around 100,000 pyramidal cells are activated syn-

chronously, the field can be measured by EEG. Thus, EEG is limited to detecting a large population of neuron synchronous activity, and estimating the asynchronous activity of a tiny number of neurons seems impossible for the EEG system. Furthermore, the EEG system was designed to measure small voltages from the human scalp; the data itself is quite sensitive to unwanted noise from muscle and the environment. Thus, it is necessary to be very careful when analyzing EEG data.

Furthermore, EEG signals vary between people. They even vary within the same person at different measurement times, because of the EEG hardware set-up and internal cognitive states of the participant. For hardware reasons, it is difficult to get the same sensor location on one person at different times, and the impedance of the sensors also alters due to changes in conductivity under the sensors. Moreover, there is also the learning effect of the typical cognitive experiment design, and participant performance might be changed in the next recording.

To minimize these effects and ensure replication, participants usually perform a large number of trials in one recording session. Thus, the signal to noise ratio can be higher. In addition, there needs to be a systematic method for removing the noise from EEG data and then estimating the location of the activated brain source. The typical solutions for those problems are discussed in the next sections, and more detail and relevant information is exposed in the methods in Chapters 3, 4, 5, and 6.

2.2 Independent Component Analysis

The independence component analysis (ICA) method has been widely used in the EEG research community to remove potential noise in the data. In EEG recording, each sensor passively records signals, which are mixed from multiple sources, including brain and non-brain signals. The source in the brain is the result of synchronous or partially synchronous activity from cortical patches. The non-brain source could be from eye activity, such as a blink or movement, muscle movement, and line noise. ICA looks for the linear transformation that can maximize statistical independence among components. Then, we can remove the "noise" components and clean the

data.

Let us assume that we have EEG data recorded from 64 channels X (channel x times), and we are interested in contributing source S to the EEG data. The problem can be represented by this formula:

$$X = WS \tag{2.1}$$

where W is the weight matrix to go from the S space to the X space.

The ICA solution provides an unmixed matrix from given EEG data to trace back to the original source. Figure 2.2 shows ICA results from a participant in the physical navigation experiment.

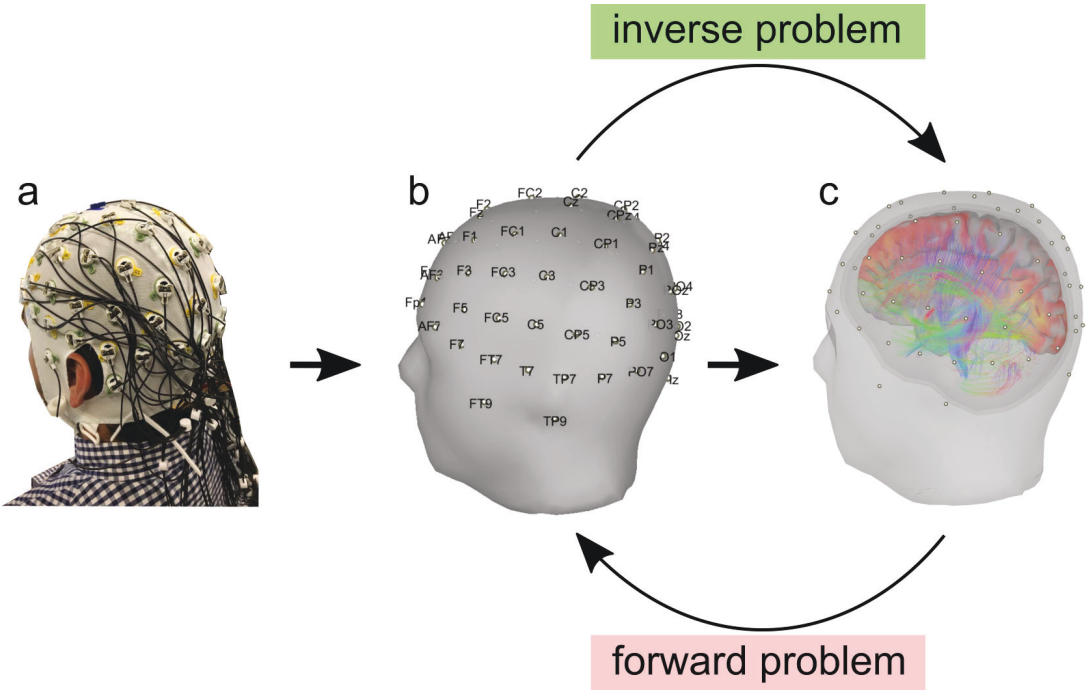

Figure 2.1 : The set-up of the EEG experiment. (a) The EEG cap. (b) The EEG channel location with the scalp template. (c) The distributed source of activation in the brain cortex.

2.3 Source localization for inverted problem

EEG data, which is measured from the head, reflects projected data from a brain source. However, localizing the brain source provides a better idea of the cognitive

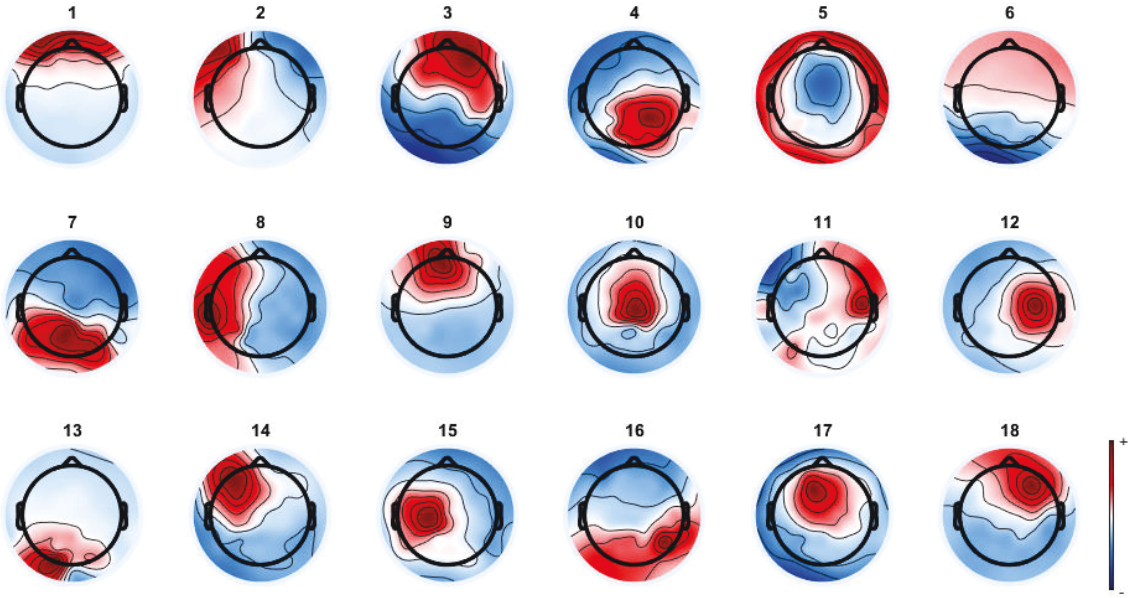

Figure 2.2 : The results of the ICA solution. The largest 18 independent components from a participant in a physical navigation study.

function. Thus, we can find out more which brain regions are related to our cognitive tasks.

In general, we can consider the EEG data can be presented as:

$$y(t_i) = Lx(t_i) + \epsilon(t_i) \tag{2.2}$$

where $y(t_i) \in R^{d\times 1}$ indicates EEG data at sample time t_i, $L \in R^{d\times n}$ represents the lead-field matrix, $x(t_i) \in R^{n\times 1}$ indicates brain source activation, and $\epsilon(t_i)$ indicates the noise at sample time t_i. Therefore, given the EEG data y, and lead-field matrix L, we can find the location of source activation.

While EEG data is normally recorded from a small sensor number, the number of potential source activations is higher, at around 2,000. There is more than one solution for the brain source projecting the same EEG scalp map without any additional assumptions. This problem is defined as ill-posed problem, and the solution for source activity at given EEG scalp map is not unique. However, several methods have been developed to solve this problem, including dipole fitting, distributed-source models, and spatial filtering. For more details and practical comparisons,

see Muñoz-Gutiérrez et al. (2018). The next two sub-sections briefly review the two methods that were used in this thesis: dipole fitting and non-adaptive distributed-source imaging methods.

2.3.1 Single and multiple dipole fitting

This method looks for a single point or small set of points that can explain the maximal variance of a given EEG scalp map. To do so, dipole fitting minimizes the error between the model and the measured potential from EEG data by estimating source parameters. The dipole strength and orientation can be estimated by linear transform, while the position is estimated non-linearly. In the given EEG scalp map after unmixing the original EEG data by ICA decomposition, we can find the dipole location by using EEGLAB. More details about this DIPFIT routine can be found in Oostenveld and Oostendorp (2002). Figure 2.3 shows dipole fitting for a participant in a physical navigation experiment (chapter 5, and 6).

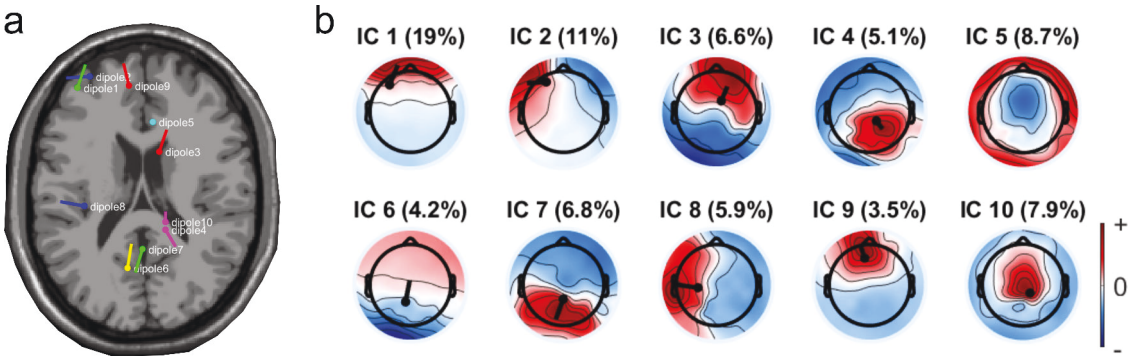

Figure 2.3 : The dipole fitting solution. (a) The first ten largest independent component dipoles location projected on the MRI template. Each dipole (coded by color) represents location and orientation. (b) The dipole locations projected on the scalp map. The number on the top indicates the IC number and its corresponding residual variance (RV).

2.3.2 Distributed source modeling

Instead of assuming that a small number of dipoles are activated at a time, distributed-source modeling assumes that thousand of dipoles all over the brain are

activated at a given time. The locations and orientation are pre-defined in a 3D volume or cortical sheet; this method estimates the strength or magnitude of the dipole. There are two typical techniques in this type: LORETA and minimum-norm estimator (MNE). Figure 2.4 shows source-distributed results from a participant in the physical navigation experiment.

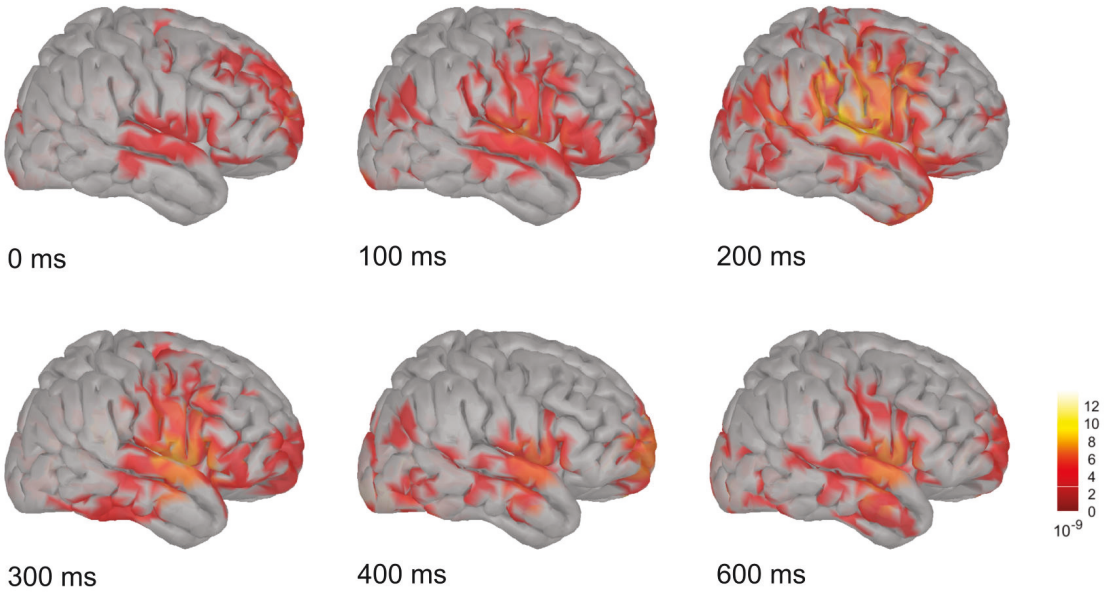

Figure 2.4 : The distributed source localization solution. The cortex source activity (right hemisphere) of a participant in the first 600 ms in the physical navigation study (chapter 5, and 6).

2.4 Group study

An independent component (IC) is different between participants; it is unlikely that a similar component will be found between participants. Therefore, in a group study, we cannot simply average the property of a component (e.g., ERP, ERSP) based on its location. Studying EEG data at a group level can be carried using a clustering method based on the attributes of the components. The next two sub-sections describe two methods that were used in this thesis: k-mean and repeated k-mean.

2.4.1 Clustering: k-means

All ICs' properties are calculated (e.g., ERP, ERSP, dipole location from dipole fitting routine, scalp map, power spectra) as an individual measured vector. To save computation time, which normally takes days with large datasets, principle component analysis (PCA) is often used for reducing the individual measured vector. Then, all attributes of ICs are composited as distance vector after normalizing with different weight factors based on their contribution (dipole location normally gets a higher weight due to its relationship with the cognitive task). Next, the k-mean method assigns each ICs to a respective cluster with a pre-defined number of clusters. Finally, we can study the ICA component activity among conditions from a given clustering solution.

Figure 2.5 shows the clustering result revealed by the dipole location of all ICs.

2.4.2 Clustering: Repeated k-means

The clustering method can assign a set of ICs into the same cluster based on their attributes. However, the cluster solution using k-mean might vary due to the initial assignment by the k-mean cluster method. Thus, the results of the clustering solution might change slightly at different run times. To overcome this issue, we can cluster more than a thousand times and then evaluate the best cluster based on our research assumption.

We first clustered the ICs based on the conventional k−means method implemented in EEGLAB. Next, we re-ran the clustering a thousand times before evaluating the best cluster of interest*, based on the region of interest (ROI) cluster centroid (Gramann et al. 2018). All ICs with an RV of less than a certain threshold (e.g., 15%) were grouped based on their attributes, such as dipole location, scalp topography, ERP, ERSPs, and mean log spectra. Subsequently, the weighted IC measurement were summed and compressed by PCA, followed by the k−mean method. The target cluster centroid with a given location in Talairach space was

*https://github.com/MariusKlug/bemobil-pipeline

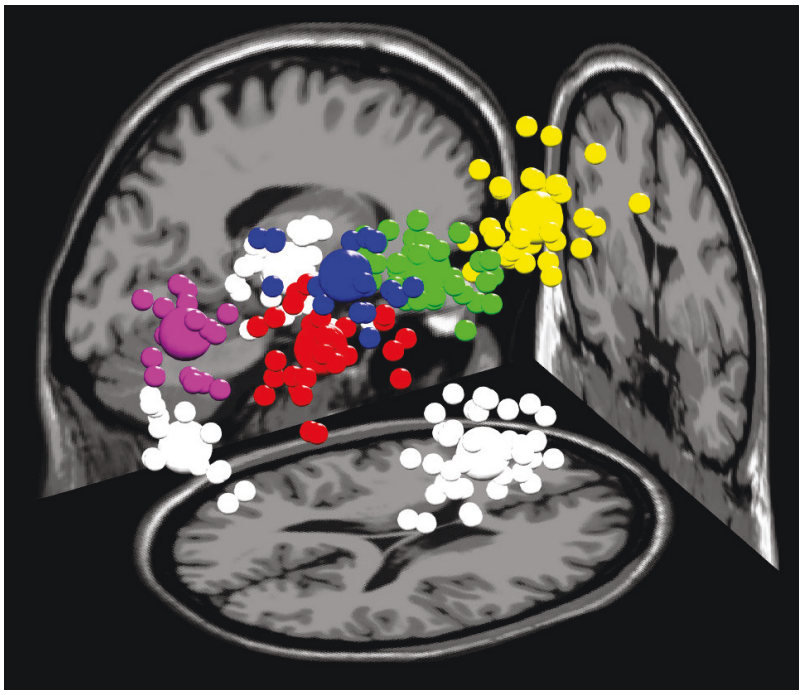

Figure 2.5 : Clustering solution. The color indicates different cluster regions: yellow, green, blue, red, pink, and white indicate frontal, sensorimotor, parietal, retrosplenial complex, occipital, and muscle, respectively. Small sphere indicates an independent component; the large sphere indicates the cluster centroid of the cluster. Figure adapted from the results of the physical navigation experiment in Chapter 5.

evaluated from the sets of ten-thousand clustering results, based on the score of each cluster solution, including: (i) the number of participants; (ii) the ratio of the number of ICs per participant; (iii) the cluster spreading (mean squared distance of each IC to the cluster centroid); (iv) the mean RV of the fitted dipoles; (v) the distance of the cluster centroid to the ROI; and (vi) the Mahalanobis distance to the median distribution of the solutions. Figure 2.6 shows the evaluation of 10,000 clustering results to find the best RSC cluster (red color).

After finding the cluster of interest, the next analysis step was based on the study hypothesis.

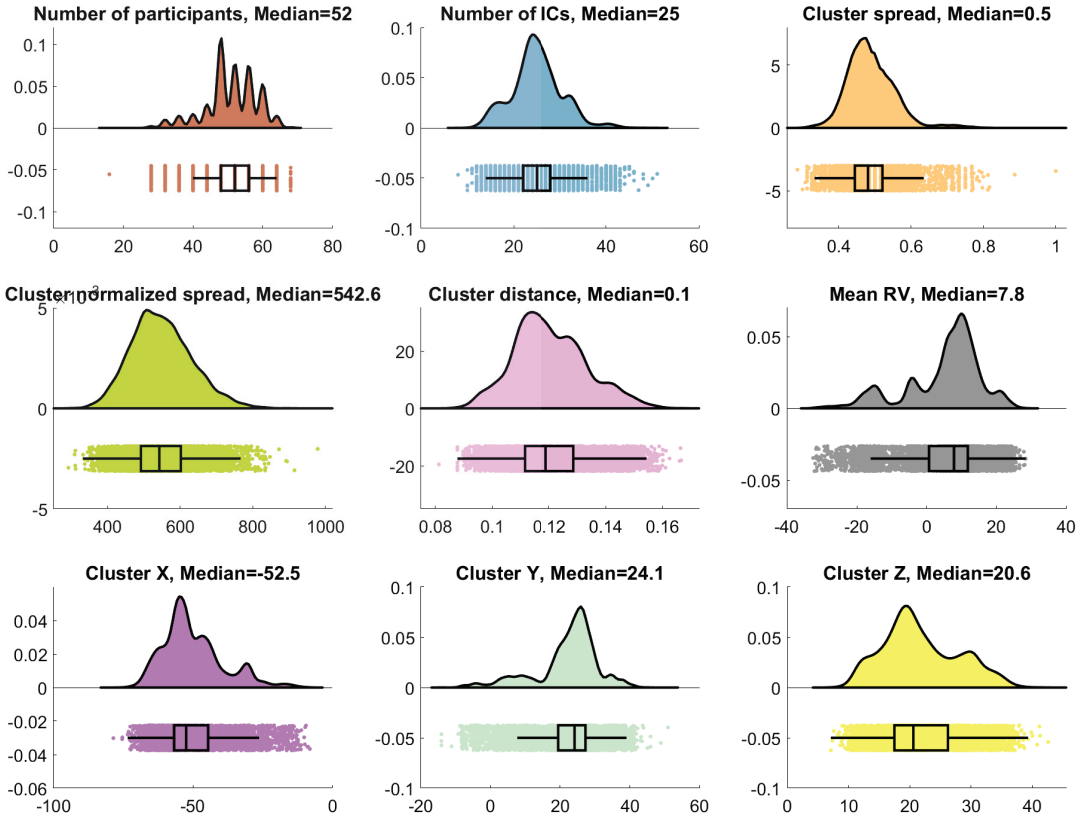

Figure 2.6 : Evaluation of multivariance from 10,000 times clustering based on the score of each cluster solution, including: (i) the number of participants; (ii) the ratio of the number of ICs per participant; (iii) the cluster spreading (mean squared distance of each IC to the cluster centroid); (iv) the mean RV of the fitted dipoles; (v) the distance of the cluster centroid to the ROI; and (vi) the Mahalanobis distance to the median distribution of the solutions.

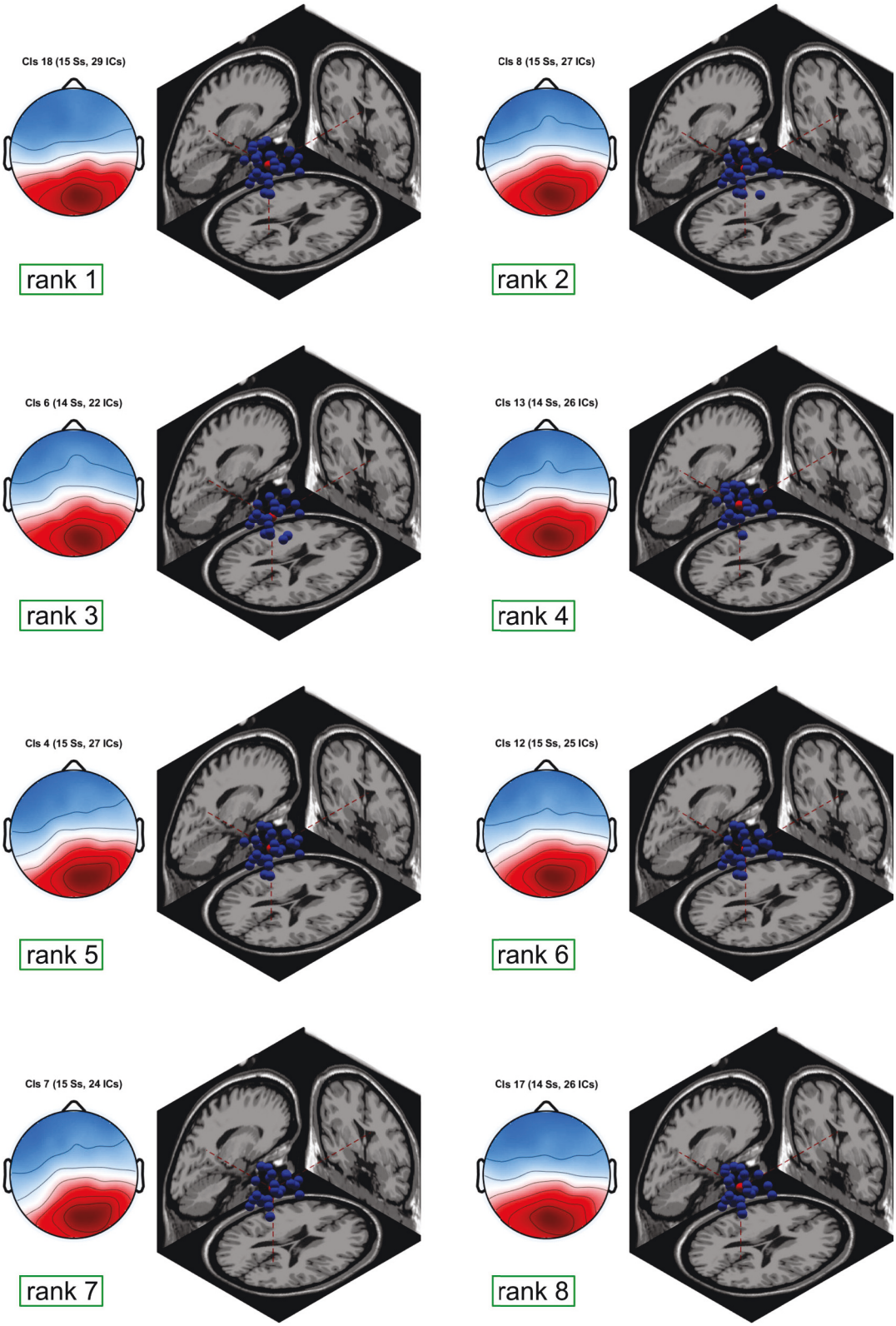

Figure 2.7 : Clustering solution for the retrosplenial complex cluster - top eight highest ranked solutions with grand scalp map and dipole location.

Chapter 3

Brain dynamics in the concurrent multitasking

This chapter investigates neural comodulation of multitasking in a simulated driving experiment. Chin-Teng Lin conceived this work. Shih-Jie Hsiao collected the data. Tien-Thong Nguyen Do and Shih-Jie Hsiao performed data analysis, with assistance from Chun-Hsiang Chuang and Yu-Kai Wang. All the authors discussed and wrote the manuscript (J-3) (Do et al. 2019).

3.1 Abstract

Distracted driving is regarded as an integrated task requiring different regions of the brain to receive sensory data, coordinate information, make decisions, and synchronize movements. In this chapter 3, we applied an independent modulator analysis (IMA) method to temporally independent electroencephalography (EEG) components to understand how the human executive control system coordinates different brain regions to simultaneously perform multiple tasks with distractions presented in different modalities. The behavioral results showed that the reaction-time (RT) in response to traffic events increased while multitasking. Moreover, the RT was longer when the distractor was presented in an auditory form versus a visual form. The IMA results showed that there were performance-related IMs coordinating different brain regions during distracted driving. The component spectral fluctuations affected by the modulators were distinct between the single- and dual-task conditions. Specifically, more modulatory weight was projected to the occipital region to address the additional distracting stimulus in both visual and auditory modality in the dual-task conditions. A comparison of modulatory weights between auditory and visual distractors showed that more modulatory weight was projected to the frontal region during the processing of the auditory distractor. This chap-

ter provides valuable insights into the temporal dynamics of attentional modulation during multitasking as well as an understanding of the underlying brain mechanisms that mediate the synchronization across brain regions and govern the allocation of attention in distracted driving.

3.2 Introduction

Driving is a complex task that requires drivers to continuously pay attention to control the car. One split second of distraction can result in an accident. Recently, there has been reported that 50 million injuries and 1.35 million deaths from road traffic crashes which is around 3700 people dying everyday globally (WHO 2018). The main reasons for road accident are various including higher population, low safety standards, distracted driving, fatigue, speeding and alcohol (WHO 2018). Distracted driving accounted for ten percent in fatal crashes in United States in 2015 (Schroeder et al. 2018). Numerous sources of distracted driving including texting, calling, passenger conversing and advertising (Drews et al. 2008; Oviedo-Trespalacios et al. 2017c, 2019a,b). For safe driving, drivers must concurrently concentrate on the road and handle incoming information and stimuli from the dashboard, road, and environment. Different regions of the brain receive sensory data, coordinate information, make decisions, and synchronize movements. Recently, new technological capabilities in vehicles have been significantly enhanced. However, interacting with these systems may impair the driver's attention. Talking on the phone while driving easily distracts the brain (Just et al. 2008). Thus, the high number of in-vehicle devices might adversely affect the attention of driver and the possibility of a fatal motor vehicle crash increases.

Distracted driving is regarded as an integrated task requiring the simultaneous execution of various cognitive, sensory and psychomotor abilities. Multitasking is an example of an interruption, in which the additional stimuli require attention while the primary task is simultaneously performed. Therefore, one of the most concerning issues addressed in dual-task studies is distracted driving, because this type of distraction is directly related to public safety. Many previous studies have

reported that concurrently performing dual tasks leads to impaired performance (Hick 1952; Hyman 1953). The Hick-Hyman law indicates that the response time is proportional to the number of stimuli (Hick 1952; Hyman 1953). Compared to dealing with only one task, there is often an extra cost to performing multiple tasks simultaneously.

Several researchers have considered attentional resources to be limited, and performance degradation in dual-task situations has been attributed to the central bottleneck (Welford 1952) or capacity sharing (Kahneman 1973). The central-bottleneck theory suggests that information can only be processed serially, that is, only one process can be engaged with at a time. Capacity-sharing theory suggests that information can be processed in parallel but with a limited amount of attentional resources, therefore different tasks must share this limited attentional resource. Many experiments have been performed that show the performance of the first task is affected in the dual-task situation (Kahneman 1973; Gottsdanker and Way 1966; Herman and Kantowitz 1970). Because both tasks needed the attentional resources at the same time, the allocation of these attentional resources will be shared between two tasks.

In addition to the fact that performance might be affected in attention-related dual tasks, many studies have reported relationships between the measured electroencephalography (EEG) spectra and attention-related processes in the past decade. The neural interference that occurs during multitasking has been revisited frequently (Anguera et al. 2013; Nijboer et al. 2014). Several studies included many trials with distincted stimulus onset asynchrony (SOA) to explore the neural correlates of shifts in attention in dual-task situations. Those results showed that both response time and accompanying EEG power varied significantly with different SOAs. The impaired task performance reflected the consequences of divided attention and shared brain resources during the dual-task situations. Increased posterior alpha and frontal theta power were observed in the presence of distraction (Lin et al. 2011; Wang et al. 2014a) , showing that an additional cost was needed to perform multiple tasks simultaneously.

An interesting question is how the human executive control system can coordinate different brain regions to simultaneously perform multiple tasks and whether the multitasking needs to recruit additional brain regions that were not involved in performance of any of the individual tasks alone. Independent component analysis (ICA) has been widely employed to explore brain temporal dynamics in EEG analysis since the 1990s (Bell and Sejnowski 1995). ICA has been demonstrated to be suitable for EEG source separation, identification, and localization (Delorme and Makeig 2004). In addition, it can remove none brain signals, such as noise made by an eyeblink, a body movement, and an indoor power line impulse. Source areas are often found to simultaneously oscillate at the same frequency. Therefore, we hypothesize that an executive control center mediates this synchronization across brain regions and governs the allocation of attentional resources during multitasking. To investigate the executive control system, an independent modulator analysis (IMA) was recruited to separate power spectral fluctuations of interest, i.e., independent components (ICs), into independent modulators (IMs), allowing us to sum up the spectral dynamics coherence across ICs. The proposed modulator analysis was applied to the spectra of temporally independent EEG components obtained from sessions using different stimulus modalities to contrast the differences between the resulting comodulators. This decomposition of spectral processes into frequency-IM processes can provide a better understanding of the potential neurophysiological mechanisms that were involved in cognitive and behavioral changes and systematically mediated the spectral activations of distinct cortical areas during multitasking. In this study, we aimed to systematically explore the executive control system that governs the coordination and allocation of attentional resources during distracted driving. The aims and hypotheses of this study are listed as follows:

1. Aim 1 - To assess behavioral changes under different stimulus modalities. Hypothesis 1 - The behavioral performance should be strongly associated with the number of tasks and stimulus modalities being engaged in the experimental paradigm. Therefore, we hypothesize that attentional interference may be generated if simultaneously performing several tasks.

2. Aim 2 - To investigate brain activities involved in attention-demanding tasks. Hypothesis 2 - Experimental designs and protocols, such as different stimulus modalities, might affect the cortical areas involved in cognitive processing. The related activations, interactions, and behavioral performance will be influenced during multitasking. Hence, we hypothesize that the stimulus modalities used in multitasking will result in different types of brain activation.

3. Aim 3 - To explore the executive control center that mediates the synchronization of power spectra across brain regions and governs allocation of attentional resources in multitasking. Hypothesis 3 - The spectral synchronization of cortical field potentials are highly affected by ortical networks. Therefore, the third hypothesis is that there is a neural modulator in the brain, which serves as an executive control center to mediate the synchronization across brain regions and to govern allocation of attentional resources during driving.

Taken together, these three hypotheses posit that the modulator(s) may have different modes of operation under different stimulus modalities used in the dual tasks.

3.3 Materials and Methods

3.3.1 Participants

Data were recorded from sixteen participants (aged 22.7 $\pm$ 1.6 years). All participants had normal or corrected-to-normal vision, and no participants took medications known to affect cognitive function or had a history of alcohol or drug abuse. All participants were students at National Chiao Tung University (NCTU) in Taiwan who participated in this study voluntarily and provided informed consent. All the components of this study were approved by the Institutional Review Board of NCTU and performed according to the Declaration of Helsinki. The participants received monetary compensation for their participation.

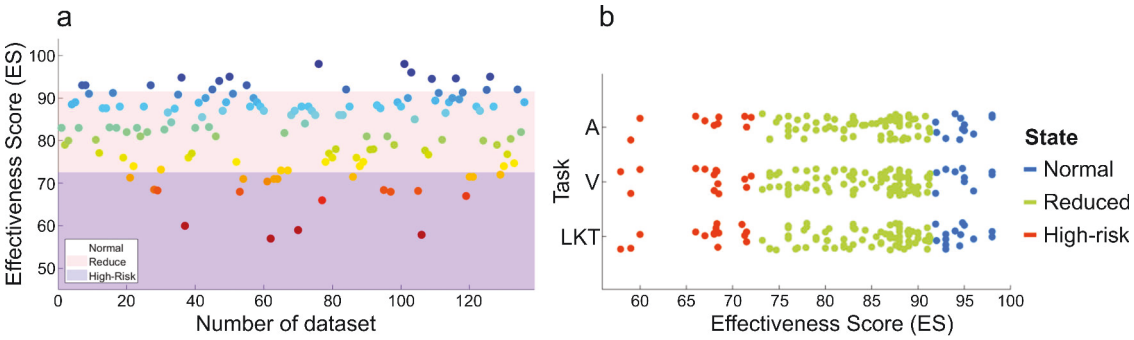

Figure 3.1 : a, Effectiveness score (ES) distributions. One dot indicates one dataset. (i), normal fatigue group (white), (ii) reduced fatigue group (light pinks) and (iii) high-risk fatigue group (light purple). b, Effectiveness score (ES) distributions between task and fatigue groups after the model validation test for effectiveness connectivity (EC) estimations.

3.3.2 Fatigue state

We applied the biomathematical fatigue model "sleep, activity, fatigue, and task effectiveness" (SAFTE) to estimate the fatigue states of the participants (Hursh et al. 2004). The SAFTE model is based on using the work/sleep pattern of participants to predict cognitive performance. In addition, the SAFTE model further records data on circadian rhythms, sleep inertia, and homeostatic drive, characterizing the sleep-wake histories of the participants to evaluate their fatigue state. SAFTE results have been validated as neurobehavioral performance predictors in experimental environments (Hursh et al. 2004, 2006; Lin et al. 2018). In this study, the fatigue state was measured using a Readiband device (Fatigue Science Readiband, Vancouver, BC), which employs the SAFTE model to estimate fatigue based on psychology. The effectiveness score (ES) is an automatically continuous output from the Readiband device based on the data collected for the previous three days. Every day, the ES index (rank from 0-100) was sent to a cloud server, and the experimenter decided whether or not the participant was in a suitable state to record the data. The participant had to come to the laboratory to collect the data within 10 hours of receiving the phone call from the experimenter. Therefore, in principle, the participant wore the Readiband every day within the experiment period. The

ES was checked again before the participant performed the experiment. The fatigue level of the participant was classified for analysis in this study based on the new ES score.

3.3.3 Experiment paradigm

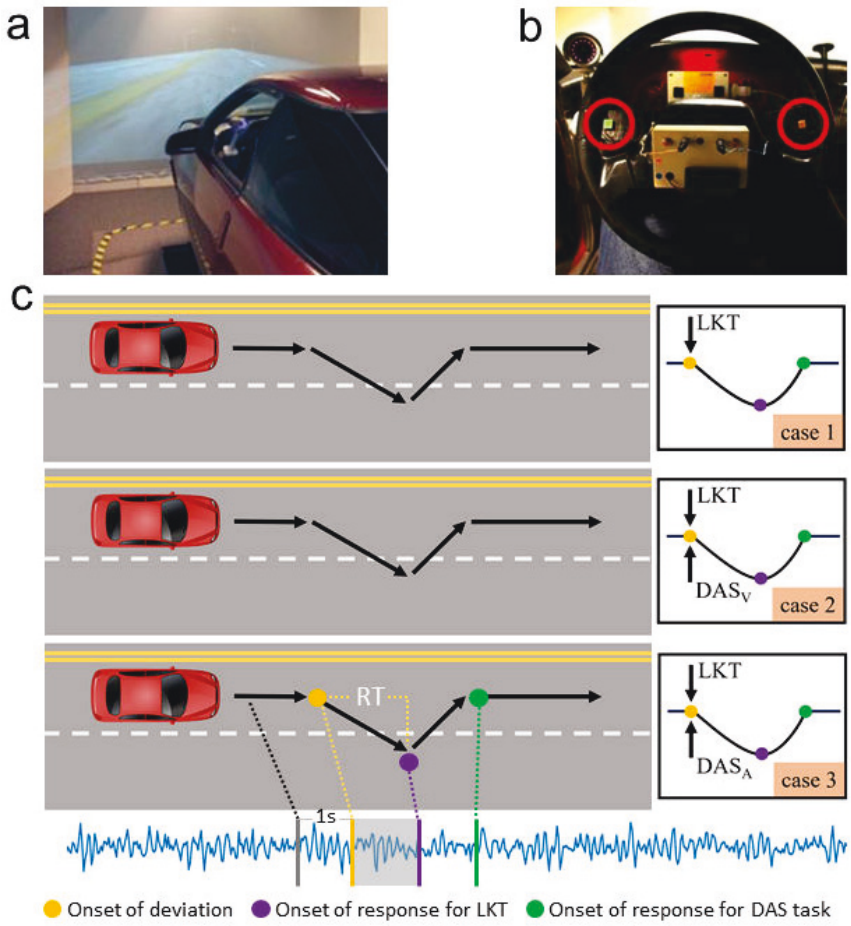

Figure 3.2 : Experimental design. (a) Virtually simulated environment for the driving task. (b) Two buttons were placed on the wheel for the DAS task response. (c) Experimental design; case 1: Lane-keeping task (LKT) only; case 2: concurrent LKT and visual dynamic attention shift (DAS$_V$) dual tasks; case 3: concurrent LKT and auditory dynamic attention shift (DAS$_A$) dual tasks.

This study adopted the event-related lane-departure paradigm in the realistic driving simulator environment (Huang et al. 2009) to assess brain dynamics under task conditions at varying fatigue states. Two task types were executed during

the experimental protocol of this study: a lane-keeping task (LKT) and a dynamic attention shift (DAS) task. The LKT task simulated a participant driving a car on a four-lane road (two lanes for each direction with constant speed at 100 km/h) at night without other traffic, as shown in Figure 3.2a. Throughout the entire experiment, the participants were required to maintain the car cruising in the third lane, as shown in Figure 3.2c. The car randomly drifted to the left or right in equal proportions. At the time of deviation onset, the participants were instructed to control the steering wheel to move the car back into the third lane as quickly as possible. The period from the deviation onset to the time point of turning the steering wheel was defined as the driving reaction time (RT, in milliseconds). In the DAS task, the participant was required to respond to the target, an animal name, and ignore the non-target by pressing the left or right buttons, which were mounted on the steering wheel (Figure 3.2b). The target appeared in the form of written (visual) red letters on the screen or spoken words (auditory). The participants performed three task cases based on a combination of LKT and DAS tasks.

The first case was LKT only (single task), the second case was concurrent LKT and visual DAS (DAS_V) dual tasks, and the third case was concurrent LKT and auditory DAS (DAS_A) dual tasks in a random order (figure 3.2c). While the target was displayed on the screen, the time from the target onset to the button press was defined as the DAS RT. All participants underwent an orientation session that described the experimental procedures and their responsibilities during the long-term study.

3.3.4 Data acquisition

All participants ideally completed this experiment nine times; however, participant S06 participated five times; S08 participated six times; S14 participated six times, and S16 participated eight times. In total, 133 datasets were collected over six months. Each experimental session lasted approximately two hours (including experimental set-up), and the sessions were conducted at roughly two-week intervals for each participant. All participants read the consent form and experiment description ten minutes before the experiment. The ES was logged before the participants

performed the experiment (Figure 3.1a). Three fatigue groups were divided based on the total ES distribution. Due to the difficulty of collecting enough datasets in the high-risk fatigue group, the fatigue groups were divided into three different fatigue groups with a new threshold that was slightly different from the original proposal from fatigue science: the normal fatigue group (ES greater than 91.5 (ESmean+ESstd)), a high-risk fatigue group (ES less than 72.6 (ESmean-ESstd)) and a reduced fatigue group (remaining datasets). EEG signals were recorded using the Synamps2 system (Compumedics Neuroscan Inc., Abbotsford, VIC) using 64 channels with Ag/AgCl electrodes and two references at the left and right mastoids (A1 and A2) according to the international 10-20 system. All electrode impedances were maintained at under 5 kOhm and were recorded with a sample rate of 1000 Hz and 32-bit quantization. The participants were seated in the car in a well sound-proofed, magnitude wrap-around virtual reality driving laboratory. The participants performed four sessions throughout the experiment in one EEG dataset; each session contains 60 trials per task condition (LKT, DAS_V and DAS_A) in random order. The participants had a rest-time of 5-10 minutes between sessions.

3.3.5 Data Processing and Analysis

In this study, all data analyses and signal processing were imported into MATLAB (version 2011a, MathWorks Inc., Natick, MA) and the EEGLAB Toolbox (version 13.0) (Delorme and Makeig 2004)

EEG data preprocessing

To remove DC drift and high frequency noises, the recorded EEG raw data were first processed by a high-pass filter and a low-pass filter at 0.5 Hz and 50 Hz, respectively. After filtering continuous EEG data, the filtered EEG data were downsampled at 250 Hz to reduce the computational complexity of EEG data. The recorded data might have included artifacts caused by muscle activity, body movement, and poor contact between the sensors and the skin. Therefore, artifacts that contaminated the EEG signals were first subjected to automatic artifact rejection provided by EEGLAB to reject those data containing extreme amplitudes and ab-

normal distribution to enhance the signal-to-noise ratio. Furthermore, to minimize artifact baseline on the EEG activity, the recording data were removed manually, e.g. the raw value of each channel is higher than 100 μV. Next, data epochs were extracted; one event-related epoch was extracted from -1.0 s (prior to the deviation onset) to 2.5 s (following the deviation onset). The one-second period before deviation was selected as baseline, and all event-related effects would be in reference to the baseline means. Time-frequency analysis and modulation analysis were then applied to the preprocessed EEG data.

3.4 Neural comodulation analysis

ICA, followed by IMA, was applied to the multichannel EEG signals to determine whether comodulatory processes mediated the spectral responses of independent EEG processes (Chuang et al. 2012, 2016). This decomposition of the spectral processes into frequency-IM processes can provide a better understanding of the potential neurophysiological mechanisms that were involved in the observed cognitive and behavioral changes.

Independent Component Analysis (ICA)

Each channel of EEG activities is a time course of mixed electrical signal activities collected from multiple electrodes placed on the scalp and sensitive to activity generated within the neurons of the brain. Therefore, EEG signals are linearly mixed source signals projected from distinct independent neuronal activations and nonbrain artifacts. ICA is an algorithm to separate a multivariate signal into non-Gaussian and statistically independent signals. The ICA decomposition of EEG time series assumed that (a) signal conduction time was instantaneous, and summation of currents at the scalp sensors was linear, (b) source activations were temporally independent of one another across the input data, and (c) statistical distributions of the source activation values were not Gaussian.

$$D = AS \tag{3.1}$$

$$U = WD \tag{3.2}$$

ICA is a statistical method to extract the independent sources contributed to mixed EEG signal, and it describes the source separation problem as a form of equation 3.1. Where D is the signal recorded from the scalp and A is a linear transform called a mixing matrix. Blind sources are statistically mutually independent. ICA estimates an 'unmixing' matrix, W, to decompose the multichannel EEG data matrix, D, into the time courses of the component activation matrix, U are statistically independent as in equation 3.2. The columns of the inverse 'unmixing' matrix, W^{-1}, represent the projection of each IC onto the original data channels, which enabled the formation of a color-coded scalp map. These projection weights provide the scalp map of each IC and evidence of the origin of components' physiology. For example, eye activity was projected mainly to frontal sites, etc. The activities from different brain sources, eye movement artifacts, muscles and channel noises were effectively separated into ICs. In the current study, ICA decomposition was implemented by the EEGLAB 'runica' toolbox function in MATLAB. Furthermore, the criteria of ICA convergence were set to the maximum steps at 1024, and the error was less than 10-7.

Component Selection and Clustering

To compare neural oscillations across subjects, component clustering was conducted to assess the consistency of ICA decompositions across subjects and sessions. The consistency of ICs across subjects was assessed semi-automatically by the k-means clustering method and visual inspection to classify the components from all subjects into distinct clusters based on measures including scalp maps, mean IC power spectra and equivalent dipole source locations. To ensure that the clusters obtained by the k-means method were sufficiently distinct, the clustering procedure was repeated for seven iterations. The ICs with equivalent dipole sources located in the medial frontal, medial central, left temporal, medial parietal, posterior-medial occipital, and bilateral occipital cortices were selected for further time-frequency analysis. Furthermore, the components in these clusters of interest for each subject were selected for further independent modulator decomposition (IMD) to assess the comodulation of independent brain processing activities among these selected ICs.

Time-Frequency Analysis

Event-related spectral perturbation (ERSP) is a spectra-temporal decomposition technique that decomposes a continuous time signal into frequencies using the fast Fourier transform (FFT). ERSP was used to explore the brain dynamics in the identified brain IC (Chuang et al. 2012). The selected IC activation for each EEG epoch was separated into the power spectra through the FFT in a frequency range between 0.5 and 50 Hz. The spectra included delta (1-3 Hz), theta (4-7 Hz), alpha (8-12 Hz), beta (13-30 Hz), and low gamma (31-50 Hz). Each EEG epoch was processed using a 256-point Hanning window with 128-point overlap. The ERSP was computed by obtaining power for each epoch and time point, subtracting the mean value of the baseline period (-1.0 s to 0 s) over the entire epoch duration and then averaging across trials. The ERSP results reflected event-related brain dynamics at different frequencies. Significance levels were computed by bootstrap resampling, extracted at random from baseline data epochs. The significance level was set at 0.05 for the ERSP results. Statistically significant ($p<0.05$) spectral changes are shown in the ERSP images; in contrast, nonsignificant time/frequency points are masked. The ERSP was time locked to the deviation onset, and the time-frequency estimates of all EEG epochs were linearly aligned with the events. In the single-task condition, the aligned events were the subject turning the steering wheel. In the dual tasks, the subject turning steering wheel and the onset of the button press were both considered.

Independent Modulator Decomposition

To model spectral fluctuations of ICs from EEG activations as the actions of IM processes, this study adopted IMA method which has been used in (Chuang et al. 2012, 2016; Onton and Makeig 2009) – see (Onton and Makeig 2009) for details on how to compute the IMA. The equation to find the IM activation as below:

$$U = WAX \tag{3.3}$$

Here, U is the IM activations across time point t $\times$ e. W is an unmixing matrix, found by the infomax ICA algorithm. A is the projection matrix. X is the matrix

of log-spectral deviations (with the size [f × c, t × e], c represented the number of selected ICs and f represented the mean log-power spectra at each frequency bin, t and e represented the time series in a single epoch and the number of epochs, respectively). To process the IMA computation, first, the time series of each epoch's normalized power spectra of selected ICs were reshaped into a 2D matrix, X, of size [f × c, t × e] (where c represented the number of selected ICs and f represented the mean log-power spectra at each frequency bin, t and e represented the time series in a single epoch and the number of epochs, respectively). Then, this matrix was reduced to p main principal components by principal component analysis (PCA) to a matrix, S, of size [p, t × e] and projection matrix, A (AX = S). After using PCA, the obtained matrix S was submitted to the infomax ICA algorithm that decomposed log-spectral power across time series for all spectral fluctuations of the selected ICs. An unmixing matrix, W, found by the infomax ICA algorithm, and its process were formulated as $S = W^{-1}U$. The rows of the output data matrix, U, are time courses of the activation of the IMs. Hence, the IMA could be formulated as $AX = S = W^{-1}U$. Given the pseudoinverse of the dimension-reduced PCA eigenvector matrix, A^{-1}, then we had $X = A^{-1}W^{-1}U$. The columns of $A^{-1}W^{-1}$ provided the relative projection weights of each IM at each frequency bin for each component, and U represented the IM activations across time point t × e, to compute the means of each IM's activation throughout the epochs.

3.5 Results of the comparison between single-task ad multiple-task conditions

3.5.1 Behavioral Performance

Our hypothesis was that behavioral performance during multitasking might be adversely affected. We focused primarily on the effect of performing the secondary task under different stimulus modalities on driving performance. The RTs from the LKT conditions were compared, as shown in figure 3.3. A hierarchical linear model analysis was conducted to assess driving performance under different conditions. figure 3.3 indicates a significant difference between the mean of the single-

and dual-task conditions. The RTs in both dual-task conditions (Case 2 and Case 3) were significantly longer than the single-task (Case 1) condition ($p < 0.05$). Furthermore, the RTs of dual tasks involving different stimulus modalities also showed a significant difference ($p < 0.05$). In the dual-task conditions, drivers' RT to lane perturbation was longer when the participants had to react to the secondary task, which was presented in either an auditory form or a visual form (figure 3.3). In this study, the driving task was considered the primary task; therefore, trials with the driving reaction as the first reaction and DAS as the second reaction were included in this analysis. The stimulus in the form of visual was dominant in the current experimental design for the LKT task. Therefore, the DAS_A's RT might take a longer time due to the stimuli modality difference (auditory vs. visual).

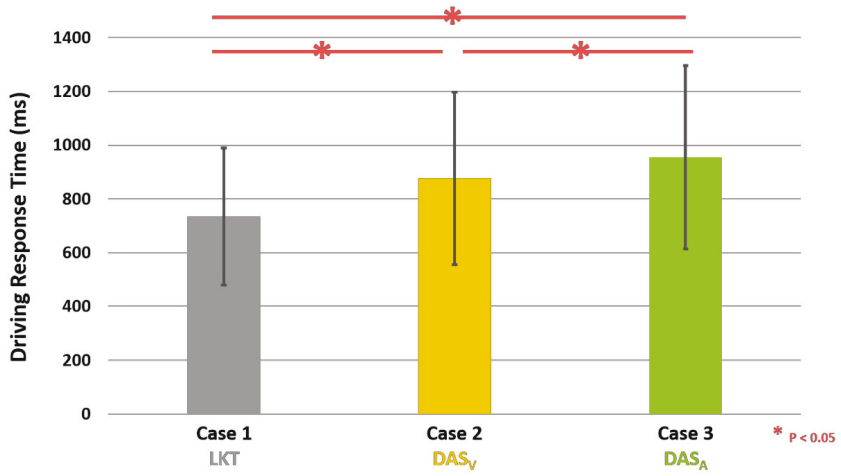

Figure 3.3 : The behavioral performance among the single- and dual-task conditions. The averaged driving response time of LKT (gray bar), DAS_V (yellow bar) and DAS_A (green bar) in each condition are listed. The averaged driving response time were significant different among three cases ($p < 0.05$).

3.5.2 Event-Related Spectral Perturbation

In addition to the behavioral changes, experimental trials that involved different workload and stimulus modalities might have produced distinctive activations and interactions in the human brain. We hypothesized that the workload or stimulus

modalities used in multitasking would result in different types of activations. To test this prediction, we applied the ERSP analysis to selected ICA components, including the frontal, central, parietal, occipital, and temporal components. figure 3.4a shows the ERSP results in the single-task condition (LKT only). The increased power in the delta band from the deviation onset to the driving response onset was mainly observed in the frontal, central and parietal areas, and the central area delta band was strongly increased. The increased power in the theta band was primarily observed in the frontal and central areas.

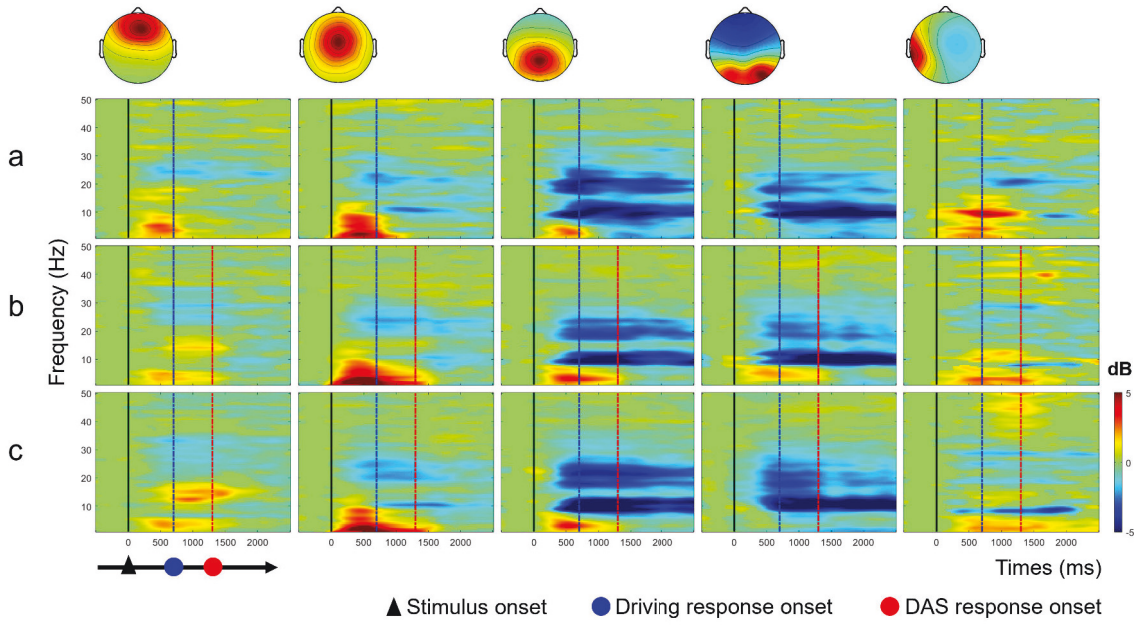

Figure 3.4 : The Event-Related Brain Dynamics in three cases (rows) across brain regions (column), including the frontal, central, parietal, occipital, and temporal components (top). a) The ERSP in the Case 1 (LKT). b) The ERSP in the Case 2 (DAS_V). c) The ERSP in the Case 3 (DAS_A). The black-vertical line indicates stimulus onset (deviation onset), the blue-vertical line indicates driving response, and the red-vertical line indicates DAS response.

After the deviation onset, decreased alpha and low beta power were also observed in the posterior area, including the parietal and occipital components. figure 3.4b shows the ERSP results in the selected components while performing in Case 2 trials (LKT and DAS_V). The delta and theta bursts can be observed in all selected

components from the deviation onset to the button press (red dotted lines in figure 3.4). Decreased power in the alpha band can also be observed in the posterior area. Increased power in the frontal alpha band appears briefly between the driving response onset and the button press onset. figure 3.4c shows the ERSP results while performing in Case 3 trials (LKT and DAS_A). Delta and theta bursts can be observed in all selected components except the occipital component from the deviation onset to the button press, but the central theta power was only observed from the deviation onset to the driving response onset. The decreased power in the alpha band was observed in the parietal and occipital components. Frontal alpha power increases appeared briefly from the driving response onset to the button press onset. Temporal gamma power increased from the driving response onset to the button press onset. During the dual-task conditions, the alpha oscillations varied in distinct brain areas (refer to figure 3.4). Increased power in the frontal alpha bands was time locked from the driving response onset to the button press onset. Instead of increased power in the alpha band in the frontal area, decreases in alpha were observed in the posterior areas (parietal and occipital area). In addition, occipital theta power was found to be significantly increased in the parietal component in both dual-task conditions and in the occipital component in the DAS_V condition.

3.5.3 Independent Modulators and Their Activation

The power spectral fluctuations from the neurons of the brain sources were further subjected to IM decomposition by forming a 2D matrix to find independent modes of comodulation across the ICs. It should be noted that the number of ICs may vary across subjects since each individual may engage distinct brain processes even during the same task (Jung et al. 2001)

Event-related activation of IMs

We selected the modulators according to the activation of the modulator relative to task performance. To assess the consistency of the IMs of interest across subjects, figure 3.5a shows the modulator activation without being time locked. Furthermore, figure 3.5b presents the event-related modulator activation in all cases

over all subjects. Each column plots the individual (thin line) and averaged (thick line) modulator activation. We found that a burst of modulator activation between the lane-deviation onset and driving response onset was observed in all cases. The multiple comparisons of the event-related modulator activation between the different cases are shown in figure 3.5c. The first column shows the event-related modulator activation difference between Case 1 and Case 2. The second column shows the difference between Case 1 and Case 3, and the last column shows the difference between the dual-case conditions. The signed-rank statistical analyses were used to examine the differences among the different workloads or stimulus modalities. The IM activation difference was significant at the 0.05 level. The results showed that the comodulatory activities during the different workloads or stimulus modalities were not significantly different.

Projected frequency weights of the modulators

To assess the consistency of the IMs of interest across subjects, figure 3.6 displays the results of the group projection weights, in which each cell represents a relative projection weight from one IM to the frequency of the IC. For each selected IM, the relative weight of projection onto all selected ICs across subjects was averaged, and the average projection weights in the frequency ranges of the delta, theta, alpha, beta and gamma bands were computed. Then, a bootstrapping test was conducted on the projection weights through all ICs of each IM, and the significant differences were plotted as red bars in figure 3.6. For example, the first modulator in the frontal component has delta and theta projection weights that were significantly higher among the various brain regions. In figure 3.6, the first column shows that the modulator regulated the delta and theta bands in the frontal component, regulated all frequency bands in the central component, regulated the delta, theta and alpha bands in the parietal component, regulated the alpha band in the occipital component, and regulated the theta band in the temporal component when performing only the LKT (Case 1). The second column modulator regulated the delta and theta bands in the frontal component, regulated the delta, theta and alpha bands in the central component, regulated the delta and theta bands in the parietal

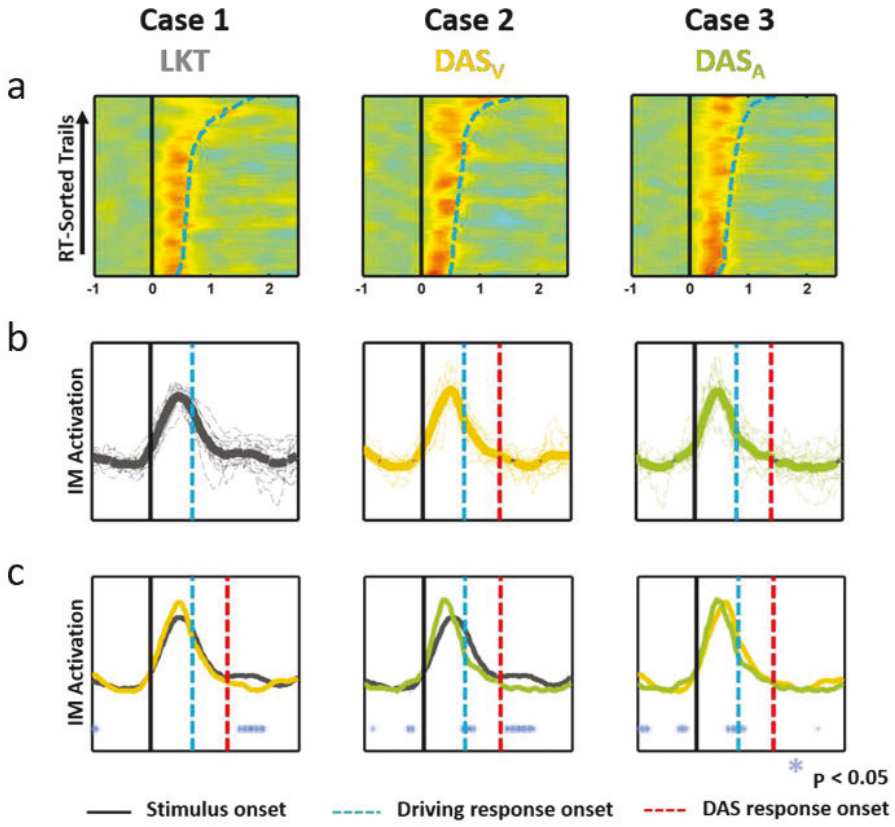

Figure 3.5 : The event-relative independent modulator activation. a) The performance-related IM activation changes in LKT, DAS$_V$, and DAS$_A$ conditions. b) The event-related IM activation changes in LKT, DAS$_V$, and DAS$_A$ conditions. c) The IM activation difference among different conditions. The first column showed the difference between Case 1 (grey curve) and Case 2 (yellow curve). The second column showed the difference between Case 1 (grey curve) and Case 3 (green curve). The last column showed the difference between Case 2 (yellow curve) and Case 3 (green curve). The IM activation difference is significant at the 0.05 level (blue *).

component, regulated the delta, theta and alpha bands in the occipital component, and regulated the beta band in the temporal component while performing LKT and the visual distractor task simultaneously (Case 2). The third column modulator regulated the delta, alpha and beta bands in the frontal component, regulated the delta, theta, alpha and beta bands in the central component, regulated the delta and theta bands in the parietal component, regulated the delta, theta and alpha bands in the occipital component, and regulated the gamma band in the temporal com-

ponent while performing the LKT and the auditory distractor task simultaneously (Case 3).

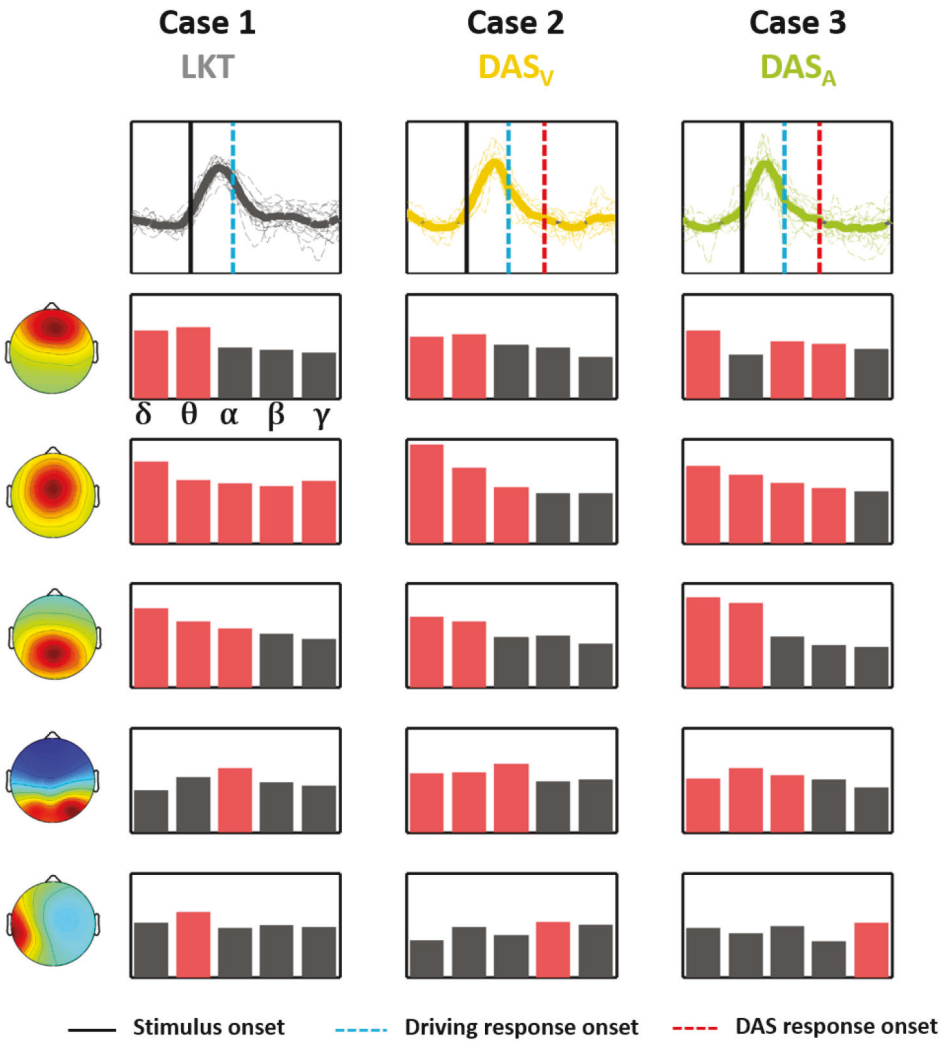

Figure 3.6 : The relative weight from IMs to each frequency band of ICs. Each column represents the relative weight of projection from the IM (the top row) to each frequency band (delta, theta, alpha, beta, and gamma band) of each selected IC (the leftmost column). For each IM, the red bar plots the significant difference among each frequency band of each selected IC.

3.6 Discussion

3.6.1 Behavioral Performance during Distracted Driving

In this study, we investigated the behavioral differences between the single- and dual-task conditions as shown in figure 3.3. The results demonstrated that the RTs of the LKT in both dual-task conditions (Case 2 and Case 3) were significantly longer than the single-task condition (refer to figure 3.3). Executing multiple tasks simultaneously leads to impaired performance in one or multiple tasks (Welford 1952; Kahneman 1973; Pashler 1994; Schubert et al. 2008; Pizzamiglio et al. 2017; Wang et al. 2018). Furthermore, the drivers' RT in response to perturbation was longer when the secondary task stimuli were presented in an auditory form. A previous study demonstrated that performance with an auditory distracter was dramatically impaired unless the auditory distracter was simple and required no cognitive processing (Tellinghuisen and Nowak 2003). Driving was considered the primary visual task and the lane-deviation event was always considered the most important issue for preventing traffic accidents. In this study, therefore, the participants almost always responded to the lane deviation first. The findings that the performance tended to decrease more when the component tasks consisted of different sensory modalities were consistent with previous studies (Näätänen 1992). This may be because the brain selects appropriate sensory inputs and suppresses different sensory inputs. As a result, the performance in the visual-based driving task was less affected by a visual distractor than by an auditory distractor. Most recent studies provide evidence that the driver self-regulates the driving speed as using mobile phone in various traffic conditions (Oviedo-Trespalacios et al. 2017a, 2018, 2017b). In this study, the velocity of the vehicle was consistently simulated with 100 km/h in the motor highway without any other traffic. Therefore, the driver did not have the opportunity to control the vehicle speed, driver may increase their reaction time of the driving task to handle the information from the distracting secondary task (refer to figure 3.3). In addition, the driver always keeps their gaze on the center of driving scenario, therefore, the distracted factor from secondary task may not be compatible to the visual-manner distracted from mobile phone such as texting and

browsing which shifted their gaze from the road. Further study is needed to investigate the self-regulation of driver to the distracted factor when driving in constant speed.

3.6.2 EEG Correlates of Distracted Driving

Compared to the behavioral changes, the physiological measurements are more sensitive to cognitive and attentional changes. In this study, we also investigated the differences in brain activation between the single- and dual-task conditions. Previous studies have shown that the frontal and parietal cortices are related to the attentional demands involved in the coordination of multiple parallel tasks (Herath et al. 2001; Schubert and Szameitat 2003; Stelzel et al. 2006). We observed that increased theta, alpha and beta band power in the frontal area appeared briefly while performing the cognitive task during the dual-task conditions (refer to figure 3.4). Human EEG studies have highlighted the importance of theta and alpha oscillations in distinct brain regions as parts of the neural network involved in attention-related processes (Klimesch 1999). Previous studies have demonstrated that increased frontal theta and beta bands were associated with distraction effects (Lin et al. 2011; Pizzamiglio et al. 2017; Wang et al. 2018). In addition, increased frontal theta oscillations were mainly associated with decision-making, orienting, conditioning, managing workload, working memory, and maintaining goal states (Klimesch 1999; Gevins et al. 1997; Sauseng et al. 2005; Kahana 2006; Tombini et al. 2009; Huang et al. 2013; Popov et al. 2018; Proskovec et al. 2019). In this study, increased frontal theta, alpha and beta power might have been correlated with the high attentional demands and executive controls in cognitive tasks that are involved in decision-making. Since the subjects needed to shift their attention between two tasks in the dual-task conditions, decision-making must be involved in the process. Therefore, the dual tasks induced more theta activity in the frontal region, as well as requiring the subjects to allocate more brain resources to accomplish both tasks. The occipital lobe is the visual cortex, which processes and relays visual stimuli in the brain. This region specializes in different visual tasks, such as visuospatial processing, color discrimination and motion perception. The occipital theta power was significantly increased

after the deviation onset, when the visual targets appeared simultaneously (refer to figure 3.4). A previous study reported that the occipital component revealed a sequence of theta increases after the onset of a visual stimulus presentation (Huang et al. 2013). In this study, the increased occipital theta was only found in the Case 2 trials. These results can be explained by assuming that the visual stimulus and the auditory stimulus might engage distinct brain resources during the driving task. Therefore, the cortical components that were induced would vary across different types of modalities. In sum, the theta oscillation in the occipital cortex might be associated with sensory processing or stimulus selection.

3.6.3 EEG Comodulatory Activity Correlates of Distracted Driving

To explore the comodulators of independent brain processes with different workload or stimulus modalities in a multitasking situation, we applied a method including PCA and a second ICA for decomposing spectra dynamics of temporally independent EEG components into the different spectral comodulators. The modulator activation trend across participants was similar even though the components' log spectra of each participants was calculated separately (refer to figure 3.5c). The statistical comparisons showed that the comodulatory activities during the different workloads or stimulus modalities were not significantly different. Our findings are not in contradiction with those of the previous studies discussed above. Moreover, the number of main spectral fluctuations mediated by the modulators was also similar (refer to figure 3.6). Regarding the attentional resources in a multiple task condition, several studies have indicated that attentional resources were limited (Welford 1952; Kahneman 1973; Gottsdanker and Way 1966; Herman and Kantowitz 1970).

3.6.4 Potential Neurophysiological Mechanisms

In the present study, we found that modulator activations were not significantly different during the different workload requirements or stimulus modalities, and the number of main spectral fluctuations mediated by the modulators were also similar. However, the component spectral fluctuations affected by the modulators were

distinct across conditions (refer to figure 3.6). Several previous studies have suggested that the components might have different spectra dynamics under different stimulus modalities engaged in the multiple tasks (Nijboer et al. 2014; Adcock et al. 2000; Just et al. 2001; Jaeggi et al. 2003; Szameitat et al. 2011). The frontal region oscillations may vary from one task combination to another (Miller and Cohen 2001; Staines et al. 2002) and are involved in managing concurrent processes (Dux et al. 2006; Kane and Engle 2002). Compared with executing only the lane deviation, performing the response to the lane deviation with a visual distractor in Case 2 involved additional processes and attention (Fernández et al. 1995; Sammer et al. 2007); therefore, the frontal region may be more activated. Although the lane deviation with visual distractor induced a higher workload, we found that the modulators mediated the same spectral dynamic in the frontal regions under Case 1 and Case 2 (refer to figure 3.6). It is possible that both tasks were visual-based. Therefore, there were no additional spectral dynamics mediated by the modulators in the frontal area. In contrast, the result of this study showed more spectral dynamics in the frontal component mediated by the modulator in Case 3. The possible explanations for the finding might be that the frontal lobe is considered to control higher-level cognitive processes and problem solving. Thus, additional attentional resources might be used in the frontal region to process auditory distractors compared with visual distractors during dual tasks. During the dual-task conditions, the equal number of spectral fluctuations mediated by the modulator was observed in the occipital area. Previous studies have suggested that the occipital region might be associated with attention processing or stimulus selection (Murray and Wojciulik 2004; Huang et al. 2013). These results can be explained by assuming that the presentation of a distracting stimulus in one of these modalities affected the processing of the occipital cortex. It is possible that more attentional resources should have been shifted into the occipital region to account for the additional distracting stimulus in the dual-task conditions.

3.6.5 Possible Neural Modulation Mechanisms

Several previous research indicated that neurotransmitters such as acetylcholine, norepinephrine, dopamine or serotonin might modulate thalamic and cortical activation (Robbins 1997; Bardo 1998). The underlying co-modulation possibility consider that the influence of cortical and thalamic projections (Oken et al. 2006; McCormick and Bal 1997; Akimoto et al. 1956; Bardo 1998; Robbins 1997). A thalamo-cortical network involves thalamus receiving sensory input from little cortical area and projecting to a higher-order cortical areas (Bertram 2010; Swick et al. 1994). Many studies have found that thalamic neurons modulating the power spectral synchrony between distinct cortical areas (Swick et al. 1994; Herculano-Houzel et al. 1999). Therefore, the neural modulator might serve as an executive control center to mediate the synchronization across brain regions and govern allocations of attention resource. An internal mechanism may affect cortex synchrony and oscillations during the information transmission and cognitive processing (Saalmann 2014). In terms of the power spectral projection weights of co-modulation, the modulator in the different condition of the present study gave rise to distinct integration of information across multiple components. Therefore, an underlying neural co-modulation mechanism might modulate the degree of synchrony thalamo-cortical activity between distinct groups of cortices according to task demands in the dual tasks.

Chapter 4

The effect of fatigue on brain connectivity in multitasking

This chapter investigates the effect of sleep-related fatigue on effective brain connectivity in a simulated driving experiment. We demonstrate that the effective connectivity increases in multitasking condition, but not in high-risk fatigue stage. Chin-Teng Lin conceived this work. Tien-Thong Nguyen Do performed data analysis, with assistance from Yu-Kai Wang. All the authors discussed and wrote the manuscript (J-2) (Do et al. 2020c).

4.1 Abstract

Multitasking has become omnipresent in daily activities, and increased brain connectivity under high workload conditions has been reported. Moreover, the effect of fatigue on neural activity has been shown in participants performing cognitive tasks, but the effect of fatigue on different cognitive workload conditions is unclear. In this study, we investigated the effect of fatigue on changes in effective connectivity (EC) across the brain network under distinctive workload conditions. There were 133 electroencephalography (EEG) datasets collected from sixteen participants over a five-month study in which high-risk, reduced, and normal states of real-world fatigue were identified through a daily sampling system. The participants were required to perform a lane-keeping task (LKT) with/without multimodal dynamic attention-shifting (DAS) tasks. The results show that the EC magnitude is positively correlated with the increased workload in normal and reduced states. However, low EC was discovered in the high-risk state under high workload condition. To the best of our knowledge, this investigation is the first EEG-based longitudinal study of real-world fatigue under multitasking conditions. These results could be beneficial

for real-life applications, and adaptive models are essential for monitoring important brain patterns under varying workload demands and fatigue states.

4.2 Introduction

Individual often handle multiple tasks simultaneously during daily activities. Examples include individuals listening to music while walking or running and students taking notes while listening to a class lecture. Although simultaneously performing multiple tasks is normal in our daily life, it may cause distractions that lead to serious consequences, especially during driving. Distracted driving causes a driver's reaction time to be fifty percent slower than normal (WHO 2018), and many reasons for distraction or attention switching exist, such as mobile phone calls, texting or listening to the radio while driving (WHO 2018; Young et al. 2007; Oviedo-Trespalacios 2018). The factors that contribute to a driver's impaired attention are related to a driver's mental status (WHO 2018) and the surrounding environment (Oviedo-Trespalacios 2018; Oviedo-Trespalacios et al. 2019b; Theofilatos et al. 2018).

Driver fatigue is one of the factors that should be considered when analysing vehicle crashes (Huang et al. 2016). Fatigue may lead to torpid reactions to the surrounding environment, such as steering the car or hitting the brakes. Across previous studies, fatigue was estimated to be responsible for between 10 and 20 percent of vehicle crashes reported in the US in 2016 (National Academies of Sciences and Medicine 2016) and led to 21 percent of all fatal crashes and 13 percent of severe injuries between 2009 and 2013 (Tefft 2014). Therefore, there is a need to regulate drivers to avoid using distracting devices, such as cell phones, while driving. Furthermore, understanding the mechanism of driver performance could help to avoid potential accidents on the road. Cognitive states are believed to be associated with behavioural performance (Borragán et al. 2019; Sievertsen et al. 2016). In addition, neurophysiology is a valid approach for exploring cognitive states (Lal and Craig 2002; Simon et al. 2011; Lal et al. 2003; Jap et al. 2009; Do et al. 2019), and many studies have explored the link between fatigue and electroencephalography (EEG) power spectra (Lal and Craig 2001; Makeig et al. 2000; Makeig and Jung 1996; Jung

et al. 1997; Schier 2000; Huang et al. 2008, 2001). Researchers have reported that the powers of the theta (4-7 Hz) and alpha (8-12 Hz) bands concurrently increase in bilateral occipital brain regions (Lin et al. 2013). An online, closed-loop system was developed to monitor user alertness and improve user responses during driving based on EEG power spectra (Wang et al. 2014b, 2015).

Furthermore, there has been increasing interest in neuroimaging research regarding brain connectivity (Friston 2011; Sporns 2014), which can be classified into three main types (Bullmore and Sporns 2009): structural connectivity (SC), functional connectivity (FC) and effective connectivity (EC). SC reflects the anatomical networks, FC is associated with the correlations among brain regions while the brain is processing information, and EC involves the causal dependencies among brain regions. FC uses an undirected graph that can describe the statistical associations among regions; however, EC uses a directed graph that illustrates the causal relationships among regions. Hence, an EC study can provide information about how the information flow is exchanged among brain regions. Therefore, EC results can be used to interpret how information is exchanged among brain areas in a task-related period. Many studies have shown increased across-network FC while performing cognitive tasks (Spadone et al. 2015; Kwon et al. 2017), working memory (2-back task) (Shine et al. 2016a) and movie watching (Betti et al. 2013) tasks. Studies have indicated that connectivity is correlated with the task load. As the load increases, more brain regions are activated to communicate, exchange information and process external environmental stimuli, and the across-network brain connectivity may therefore increase. However, notably, FC has also been reported to decrease across the brain network during semantic similarity tasks (DeSalvo et al. 2014) and movie watching (Betti et al. 2013).

Although previous studies have provided insights into complex brain networks that are correlated with task costs, whether fatigue state variability during the performance of a task is related to fluctuations in brain network organization remains unknown. Fonseca, et al. (Fonseca et al. 2018) showed evidence of the relationship between sleep-related fatigue and EC in a simulated driving experiment. Borragán,

et al. (Borragán et al. 2019) showed that prefrontal connectivity decreased with participants' fatigue levels, which were defined by sleep deprivation. In addition, considering time-on-task as fatigue, Huang, et al. (Huang et al. 2015) showed evidence of compensation between cortico-cortical EC and driving performance, ranging from alertness to an intermediate level of vigilance. Furthermore, this compensation seemed to decline from an intermediate to drowsy level of vigilance (Huang et al. 2015). However, the changes in brain connectivity remained unclear considering both factors, multitasking, and real-world fatigue. In previous studies (Borragán et al. 2019), fatigue levels have been monitored by sleep deprivation, which is not sufficiently natural. Although several studies have identified evidence of the fatigue state and multitasking factors influencing brain connectivity, there is still limited information on the effects of both factors on brain neural networks during cognitive tasks. In this study, we used a state-of-the-art biomathematical fatigue model called Sleep, Activity, Fatigue, and Task Effectiveness (SAFTE) to assess fatigue levels. Notably, longitudinal recording can benefit from tracking personal real-world fatigue for further applications, such as behaviour prediction or task assignment. To do so, we investigated the ECs of network patterns under different task load conditions and dynamic fatigue states. The fatigue state was measured based on a biomathematical fatigue model (Hursh et al. 2004). We hypothesized that the EC in high-attention load conditions (concurrent dual tasks) enhances brain network activation compared to that induced under low-attention load conditions (e.g., a single task). Furthermore, we hypothesized that EC varies under different fatigue states for each task condition.

4.3 Related works

Brain connectivity has been extensively investigated under altered task load conditions, revealing increasing brain connectivity with the level of the task load demand (Cole et al. 2014; Spadone et al. 2015; Kwon et al. 2017; Shine et al. 2016a; Betti et al. 2013). Furthermore, results have shown that brain connectivity can be physiologically modulated, including by anaesthesia, fatigue, and ageing (Peltier and Shah 2011). For instance, a study based on resting-state fMRI demonstrated

a significantly decreased interhemispheric correlation in the motor cortices after a muscle fatigue task (Peltier et al. 2005). Studies on simulated driving scenarios have shown a clear relationship between connectivity among brain areas and fatigue related to prolonged driving (Xu et al. 2017; Al-Shargie et al. 2019). Al-Shargie, et al. (Al-Shargie et al. 2019) revealed that the brain connectivity network is negatively correlated with increasing fatigue level, defined as prolonged time-on-task driving. Furthermore, another study of simulated driving scenarios using effective brain connectivity highlighted the relationship between driving performance and effective connectivity, suggesting that EC patterns are affected by distinctive sleep-related fatigue (Fonseca et al. 2018). Moreover, impairments in prefrontal cortical connectivity led to decreased attention in cognitive fatigue, which was defined as sleep-related fatigue (Borragán et al. 2019).

Nevertheless, research has generally focused on the effects of brain connectivity on task load conditions or the fatigue status rather than considering both factors together. There is still limited information about the effect of sleep-related fatigue on brain connectivity under different workload conditions. In this study, we investigated brain connectivity under different task load conditions in various fatigue states. We hypothesized that brain connectivity is positively correlated with the task load demand; however, this correlation is dependent on the fatigue state of participants.

4.4 Meterials and methods

4.4.1 Experimental Design

Refer to the Chapter 3, section 3.3.

4.4.2 EEG data processing

Figure 4.1 lists the processing steps in the current study. Raw EEG data were subjected to bandpass filtering at 1-50 Hz before being downsized to a sample rate of 250 Hz using the EEGLAB toolbox (Delorme and Makeig 2004) in MATLAB (version 2013b, MathWorks Inc., Natick, MA). Some portions of data included artificial noise, which was manually removed. The artifact noise was defined by their

raw data quality such as value has strong peak comparing to the rest (threshold value = 100 μV). Pre-processed EEG data were subsequently subjected to independent component analysis (ICA) (Makeig et al. 1996) to decompose the independent sources of information. The function 'runica.m' in EEGLAB was used to decompose the Independent Components (ICs) which contributes to the EEG data (maximum step was 2014 and error less than 10^{-7}). Then, dipole fitting routine (dippole2.m) was applied to find the ICs location. Subsequently, the non-brain components were removed (48.3 $\pm$ 5.4 ICs) based on their ICs properties such as location, topographic, power spectrum. The main non-brain components were from eye-blind, eye movement, muscle and sensor noise components. After that, the remaining brain components (13,5 $\pm$ 5.3 ICs) were back-projected to the EEG channel space. Subsequently, the data was divided into task conditions with the epoch length [-1 2.5] second within the task event onset. The period [-1 0] second of the epoch were used as the baseline correction for all the epoch data. Then, the bad epochs in those task conditions was rejected based on their extreme value (threshold was set to 100μV). Next, the ECs were estimated in the channel domain from the cleaned datasets.

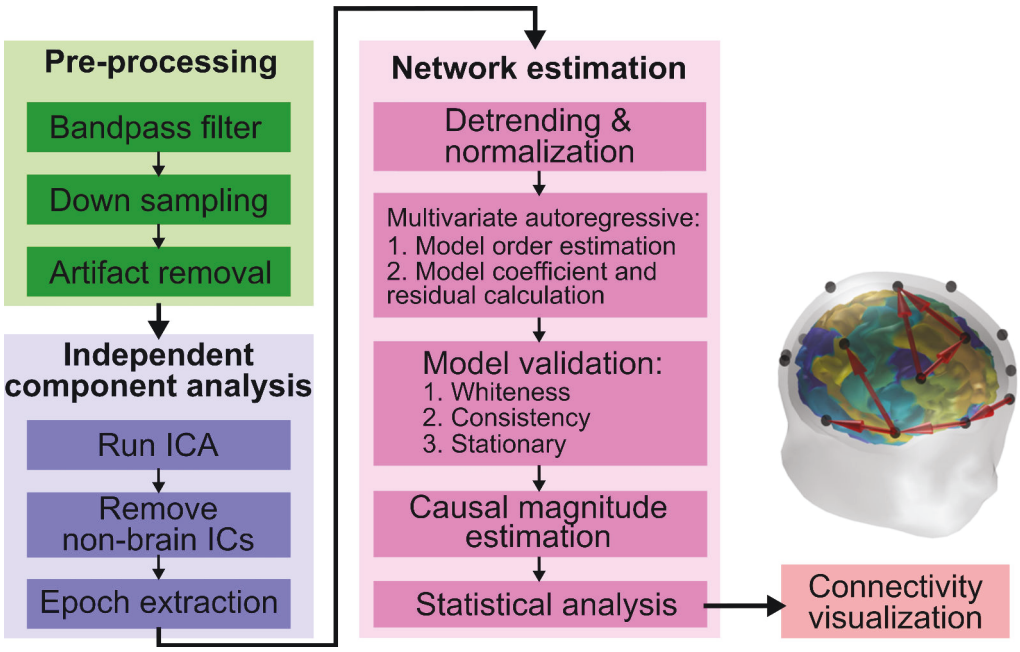

Figure 4.1 : Flowchart of effective connectivity estimation.

4.4.3 Effective connectivity

All datasets with pre-processing steps were used to calculate the effective brain connectivity. The multivariate linear dynamical (autoregressive) model was fit to the process activation time series after stimulus onset to the aligned RT at 667 milliseconds (median of RT). Time series EEG data were subsequently extracted for all frequency bands: delta (1-3 Hz), theta (4-7 Hz), alpha (8-12 Hz), and beta (13-30 Hz).

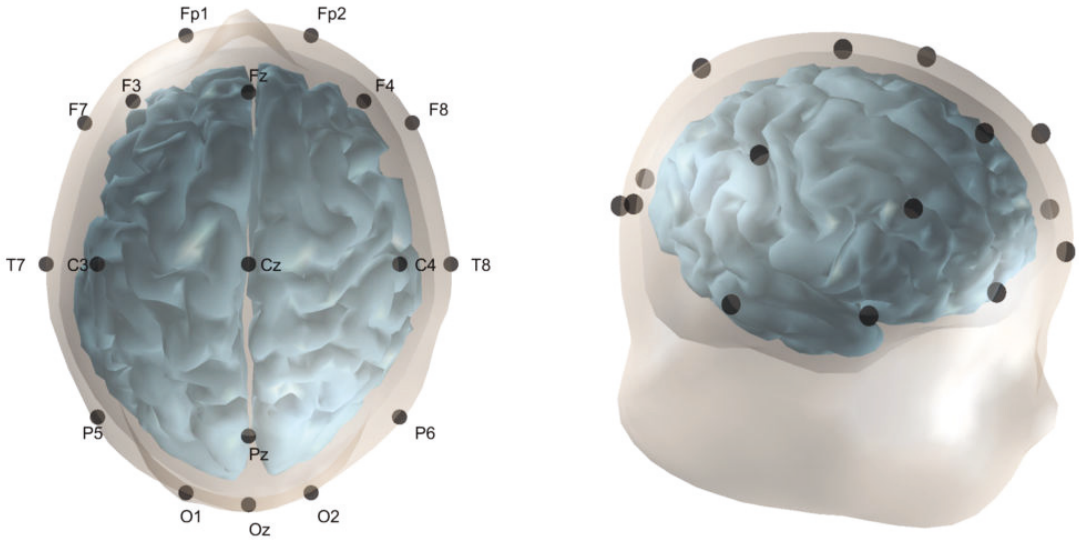

Figure 4.2 : EEG channels selected for estimating effective connectivity.

EC was estimated based on Granger causality (GC) to obtain the flow of information exchanged between the brain regions. GC was introduced for the first time in the econometric time series analysis (Granger 1969). Time series data X_{1t} is deemed Granger causal to another time series X_{2t} when the knowledge of history X_{1t} can improve the prediction of X_{2t}. Multiple-channel data X at time t may be represented as a stationary, stable vector autoregressive (VAR) with order p as follows:

$$X_t = v + \sum_{k=1}^{p} A_k X_{t-k} + u_t, \tag{4.1}$$

where p is the model order, v is the mean of X, A_k is the model coefficient matrix, and u_t is the zero-mean white noise process. In this study, the model fitting p was

Brain Area	**EEG channels**
Frontal	Fp1, Fp2, Fz, F3, F4, F7, F8
Central	Cz
Motor	C3, C4
Temporal	T7, T8
Parietal	Pz, P5, P6
Occipital	Oz, O1, O2

Table 4.1 : Brain areas and respective EEG channels selected for estimating effective connectivity.

selected based on the Akaike information criterion (AIC):

$$AIC\,(p) = ln\left|\tilde{\Sigma}(p)\right| + \frac{2}{\hat{T}}pM^2 \tag{4.2}$$

where $ln\left|\tilde{\Sigma}(p)\right|$ is the determinant logarithm of the estimated noise covariance matrix for the VAR model with order p fit to M-channel data, and $\hat{T}$ is the total data points (sample data points per trial x N trials).

The model fitting was subsequently validated by three tests:

- Whiteness test: to ensure the residual of fitted model is small and uncorrelated (white). The fitted model must pass two tests to be considered as whiteness: autocorrelated function test (ACF) and Portmanteau Tests by checking the statistic test of Box-Pierce (BPP), Ljung-Box (LBP), and Li-McLeod (LMP) (Lütkepohl 2005; Arranz 2005).

- Percentage of consistency (PC) test: to check the fraction of correlation structure between our model and original data (Ding et al. 2000). The higher PC indicates for the better model for generating the original data.

- Stationary of the model test: to ensure the original data and VAR[p] model fulfill the stationary and stable properties. Therefore, the VAR[p] process will not diverge to the infinity (Lütkepohl 2005).

After the modal validation step, the causal magnitude was estimated via the following formula:

$$F_{ij} = \ln\left(\frac{\overline{\Sigma_{ij}}}{\Sigma_{ij}}\right) = \ln\left(\frac{var(x_t^{(i)}|x_{(.)}^{(i)})}{var(x_t^{(i)}|x_{(.)}^{(i)}, x_{(.)}^{(j)})}\right) \tag{4.3}$$

where F_{ij} indicates the GC from process j to process i. Finally, Wilcoxon signed-rank tests were used to test the significances of the differences between conditions while correcting for the FDR. Source of Information Flow (SIFT) (Delorme et al. 2011) from the EEGLAB-compatible toolbox was used to estimate EEG ECs. All data processing steps are demonstrated in figure 4.1.

4.5 Results

We analysed the behavioural data based on the RT of participants. The behaviour results revealed that both task loads and fatigue states affected the RT of participants (figure 4.3). Then, we further examined the EC magnitude among brain regions across four frequency bands, including the delta, theta, alpha, and beta bands (figure 4.4, figure 4.5, figure 4.6). The EC results showed significantly increased brain connectivity with increasing task load level in both the normal and reduced fatigue groups. In contrast, the opposite trend was observed in the high-risk fatigue group. The results demonstrated that fatigue and the task load affected brain connectivity.

4.5.1 Behavioral Performance

The performance of the participants was measured using the RT required to response to the first stimulus onset either steering a car back into a fixed lane or pressing the bottom for DAS task after deviation onset for LKT. The average RTs were compared among three task conditions (LKT: lane keeping task only, DAS_V: concurrent LKT and visual dynamic attention-shifting, and DAS_A: concurrent LKT and auditory dynamic attention-shifting) and three fatigue states (normal, reduced and high-risk) via two-way repeated measures analysis of variance (ANOVA) (3x3 design). The ANOVA showed a significant main effect of the tasks on RT (F=4.32,

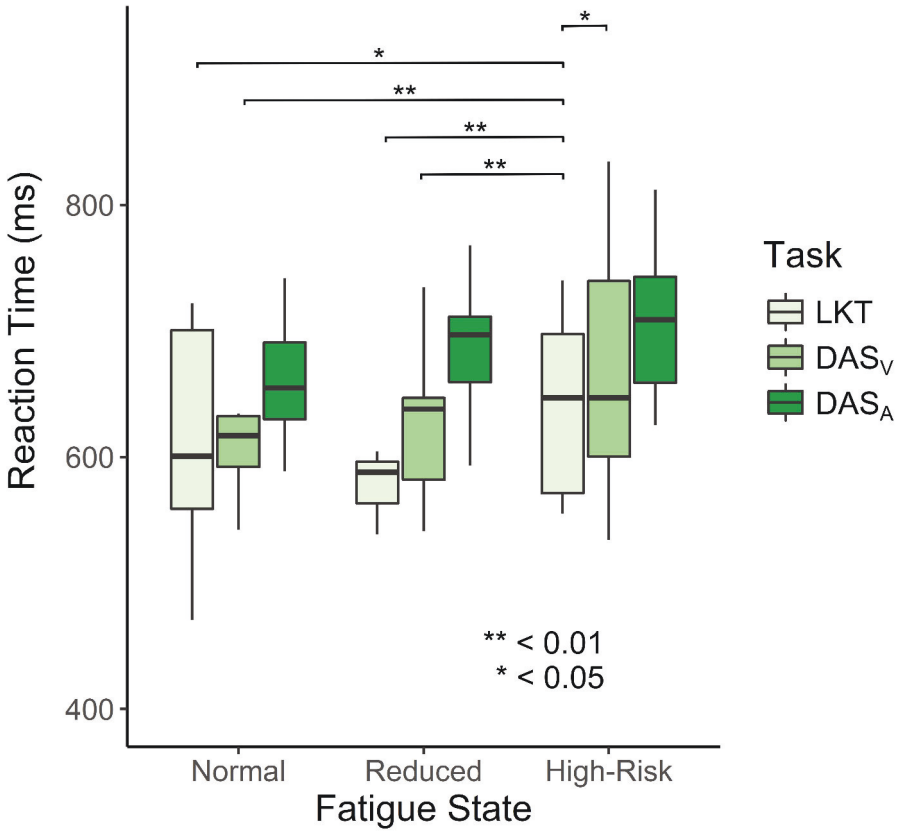

Figure 4.3 : Reaction time and effectiveness score. Reaction time of lane-keeping task (LKT) across three tasks in three fatigue groups. The RTs of the LKT significantly increase in the high-risk state ($p < 0.05$). There is no significant difference among the fatigue states when performing the DAS_V and DAS_A.

$p < 0.05$) as well as an interaction between the tasks and fatigue states (F=4.99, $p < 0.005$) (figure 3.2). A post hoc Tukey test showed that the LKT task in high-risk and normal, high-risk and reduced groups differed significantly ($p < 0.05$).

4.5.2 Comparisons of ECs between single- and dual-task conditions in different fatigue states

Subject	**ES**	**Model Order**[1,2]			**Whiteness**[1,2,3]			**Consistency**[1,2,3]			**Stationarity**[1,2,3]		
S01	93	4	8	8	100	77	80	77	90	90	100	100	100
	93	4	5	5	100	94	91	80	84	86	100	100	100
	91	4	6	5	100	77	82	76	86	85	100	100	100
	88.5	4	7	8	100	78	83	77	90	90	100	100	100

	89	4	9	8	100	80	81	82	92	91	100	100	100
	83	4	8	8	100	77	83	81	92	92	100	100	100
	83	4	7	9	100	84	79	80	91	92	100	100	100
	79	4	5	5	100	78	77	81	86	85	100	100	100
	80	4	4	4	88	99	92	81	80	82	100	100	100
S02	91.2	4	5	6	100	94	91	76	84	88	100	100	100
	83	4	5	6	88	87	88	76	83	87	100	100	100
	88	4	5	5	100	93	94	77	86	86	100	100	100
	87.6	4	5	5	98	92	96	83	85	86	100	100	100
	87.6	4	5	6	100	90	96	82	84	87	100	100	100
	83.1	4	6	6	100	93	92	79	88	88	100	100	100
	41.2	4	4	4	92	97	91	84	84	82	100	100	100
	80.2	4	5	5	100	94	91	81	84	86	100	100	100
S03	88	5	5		100	96		84	84		100	100	
	82	5	5	5	100	71	77	84	85	84	100	100	100
	93	5			100			86			100		
	74	5	6		100	93		85	86		100	100	
	83	4	4	6	100	87	80	83	84	86	100	100	100
	81	5	5		100	77		85	84		100	100	
	76	4	5	6	100	91	79	81	83	85	100	100	100
	82	5		7	100		73	84		87	100		100
	71.3	4	5	5	92	73	82	83	84	85	100	100	100
S04	87.5	5	6	6	100	85	90	84	85	84	100	100	100
	90.8	4		4	99		94	83		82	100		100
	94.8	4	6	6	100	80	71	82	86	85	100	100	100
	82.6	4	4	4	100	92	96	79	78	76	100	100	100
	86.6		6	7		83	87		86	87		100	100
	84.3	5	5	6	93	76	87	85	84	87	100	100	100
	68.5	5	5	5	100	89	83	84	84	84	100	100	100
	68.3	4	4		100	71		81	82		100	100	
	73.2	3	5	5	100	80	74	58	85	85	100	100	100
S05	90	3	5	5	100	94	94	52	83	81	100	100	100
	83.2	3	5	5	100	90	81	63	85	85	100	100	100
	92	4	5	5	100	94	96	81	84	83	100	100	100
	83		5	6		90	82		83	87		100	100
	88.9	4	4	5	96	96	97	80	81	84	100	100	100
	85.5	4	5	4	100	94	96	79	84	77	100	100	100

	60	3	4	4	100	89	94	70	75	75	100	100	100
	76	4	5	4	100	88	97	79	83	82	100	100	100
	77	4	6	5	99	89	85	78	86	83	100	100	100
S06	95	5	6	7	100	83	75	84	87	89	100	100	100
	91	3	4	4	99	80	80	65	82	81	100	100	100
	94	4	4	5	100	92	91	81	79	83	100	100	100
	87	4	5	5	100	77	82	80	85	86	100	100	100
	89	4	5	5	100	86	79	83	84	84	100	100	100
S07	88	4			100			84			100		
	87	4	6	6	100	92	89	83	89	88	100	100	100
	93	5		7	100		78	88		93	100		100
	88	3		6	100		80	62		87	100		100
	90	5			100			88			100		
	75		6	7		85	81		86	89		100	100
	68	4	6	6	100	75	89	83	89	88	100	100	100
	71	4	7	6	100	75	87	83	91	88	100	100	100
S08	71		4	4		89	82		72	77		100	100
	73	4	6	5	100	80	81	77	88	85	100	100	100
	81.8	4	5	5	100	94	92	75	87	86	100	100	100
	57	4	5	5	100	80	89	75	85	85	100	100	100
S09	87		5	5		95	82		87	87		100	100
	86	3	6	5	100	85	98	72	88	86	100	100	100
	98	5	6	6	100	100	92	88	90	90	100	100	100
	88	4	5	4	100	86	100	86	87	85	100	100	100
	84	4	4	3	100	98	100	83	79	65	100	100	100
	88	4	4	5	100	100	77	84	84	87	100	100	100
	86	3	4	4	100	98	96	68	83	83	100	100	100
	87	3	3	4	100	96	96	71	70	84	100	100	100
	59	3	4	4	100	99	92	70	80	82	100	100	100
S10	76	3	4	5	100	88	87	64	77	86	100	100	100
	78	3	4	4	100	87	95	60	76	81	100	100	100
	86	4	4	4	100	98	91	82	80	77	100	100	100
	66	4	4	4	100	100	100	83	82	82	100	100	100
S11	78	4	5	6	100	80	80	82	85	86	100	100	100
	88.3		3	3		94	98		63	60		100	100
	87.6		4	4		93	94		85	87		100	100
	75		4	4		83	80		84	82		100	100

	77.9	3	4	4	99	93	96	64	84	84	100	100	100
	76	4	5	4	100	92	94	83	85	83	100	100	100
	74	4	4	4	100	98	100	83	84	83	100	100	100
S12	98	4	6	5	100	88	92	83	88	85	100	100	100
	90	4	4	5	100	95	89	82	81	85	100	100	100
	96	4	6	6	100	87	92	83	86	88	100	100	100
	79		6	7		80	82		88	91		100	100
	89	3	4	5	100	95	99	56	78	83	100	100	100
	88	4	6	6	100	80	86	83	89	90	100	100	100
	68.4	3	5	5	100	91	86	61	84	85	100	100	100
	81	4	5	5	100	85	99	81	85	85	100	100	100
	68	5	5	5	100	97	89	84	84	84	100	100	100
S13	89.4	3	6	6	100	78	81	72	91	91	100	100	100
	91.2	4	8	6	96	73	80	87	92	89	100	100	100
	80.2	4	5	6	100	86	88	86	87	89	100	100	100
	77.7	5	7	8	100	82	71	87	91	92	100	100	100
	85	4	6	7	100	77	80	86	91	91	100	100	100
	68.2	3	5	6	100	82	72	70	86	89	100	100	100
	57.9	4	4	4	92	72	71	87	85	87	100	100	100
S14	94.6	5		7	100		78	83		88	100		100
	89.7	4	4	4	100	100	82	83	84	83	100	100	100
	91.3	4	6	4	100	80	80	84	87	82	100	100	100
	86.5	4	5	8	100	93	79	81	84	88	100	100	100
	89	3	5	5	100	95	76	63	84	85	100	100	100
	90	3	4	5	100	94	81	64	81	83	100	100	100
S15	91.9	4	6	6	98	73	81	80	89	87	100	100	100
	95		5	5		94	97		85	85		100	100
	88		5	5		76	96		88	86		100	100
	88	4	5	5	99	80	79	83	88	89	100	100	100
	87	4	6	8	100	84	87	82	90	92	100	100	100
	80	3	5	4	100	93	99	67	85	82	100	100	100
	67	4	6	8	100	81	85	85	91	93	100	100	100
	71.5	4			100			83			100		
	71.5	4	6	6	100	89	80	82	86	87	100	100	100
S16	82	5	5	5	99	85	91	82	83	84	100	100	100
	89	4	4	4	100	95	90	82	79	82	100	100	100
	76.8	3	5	4	100	85	79	62	85	79	100	100	100

	80.4	4	4	5	100	87	85	83	82	87	100	100	100
	74.7	3	4	4	94	86	100	66	76	83	100	100	100
	79	4	4		92	92		84	84		100	100	
	72		4	4		90	100		81	83		100	100
	74		4	4		97	91		84	82		100	100

Table 4.2 : Validation results of effective connectivity model estimation.

Computational analysis was performed using the Advanced Research Computing Laboratory server at the University of Technology Sydney (UTS), and the results of the validation tests are shown in table 4.2. All the comparison used the Wilcoxon signed-rank test, followed by FDR-adjusted $p<0.05$. Overall, the dual-task condition showed an increased EC across-network among the frontal, central, parietal, occipital, motor, and temporal areas (figure 4.4 and 4.6). In addition, the EC under workload task also varies in different fatigue states (figure 4.5, 4.6). The increased and decreased edges were used from the EC connectivity matrix after the statistic test between task conditions (Wilcoxon signed-rank test, FDR-adjusted $p<0.05$). Then the total number of increased and decreased edges were calculated (figure 4.6). Compared to the single-task condition (LKT), more increased edges and less decreased edges of brain connectivity were observed in the normal and reduced fatigue groups (figure 4.6). However, there were more decreased edges of brain connectivity than increased edges in the high-risk fatigue group in the delta, theta, alpha and beta bands. Furthermore, the number of significant increase edges in A case is higher or equal to V, indicates the enhance brain connectivity among brain regions when the task difficulty increases. Of note, the reduced fatigue group showed the highest number of increased edges across the delta, theta, alpha and beta bands in both cases V and A (with the exception of delta and theta bands in case V). In both V and A cases, the number of increased edges had an inverted U-shape trend in the alpha and beta bands (figure 4.6). The number of increased edges in the A case also showed the inverted U-shape trend in all bands (figure 4.6); however, the V case showed a linear decrease trend in the delta and theta bands. Those results indicate the effect of fatigue to the brain connectivity.

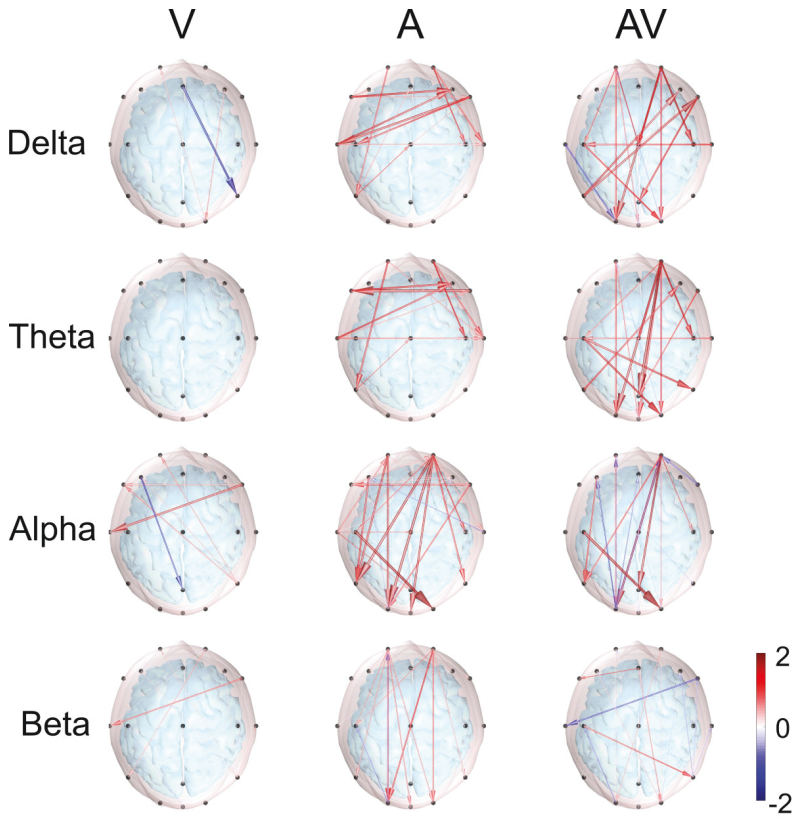

Figure 4.4 : Topographical comparisons of significant EEG effective connectivity differences ($p < 0.05$) between task conditions. The first column shows a comparison between the concurrent dual-task DAS_V and LKT (V), the second column shows a comparison between the concurrent dual-task DAS_A and LKT (A), and the third column shows a comparison between the concurrent dual-task DAS_A and DAS_V (AV). Line colors indicate the differences in connectivity strength between electrode pairs, with red indicating positive differences (more information flow) and blue indicating negative differences (less information flow). The directions of the arrows represent the direct paths of inter-channel information flow.

4.6 Discussion

Attention and cognition comprise a complex and dynamic process that involves multiple brain cortical and subcortical regions (Gonzalez-Castillo and Bandettini 2017). The resting state and task performance periods are reportedly altered at both the neuronal and system levels (Gonzalez-Castillo and Bandettini 2017). Dur-

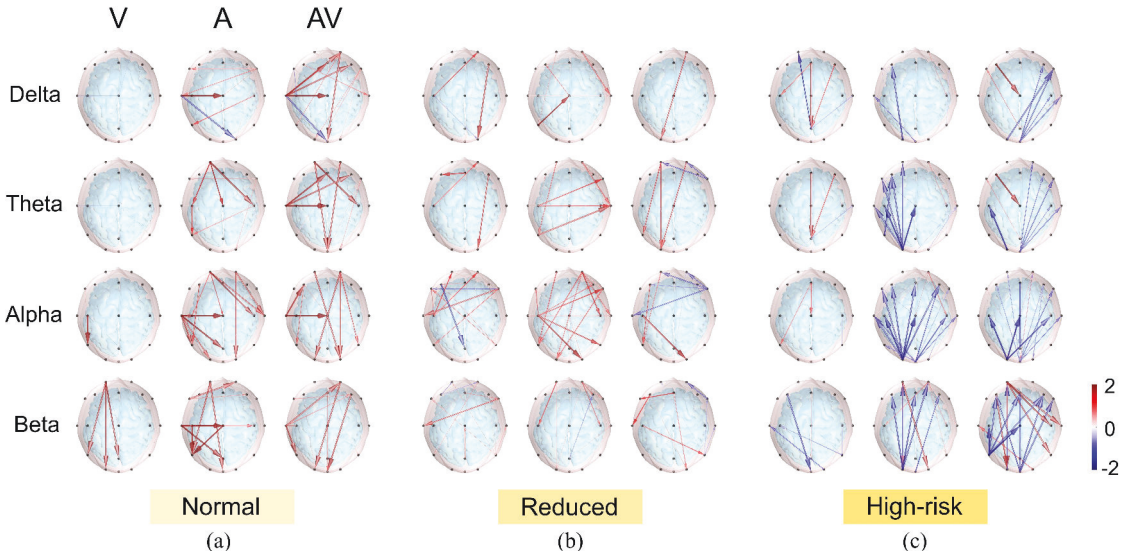

Figure 4.5 : Topographical comparisons of significant EEG effective connectivity differences ($p < 0.01$) between task conditions in each fatigue group. (a) Normal. (b) Reduced. (c) High-risk. The first column shows a comparison between the concurrent dual-task DAS_V and LKT (V), the second column shows a comparison between the concurrent dual-task DAS_A and LKT (A), and the third column shows a comparison between the concurrent dual-task DAS_A and DAS_V (AV). Line colors indicate the differences in connectivity strength between electrode pairs, with red indicating positive differences (more information flow) and blue indicating negative differences (less information flow). The directions of the arrows represent the direct paths of inter-channel information flow (note: V case used $p<0.05$).

ing the period of task performance, the brain typically converts to a connectivity network of higher order than that in the resting state and reorganizes the network based on task properties. Many studies have reported increased across-network connectivity during task performance compared to that in the resting state during visual attention tasks (Spadone et al. 2015; Kwon et al. 2017), cognitive tasks (Cole et al. 2014; Wang et al. 2016), and working memory tasks (Shine et al. 2016a). We hypothesized that the brain across-network connectivity may correlate with the task load. In figure 4.4, we applied GC to calculate the differences in ECs under different fatigue states as participants performed the LKT (single task), DAS_V (dual task) and DAS_A (dual task). The LKT requires multiple senses to safely control a car,

e.g., motor resources to control the steering wheel and visual sensing to observe the road traffic (Lin et al. 2016). We simulated a real situation on the street in which the participants were instructed to keep the car in the fixed lane and identify the name of an animal displayed visually or auditorily. The DAS_V task employed the visual modality; however, it may have required more memory attention than only performing the LKT. Thus, the period from the concurrent stimuli event onset to the participant's first RT is critical because more brain resources are required to process the dual/multiple tasks, including moving the car back into the fixed lane and processing external information for the DAS task. Figure 4.4 shows that the information flow was enhanced in the dual task compared to that in the single task in the delta, theta, alpha, and beta bands. In addition, the DAS_A task employed an auditory modality, which was substantially different from the visual modality in the LKT, and the brain therefore tended to communicate more. More information flows were exchanged within this period with the exception of connections in the left hemisphere in the delta, alpha and beta bands (figure 4.4). These results suggested that the communication pathway between the frontal-executive and occipito-parietal-perceptual regions was influenced by the dual-task condition, which was consistent with previous studies (Serrien 2009; Kim et al. 2017) reporting that an enhanced connectivity strength was correlated with task load.

The prefrontal area has been well established to function in the working memory process (Esposito et al. 1995), and this area is active during dual tasks that engage the central executive system (Zanto et al. 2011). We hypothesized that when individuals attempt to maintain their performance under demanding mental tasks (LKT-DAS_V and LKT-DAS_A dual tasks), the prefrontal region is activated. However, the capacity of the brain may be correlated with the fatigue state, as the connectivity strength was reduced as a result of the limited remaining resources in the high-risk group. However, the brain connectivity related to fatigue is not well understood. Han et al. (2019) has shown that brain connectivity based on fatigue state during the driving task linearly increased in delta and theta band, while Wang, et al. (Wang et al. 2016) shown that there was a compensation between neural ac-

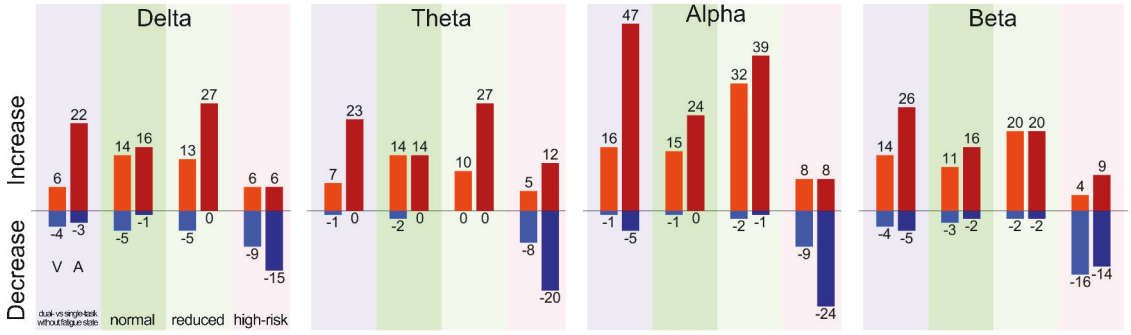

Figure 4.6 : Number of significantly different brain connectivity edges between the dual- and single-task conditions across brain networks ($p < 0.05$) in delta, theta, alpha and beta bands. The green background indicates the normal fatigue group, the light green background indicates the reduced fatigue group, the light red background indicates the high-risk fatigue group and the blue background indicates the dual- vs single-task without considering the fatigue state. The number indicates the number of brain connectivity edge significant differences ($p < 0.05$). The light red/blue bar indicates the number of significant edge increase/decrease differences in the concurrent dual-task DAS_V vs single-task LKT comparison. The dark red/blue bar indicates the number of significant edge increase/decrease differences in the comparison of the concurrent dual-task DAS_A vs single-task LKT.

tivity in response to cognitive fatigue. In this study, we demonstrated that EC varied under different states of fatigue (ref. figure 4.4, 4.5 and 4.6). In the reduced and normal fatigue groups, information flow was enhanced in the dual-task condition compared to that in the single-task condition across brain regions in the delta, theta, alpha and beta bands (ref. figure 4.4, 4.5 and 4.6). In contrast, the high-risk group showed the reversed trend, as information flow was reduced across all brain regions with the exception of the frontal region (ref. figure 4.5 and 4.6). Furthermore, the distribution of the edges difference in the multitasking (figure 4.6) is likely inversed U-shape among three distinctive states, which is inline with the previous studies (Wang et al. 2016; Huang et al. 2015). The possible explanation for this phenomenon is that there was maybe a compensation between brain connectivity to fatigue state of the participants. Our findings provide new evidence of across-

network brain connections at different fatigue states and thus serve as promising candidates for real-world applications. In contrast to the reduced and normal fatigue groups, the high-risk fatigue group showed decreased magnitude connectivity between brain regions, particularly from or to the occipital and parietal regions. In contrast to the intuitive concept that EC increases as workload increases, EC decreases as workload increases for individuals with high fatigue. Thus, in real-world applications, one single fatigue model cannot fit individuals with different fatigue statuses, and multiple fatigue models that can adapt to varying fatigue states are required to address individual variations. This study also provides a view of the frontal area, an important region that may process information independent of the fatigue state. The magnitude of connectivity in the frontal region was enhanced in the dual-task compared to that in the single-task in the three fatigue groups. Most importantly, this study identified the brain connectivity related to fatigue states.

Chapter 5

Heading computation in active navigation

This chapter investigates the consistency of RFP in active navigation condition. Furthermore, we explore the heading computation in a physical navigation experiment. Chin-Teng Lin and Klaus Gramann conceived this work. Tien-Thong Nguyen Do performed data collection and analysis, with assistance from Klaus Gramann. All the authors discussed and wrote the manuscript (J-4) (Do et al. 2020b).

5.1 Abstract

Spatial navigation is a complex cognitive process based on multiple senses that are integrated and processed by a wide network of brain areas. Previous studies have revealed the retrosplenial complex (RSC) to be modulated in a task-related manner during navigation. However, these studies restricted participants' movement to stationary setups, which might have impacted heading computations due to the absence of vestibular and proprioceptive inputs. Here, we present evidence of human RSC theta oscillation (4-8 Hz) in an active spatial navigation task where participants actively ambulated from one location to several other points while the position of a landmark and the starting location were updated. The results revealed theta power in the RSC to be pronounced during heading changes but not during translational movements, indicating that physical rotations induce human RSC theta activity. This finding provides evidence of head-direction computation in RSC in healthy humans during active spatial navigation.

5.2 Introduction

Spatial navigation is an essential human skill that helps individuals track their changes in position and orientation by integrating self-motion cues from linear and

angular motion (McNaughton et al. 2006). Spatial navigation involves several brain regions for spatial information processing (Doeller et al. 2010; Ekstrom et al. 2003), including the retrosplenial complex (RSC) (Epstein 2008), to translate spatial representations based on egocentric and allocentric reference frames (Vann et al. 2009). Head direction (HD) cells that compute HD and orientation (Clark et al. 2010) provide vital information for the translation of information based on distinctive spatial reference frames. HD cells have been found in several brain regions, including the parahippocampal (Bellmund et al. 2016; Vass and Epstein 2017) and entorhinal regions (Chadwick et al. 2015) as well as the thalamus (Shine et al. 2016b) and the RSC (Baumann and Mattingley 2010; Marchette et al. 2014; Shine et al. 2016b). Theta oscillations have been described as an essential frequency underlying the computation of HD and spatial coding in grid cell models (Brandon et al. 2011; Koenig et al. 2011; Maidenbaum et al. 2018; Winter et al. 2015) in actively orienting rodents. Due to its anatomical connections, the RSC is also a central hub in a human brain network underlying several cognitive functions, including spatial orientation. The RSC has a direct connection to V4 (occipital), the parietal cortex, and the hippocampus and indirect connections to the middle prefrontal cortex (Vann et al. 2009). HD cells in the RSC encode both local and global landmarks simultaneously (Vann et al. 2009), supporting the central role of the RSC in encoding and translating different spatial representations.

Several brain imaging studies using electroencephalography (EEG) to investigate the fast-paced time course of the neural basis of spatial cognitive processes have shown that the RSC translates between egocentric and allocentric spatial information (Gramann et al. 2010; Lin et al. 2015). The RSC works with the occipital and parietal cortices to translate egocentric visual-spatial information embedded in an egocentric (retinotopic) reference frame into an allocentric reference frame (Vann et al. 2009; Lin et al. 2017). Most previous studies, however, were conducted in a stationary setup, and they did not investigate the neural mechanisms contributing to navigation in real-world environments, including motor efference, visual, proprioception, vestibular, and kinesthetic system information input or subject-driven

allocation of attention (Cullen and Taube 2017; Gramann 2013). During active navigation, proprioceptive and motor-related signals significantly contribute to the estimation of self-motion, leading to higher accuracy in estimating travel distance and self-velocity (Becker et al. 2002; Frissen et al. 2011; Jürgens and Becker 2006; Telford et al. 1995). Importantly, heading changes in naturalistic navigation are associated with vestibular input, which, together with the visual system and proprioception, is the driving input for HD cells (Cullen and Taube 2017; McNaughton et al. 2006; Stackman et al. 2003). Although a few studies examined active spatial navigation in humans, their experimental designs did not reflect the brain dynamics associated with unrestricted near-real-life navigation experiences (Ehinger et al. 2014; Lin et al. 2015), or they relied on specific patient populations (Bohbot et al. 2017). In summary, there is little knowledge about the brain dynamics underlying spatial navigation in actively navigating human participants and how these dynamics subserve the computation and translation of spatial information embedded in distinct frames of reference for orientation.

In the present study, we investigated the brain dynamics of healthy human participants during active navigation. In an effort to overcome the restrictions of established imaging modalities, we adapted the Mobile Brain/Body Imaging (MoBI) approach (Gramann et al. 2011, 2014b; Makeig et al. 2009), allowing physical movement of the participants. Thus, we recorded high-density EEG synchronized to head-mounted virtual reality (VR) while participants physically performed a spatial navigation task. Participants tracked their location and orientation by using self-motion cues from the visual, vestibular, proprioception, and kinesthetic systems as well as motor efferences. At the end of the trial, after traversing paths that included several turns and straight segments, participants pointed to previously encoded landmark locations. Their brain dynamics were analysed using independent component analyses (ICA) on high-density EEG data and subsequent source reconstruction. This approach allowed us to assess the brain dynamics originating in or near the RSC during the active navigation, focusing on i) the effect of active locomotion on brain dynamics in participants preferentially using an egocentric reference frame

or an allocentric reference frame for navigation (Gramann et al. 2005) and ii) how multisensory convergence during the active movement changes the use of reference frames underlying active navigation compared with established desktop setups. The results demonstrate that active movement through space significantly changes the preferred use of spatial reference frames. Furthermore, naturalistic navigation reveals strong theta synchronization in the RSC during navigation phases that require heading computation and a substantial covariation of alpha desynchronization with the accuracy in a landmark pointing task.

5.3 Materials and Methods

5.3.1 Participants

Eighteen healthy adults (age 27.8±4.2, 2 females) participated in this experiment. All participants reported normal or corrected-to-normal vision. Each received $60 for their participation. The protocol was approved by the University of Technology Sydney (UTS) (Grant number: UTS HREC REF NO. ETH17-2095).

5.3.2 Experiment design and tasks

Reference Frame Proclivity Test (RFPT)

Prior to the main experiment, the participants completed an online RFPT (Gramann et al. 2010, 2005; Goeke et al. 2015) to classify them as allocentric, egocentric, or mixed-strategy navigators. In the test, participants had to navigate through a tunnel on the flat screen monitor that included direction changes of various angles in the horizontal plane (figure 5.1). When they reached the end, they were asked to select which one of two homing vectors pointed back to the start of the tunnel. This choice, made over 40 trials, determined their navigation style: egocentric or allocentric if they consistently used that reference frame in at least 70% of the trials, or mixed-strategy navigators if they switched between frames. Of the 18 participants, five were egocentric navigators, seven were allocentric, and six were mixed.

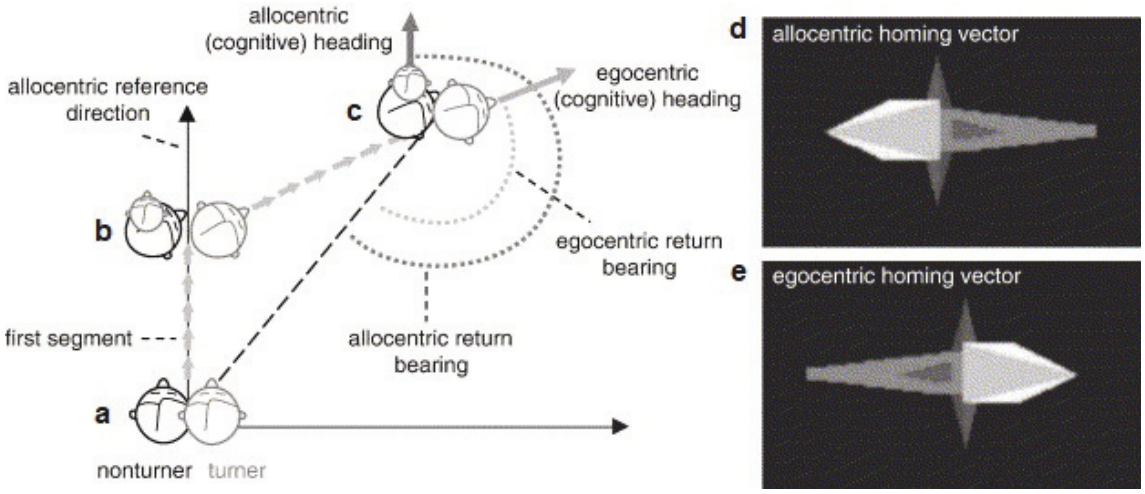

Figure 5.1 : Depiction of a passage through a tunnel with a turn to the right, with nonparallel start and end segments. The left-side displays a nonturner (dark grey head representing the perceived heading and the small light grey head representing the cognitive heading) using an allocentric frame of reference, with the navigator's heading during the first segment (a), during the turn (b), and during the last segment (c) of the tunnel passage. Note that the perceived and the cognitive heading diverge during the turn. On the right, a turner (light grey head representing the perceived cognitive heading which is assumed to be identical to the cognitive heading) is displayed who uses an egocentric frame of reference. During the first segment (a), the turner's heading is the same as that of a nonturner. During the turn, the axis of orientation changes (b). At the end of the tunnel, the turner's cognitive heading is different from that of a nonturner. Note that turners build up an additional allocentric frame of reference if they are forced to react based on an allocentric frame. There is no depiction of an additional allocentric reference frame for turners to emphasize the preferred use of an egocentric frame of reference by this strategy group. To the right-side of the figure, examples of homing vectors are displayed with the correct angular adjustment for a tunnel with one turn of 60° to the right, with panel D depicting the correct homing vector for nonturners, and panel E that for turners. Reprinted from Brain Research, Vol 1118, K. Gramann, H.J. Müller, B. Schönebeck, G. Debus, The neural basis of ego- and allocentric reference frames in spatial navigation: Evidence from spatio-temporal coupled current density reconstruction, Pages No. 116-129, Copyright (2021), with permission from Elsevier.

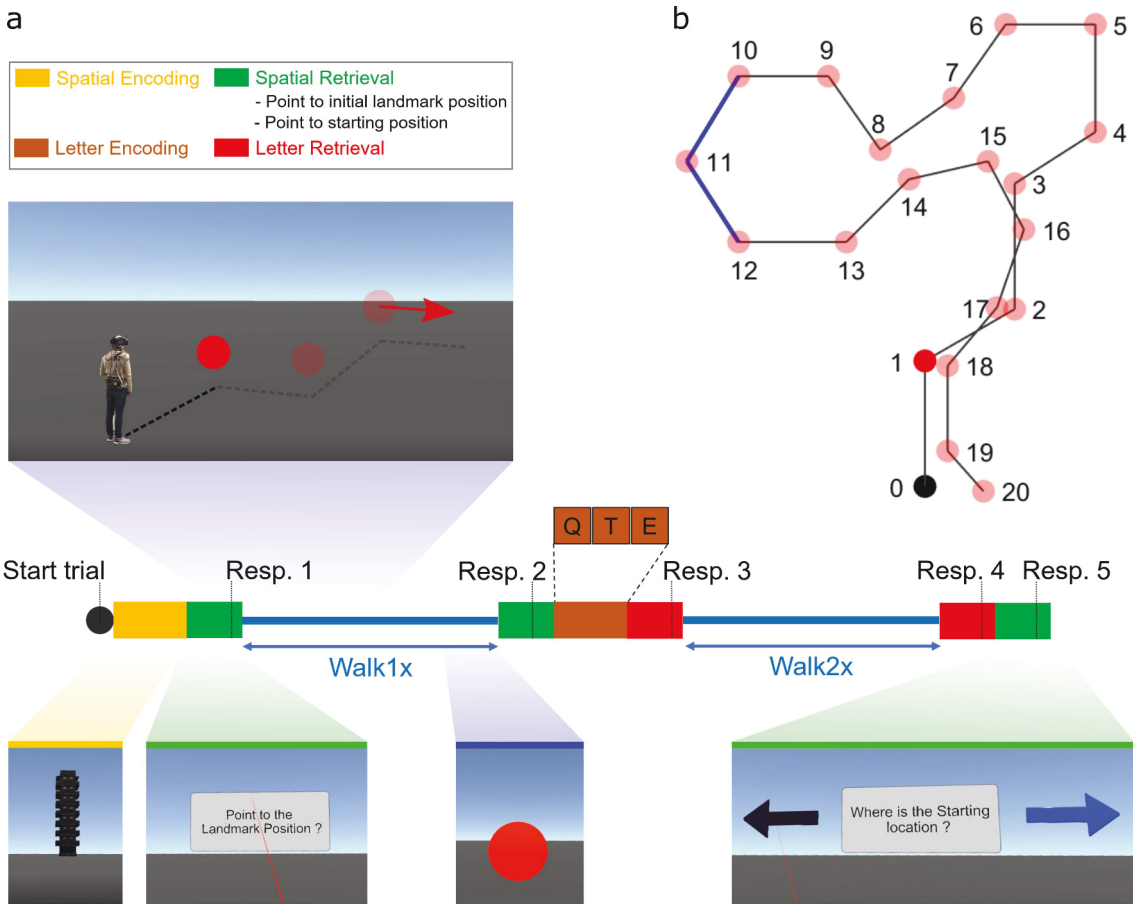

Figure 5.2 : Experiment Design. a. Trial representation. At beginning of the trial, participant had 4 seconds to remember a landmark position which appeared in front of them (around 200 meters). Then participant performed navigation in walk1x and walk2x with random 2 or 3 turns within each walk. In the middle of the trial, participant performed the letter encoding task with random of 3, or 5, or 7 letters. The green squares indicated for the spatial retrieval task, while red squares indicated for the letter retrieval task. b. There were 20 turning points (4 walking paths, path 1 - $\text{point}_{0.1.2.3.4.5}$, path 2 - $\text{point}_{5.6.7.8.9.10}$), path 3 - $\text{point}_{10.11.12.13.14.15}$) and path 4 - $\text{point}_{15.16.17.18.19.20}$) in this experiment. The red dots indicated for the turning points. The reference frame proclivity test (RFPT) was based on the participant response in path 3 at dot number 12, the participant was considered using egocentric or allocentric if their response was left or right arrow respectively.

Main Experiment Design

The experiment comprised a series of straightforward physical navigation exercises interspersed with spatial encoding/retrieval tasks but complicated by letter encoding/retrieval tasks to impose an additional cognitive workload on the participants. Each participant first performed four learning trials to familiarize themselves with the tasks and instructions and subsequently completed 23 sessions, with each session consisting of four trials, over the course of the full experiment. Each trial proceeded as follows. First, participants were shown a global landmark and given 4 seconds to remember its position before it disappeared. Participants were then given the instruction: "Point to the landmark location". They responded by pointing a controller at their reckoned location and clicking the hair-trigger (R1, figure 5.2a). A beep sounded to indicate their response had been registered and that they that should now start the first navigation task – straight walking with two to three direction changes over the walk while keeping track of their location in the space. More specifically, participants walked forward toward a floating red sphere at eye height, which disappeared once they reached it. A new red sphere then appeared, showing the next direction and distance, disappearing once they reached that, and so on. In figure 5.2a, this task is denoted as "walk 1x", where 1 indicates the first walk and x indicates the number of red spheres. Once participants reached the last red sphere, they stopped walking and the text "Attention" appeared in front of them for 3 seconds, signaling the first spatial retrieval task was about to begin. First, participants were instructed to "Point to the landmark location" by pointing their controller to the landmark location as they remembered it and clicking the hair-trigger (R2a, figure 5.2a). Next, two homing arrows appeared in front of them – one pointing left, the other right – and they were asked: "Where is the starting location?". Responses were given by pointing their controller at one of the arrows and clicking the trigger (R2b, figure 5.2a). The letter encoding task to impose additional cognitive burden followed. The participants were shown a series of 3, 5, or 7 letters of the English alphabet at one-second intervals between letters and asked to remember them. The number of letters chosen and the order the letters appeared

were both random. Three levels of difficulty were included to avoid familiarity with the task, ensuring the cognitive load stayed high. Then, three seconds after the last letter appeared, participants were shown a random letter and asked whether or not that letter belonged to their letter list. Clicking the trigger indicated yes; pressing the touchpad indicated no (R3, figure 5.2a). Participants then had 2 seconds of rest before starting the second walk. A beep sound signaled the beginning of the second navigation task (walk 2x, figure 5.2a), which followed the same straight walk to the red sphere format as the first. However, this time, the participants had to remember their letter list as well as keep track of their orientation to the landmark location and starting position. When the second walk was finished, the participants were asked to do three things: first, to confirm whether or not a random letter belonged to their letter list (R4, figure 5.2a); second, to point to the landmark location; and, third, to point to the starting location (R5a and R5b, figure 5.2a). The next trial started when the participant indicated their readiness by clicking both bottom grips on the controller. The maths of four trials with 2 to 3 random turns in each of two walks meant that each session consisted of a total of 20 turns, as shown in figure 5.2b. After 20 turns, the participant reset his or her location to dot number 0 before starting the next session to ensure that the total navigation segments were within the experimental space. The RFPT in the active walk condition was assessed only at point 12 (figure 5.2b) based on the participant's response to the left arrow (egocentric) or right arrow (allocentric).

Data Recordings

The scenario was developed in Unity (version 2017.3) with the VRTK plug-in and performed in a VR environment using a head-mounted display (HTC Vive Pro; 2x 1440 x 1600 resolution, 90 Hz refresh rate, 110° field of view). All data streams from the EEG cap, eye-tracking device, and head-mounted display were synchronized by Lab Streaming Layer (Kothe 2014). The EEG data were recorded from 64 active electrodes placed equidistantly on an elastic cap (EASYCAP, Herrsching, Germany) with a sampling rate of 500 Hz (LiveAmps System, Brain Products, Gilching, Germany). The data were referenced to the electrode located closest to the standard

position, FCz. The impedance of all sensors was kept below 5 kΩ.

5.3.3 EEG analysis

Pre-processing

All pre-processing steps were performed using MABLAB version 2018a (Mathworks Inc., Natick, Massachusetts, USA) and custom scripts based on EEGLAB version 14.1.2 (Delorme and Makeig 2004). The raw EEG data were downsampled to 250 Hz before applying a bandpass filter (1-100 Hz). Line noise (50 Hz) and associated harmonics were removed using the cleanline function in EEGLAB. Dead channels were then removed based on flatline periods (threshold=3 seconds), correlations with other channels (threshold=0.85), and abnormal data distributions (standard deviation=4). Missing channels were interpolated by spherical splines before re-referencing to the average of all channels. Noisy portions of continuous data were removed through automatic continuous data cleaning based on the spectrum value (threshold=10 dB) and power. criteria of maximum bad channels (maximum fraction of bad channels=0.15) and relative to a robust estimate of the clean EEG power distribution in the channel ([minimum, maximum]=[-3.5 5]). Then, adaptive mixed independence component analysis (AMICA) (Delorme et al. 2012; Palmer et al. 2006) was used to decompose the data into a series of statistically maximally independent components (ICs) with the time source as the unit. The approximate source location of each IC was computed using the equivalent dipole models in EEGLAB's DIFIT2 routines (Oostenveld and Oostendorp 2002). Last, the spatial filter matrix and dipole models were copied back to the pre-processed but uncleaned EEG data (no cleaning in the time domain) for further analysis (figure 5.3).

Event-Related Spectral Perturbation (ERSP)

Epoched data sets for each walking condition (walk1x or walk2x) were extracted at the onset of navigation for a length of 14.5 seconds, including a baseline period of 2.5 seconds prior. Bad epochs were identified and removed in the sensor space (for strongly affected head and body motion artifacts) and subsequently in the component space (for artifact noise in the ICs). (i) In the sensor space, the bad epochs

were labeled based on the epoch mean, standard deviation (std=5), absolute raw value (threshold value=1000 µV), and kurtosis activity (refer to the pop_autorej.m function in EEGLAB). From 2714 epochs, 12.5% were deemed bad and removed. (ii) In the component space, the time-warped ERSP patterns for each epoch were calculated by computing single spectrograms for each IC and single trial based on the newtimef() function using the standard parameters. The timewarp option was used to linearly warp each epoch to a standard length based on the median time point of sphere collision events. The time period before the onset of the active navigation at the beginning of the trial was used as the baseline to estimate the ERSP for each epoch with divisive baseline correction (Grandchamp and Delorme 2011) to minimize single-trial noise. Epochs were then identified as bad if the z-score of the ERSP epoch was larger than 3 standard deviations from the median of all ERSP epochs (see the power panels in (figure 5.4, figure 5.5, and figure 5.6) Approximately 6% of the epochs were bad and removed based on their ERSP in the component space.

Clustering

We first clustered the ICs based on the conventional EEGLAB k−means method. Then, we repeated the clustering process 10000 times before performing an evaluation to identify the best cluster of interest (COI) based on the region of interest (ROI) cluster centroid (Gramann et al. 2018). All ICs with an RV of less than 30% for all participants were grouped based on their dipole locations (weight=6), ERSPs (weight=3), mean log spectra (weight=1), and scalp topography (weight=1). Then, the weighted IC measures were summed and compressed with principal component analysis (PCA), resulting in a 10-dimensional vector, followed by the k−mean method (with 25 clusters). The target cluster centroid in Talairach space (RSC, x=0, y=-45, z=10) was evaluated from 10000 clustering results based on the score of each cluster solution, including: (i) the number of participants (weight=2); (ii) ratio of the number of ICs per participant (weight=-3); (iii) cluster spreading (mean squared distance of each IC to the cluster centroid) (weight=-1); (iv) mean RV of the fitted dipoles (weight=-1); (v) distance of the cluster centroid to the ROI (weight=-

3); and (vi) Mahalanobis distance to the median distribution of the 10000 solutions (weight=-1). The final COI score of -1.7 was derived from 15 participants, 29 ICs, a spread of 677, a mean RV of 11.76%, and a distance of 7.3 units in Talairach space. In the ERSP group-level analysis, the ERSP at COI was calculated first at the IC level, then at the participant level, and finally at the group level. The time-frequency data of all ICs of the same participant were averaged. Then, the ERSPs of all participants were averaged for the final ERSP at the group level. The statistical test for ERSPs was performed by a permutation test with 2000 permutations and a multiple comparison correction using the false discovery rate (FDR, α=0.05).

5.4 Results

5.4.1 Behavior

The navigation routes participants were asked to follow were pre-defined. First, they were shown a global landmark and asked to point to it. After the landmark disappeared, they followed a path with several turns and, after two or three changes in course, they were asked to point to the (now invisible) landmark. The navigation task resumed with two or three more turns, and the trial concluded by asking them to point to the invisible landmark a final time. The landmark pointing error (in degrees) was statistically significantly different at the different number of turns (NT) using the Friedman test, ($\chi^2(5)$=53.34, p<.0001). The pairwise Wilcoxon signed rank test (with false discovery rate-FDR corrected) between groups revealed statistically significant differences in landmark pointing error between NT0 and NT2 (p=.000046); NT0 and NT3 (p=.000046); NT0 and NT4 (p=.000046); NT0 and NT5 (p=.000046); NT0 and NT6 (p=.000046); NT2 and NT4 (p=.007); NT3 and NT4 (p=.00011); NT3 and NT6 (p=.003). The median error was 5.79° (degrees) with 0 turns, 29.63° after 2 turns, 32.76° after 3 turns, 45.57° after 4 turns, 44.94° after 5 turns, and 60.99° after 6 turns (figure 5.9).

5.4.2 Event-related Spectral Perturbation (ERSP)

Repeated k-means clustering of independent components (ICs) resulted in 25 clusters with centroids located in several structures of the brain including the frontal cortex, the left and right motor cortices, the parietal cortex, the RSC, and the occipital cortex. Focusing on power spectrum changes in the RSC cluster, we computed event-related spectral perturbation (ERSP) in the frequency range of 3 to 50 Hz (figure 5.10). Broadband alpha and beta desynchronization were prominent during the straight segments of navigation, replicating previous results from both passive and active navigation studies (Gramann et al. 2010; Lin et al. 2015; Ehinger et al. 2014). In addition, a prominent theta burst became apparent directly after each turn, i.e., at the time when people were computing heading changes before proceeding along the next straight path. Moreover, the theta burst was present during all turns, while the alpha and low beta desynchronization became more desynchronized as the number of turns increased (figure 5.7).

5.4.3 Neural Correlations with Spatial Updating

Heading computations

Next, we calculated the correlations between power modulations in the RSC and the landmark pointing errors. For a comprehensive analysis, we divided the power modulations into different frequency bands and the pointing errors by allocentric or egocentric reference frames for the entire course of the navigation task. Further, to assess the impact of rotational compared with translational movement on RSC spectral modulations, we extracted the first 10% of each segment, which included the turn, and the middle 10% of each segment (50-60%), where participants were only moving in a straight line, and calculated the correlations between power in different bands and pointing errors with just these segments.

Participant-level Analysis

The allocentric group showed a significant positive correlation between errors in the landmark pointing tasks and power changes in the following broadband frequency

ranges: theta (r(34)=0.48, p=.00048), low alpha (r(34)=0.5, p=.00051), high alpha (r(34)=0.46, p=.00047) and beta band (r(34)=0.4, p=.0012) (FDR-corrected) (see figure 5.11A). Egocentric participants demonstrated a negative correlation between the performance pointing task (error) and power changes in the following frequency ranges: low alpha (r(22)=-0.34, p=.0.006), and high alpha (r(22)=-0.24, p=.011) (FDR-corrected)(figure 5.11A). The inverse pattern of correlation coefficients of power and individual performance error for allocentric and egocentric participants was consistent across the entire navigation phase (10x10% time bins) (supplementary figure 5.8), revealing that RSC activity depends on their stationary reference frames used to encode and integrate the spatial information.

Trial-level Analysis

In contrast to previous stationary navigation studies (Lin et al. 2015; Ehinger et al. 2014), participants moved actively through the environment, receiving sensory feedback from not only the visual system but also converging sensory evidence about changes in position and orientation from their vestibular and proprioceptive systems. This phenomenon opens the possibility that the participants' preferred use of spatial reference frames might change depending on the sensory input available to them (Gramann 2013; Goeke et al. 2015). Therefore, we further investigated the relationship between individual performance error and power changes in RSC on a single-trial level. The pointing response at the end of the path required a binary decision regarding whether the homing location was located to the left or right with respect to the current position and orientation of the navigators (at point 12, figure 5.2B). The results of the single-trial reference frame classification demonstrated that a large portion of participants preferentially used an egocentric reference frame in stationary setups but switched to an allocentric reference frame with active navigation (figure 5.9B). In contrast, participants with a preference for using an allocentric reference frame in stationary setups kept the same allocentric reference frame in the active navigation scenario (figure 5.9B). Importantly, whenever participants used an allocentric reference frame in the pointing task, irrespective of their habitual proclivity toward an egocentric or an allocentric reference frame in stationary settings,

there was a positive correlation between the pointing error and power changes in the lower alpha band (r(100)=0.37, p=.000037 for stationary allocentric; r(44)=0.17, p=.015 for stationary egocentric), higher alpha band (r(100)=0.13, p=.013 for stationary allocentric; r(44)=0.13, p=.016 for stationary egocentric), and beta band (r(100)=0.34, p=.00009 for stationary allocentric; r(44)=0.0012, p=.0.00015 for stationary egocentric). However, pointing based on an egocentric reference frame (in physical navigation) still revealed a negative covariation with power in the higher alpha band (r(12)=-0.10, p=.024) (dark-blue color, figure 5.11A) and the beta band (r(12)=-0.86, p=.000035 for stationary egocentric). Thus, the single-trial reference frame analyses clearly revealed a systematic and more pronounced desynchronization in the alpha band whenever an allocentric reference frame was used to respond to a homing challenge.

5.5 Discussion

Spatial navigation is vital to purposeful movement as it requires a representation of our position and orientation in space as well as our homing trajectories. In this study, we explored these processes through a typical stationary navigation task but also a physical navigation task where the participants actually moved through a large virtual space while we recorded and analyzed their brain dynamics using a MoBI approach (Makeig et al. 2009; Gramann et al. 2011, 2014b; Jungnickel et al. 2019). We found that participants with a proclivity for using an egocentric reference frame in stationary navigation tasks switched to an allocentric reference frame during physical navigation. In contrast, participants with an allocentric proclivity in stationary tasks still used the same reference frame during physical navigation. Importantly, using this modified MoBI approach provided this first-ever opportunity to describe theta synchronization in the RSC during heading computation in actively rotating navigators. From our analyses, we find that alpha desynchronization in the RSC occurs when retrieving spatial information from an allocentric reference frame and translating it into an egocentric location pointing response.

Remarkably, navigators switched from their preferred egocentric reference frame

to an allocentric reference frame when they were allowed to actively move through space. Thus, the reference frame proclivity (RFP) observed in stationary navigation tasks is not consistent with that observed in active navigation tasks, including naturally occurring sensory feedback from the visual, vestibular, proprioception, and kinesthetic systems. More specifically, the majority of egocentric navigators switched to an allocentric reference frame during physical navigation, while the allocentric group consistently used their preferred allocentric strategy. To anchor a cognitive map with the environment, navigators can use local and global landmarks (e.g., a mailbox, a building) and/or self-motion cues. In our navigation scenario, we gave the participants a single prominent landmark only at the very beginning of a trial that was invisible for the rest of the navigation task. Participants then moved through space, walking straight toward a point and then locating and changing directions several times while moving away from their starting location (figure 5.2). Consequently, the participants tended to derive their orientations and positions in space by converging multiple sensory inputs to represent the original global landmark position. Most participants, including the egocentric strategy group, responded as allocentric navigators in the homing direction test (figure 5.9B). This finding suggests that human spatial navigation strategies are quite flexible, exploit multisensory information, and depend on the particular type of response that is required at the given moment. In contrast to previous desktop experiments asking for a simple homing response that demonstrated a preference for distinct reference frames (Gramann et al. 2005, 2010; Lin et al. 2015) the current task showed that the majority of participants preferred an allocentric reference frame. Having to constantly update one's own position as well as the position of other entities in space (landmark, home) likely fosters the use of an allocentric reference frame.

Moreover, the behavioral results in the landmark pointing task (figure 5.9A) followed the leaky integrator model (Lappe et al. 2007; Harris and Wolbers 2012). This model assumes that the encoded orientation, as the variable state, is incremented with movement by multiplying the actual orientation gain factor. This process tends to decay by an orientation-dependent leaky factor. In our trials, there were no vis-

ible landmarks within the navigation task. Therefore, participants could not use external landmarks to anchor their cognitive map. Instead, they had to derive their orientation with each turn based on idiothetic information only. Thus, errors accumulated at each turning point (figure 5.9A) and increased somewhat proportionally to the number of turns in the scenario. In other words, the errors in the landmark pointing task (at R1, R2a, and R5a, figure 5.2) are correlated to the number of turning points (figure 5.9A).

Using a spatial filter approach and subsequent clustering of independent components, we demonstrate the RSC to reflect specific aspects of the navigation task. EEG contains subcortical activity and allows to localize deeper brain structures (Seeber et al. 2019). Previous desktop studies have already revealed navigation-related activity in or near the RSC (Gramann et al. 2010; Chiu et al. 2012; Lin et al. 2015). However, even though theta oscillation is an important mechanism for computing head orientation and providing a grid cell network (Brandon et al. 2011; Koenig et al. 2011; Winter et al. 2015), it has not been reported in human brain imaging studies using stationary setups. Notably, we found a strong theta synchronization in the RSC during periods of heading changes, which indicates that physical rotations induce RSC activity (figure 5.10). This has not been reported in previous stationary studies. This theta oscillation was robustly observed with each turn by navigators along the path. Through MoBI, our participants were able to make use of naturally occurring spatial information, such as motor efference and cues from the visual, vestibular, proprioception, and kinesthetic systems. Therefore, participants could extract their head direction from HD cells activity (Shine et al. 2016b; Chen et al. 2018), which is often eliminated in stationary setups. In addition, there is evidence that the firing rate of HD cells decreases with restraints during navigation. Compared with those in active locomotion, loosely restrained rats in passive movement showed a nearly 24% reduction in the peak firing rates of HD cells (Zugaro et al. 2001; Bassett et al. 2005), while tightly restrained rats (Taube 1995; Knierim et al. 1995) showed near or complete suppression. The suppression of the HD cell firing rate is due to disruption of the vestibular system, which is the essential sig-

nal for estimating head direction (Cullen and Taube 2017; Stackman et al. 2003; Muir et al. 2009). In previous human spatial navigation studies, the population was limited to stationary participants. Thus, the vestibular information for HD signals may have been eliminated (Gramann 2013). In this study, the participants received vestibular information in addition to all other naturally occurring sensory modalities while turning and walking. Accordingly, sufficient multi-modal sensory information was available for them to compute their head directions. Therefore, theta oscillation occurred after each turning onset (figure 5.10), indicating heading computation activity in the RSC, providing evidence of heading computation in healthy participants in a physical spatial locomotion study replicating similar theta activity in participants rotating on the spot (Gramann et al. 2018).

Furthermore, we replicated RSC alpha suppression, which has been previously observed in spatial learning for maintaining orientation in both passive (Gramann et al. 2010; Plank et al. 2010; Chiu et al. 2012; Lin et al. 2015) and active navigation tasks (Ehinger et al. 2014). This alpha desynchronization might indicate ongoing spatial transformations from egocentric to allocentric coordinates and vice versa (Gramann et al. 2010). Although Kim and Maguire (2019) demonstrated that RSC activity is correlated with behavioral performance in three-dimensional space, how the use of distinct reference frames during navigation impacts RSC activity was still unclear. Remarkably, in this study, we found that RSC activity systematically covaried with behavioral responses, and that this correlation depended on the reference frame used. The use of an allocentric strategy revealed a positive correlation of individual performance and alpha power, while an egocentric strategy was associated with a negative correlation (figure 5.11). This general pattern was confirmed using a single-trial analysis approach that identified the reference frame underlying the single-trial pointing response of participants irrespective of their general reference frame proclivity. The results clearly indicate that only the use of an allocentric response and not the use of an egocentric response was associated with desynchronization in alpha band activity.

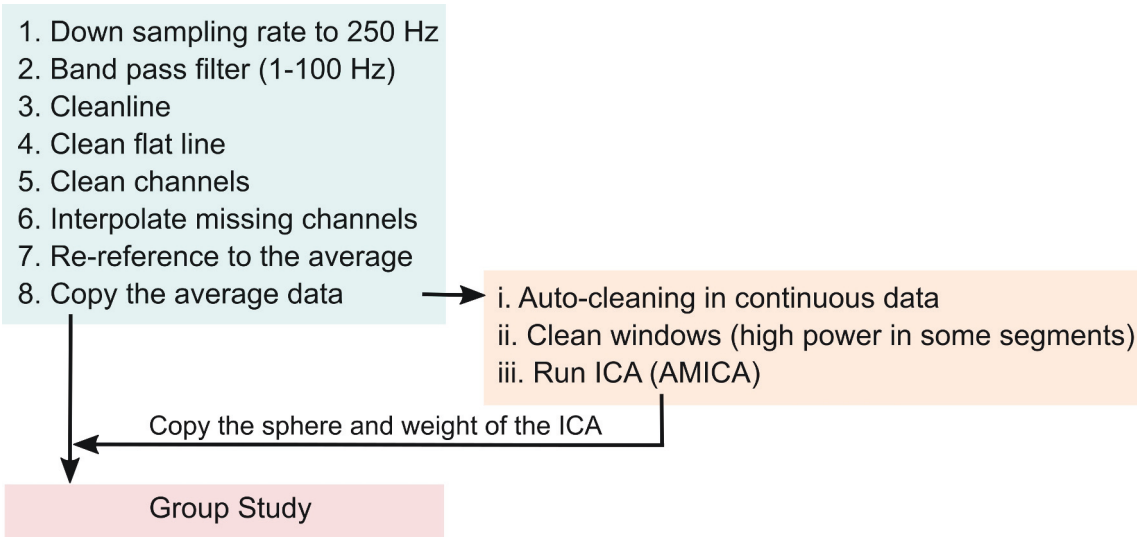

Figure 5.3 : The pipeline of EEG preprocessing.

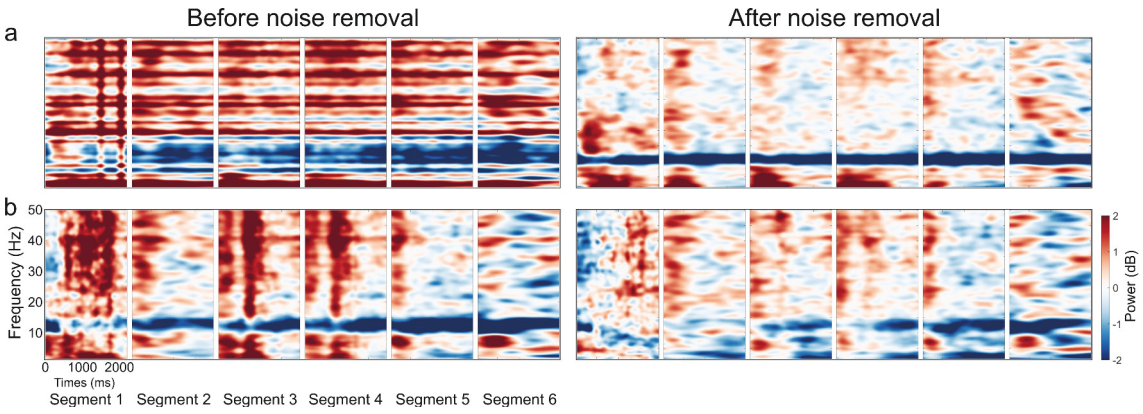

Figure 5.4 : The ERSP before and after noise removal. The RSP ERSP before and after noise removal at the participant level. The left figure shows the average ERSP for participants before noise removal. The right figure shows the average ERSP for participants after noise removal at: (a) one egocentric participant; and (b) one allocentric participant.

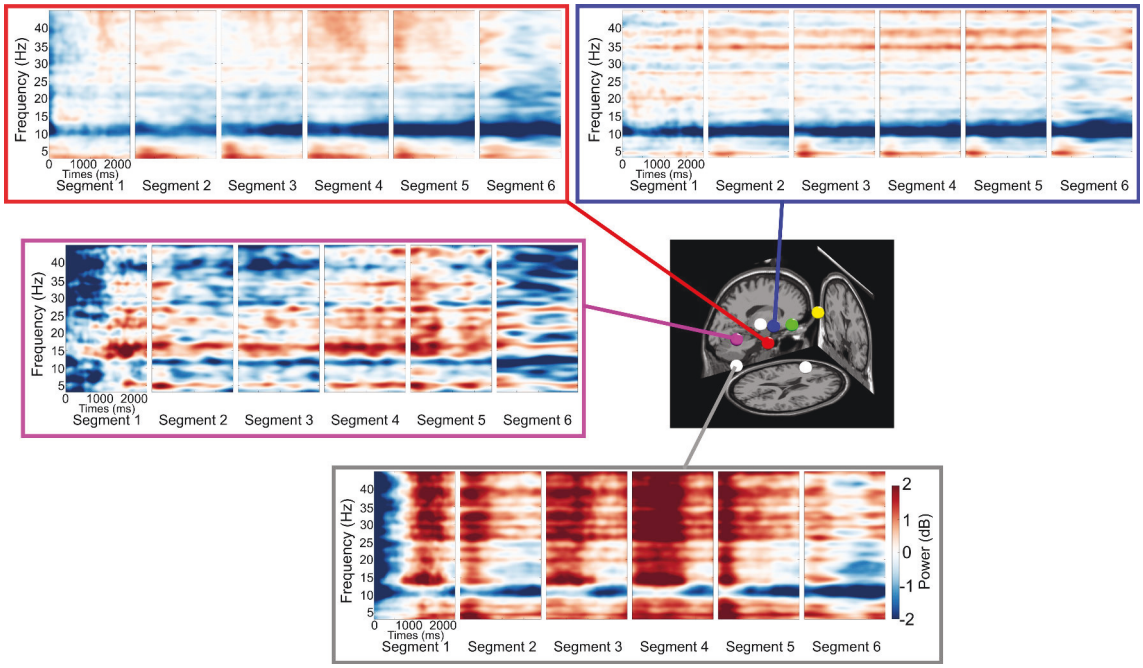

Figure 5.5 : ERSP in several brain regions. The ERSP in different brain regions in or near the RSC (red), parietal cortex (blue), occipital cortex (pink), and neck (white).

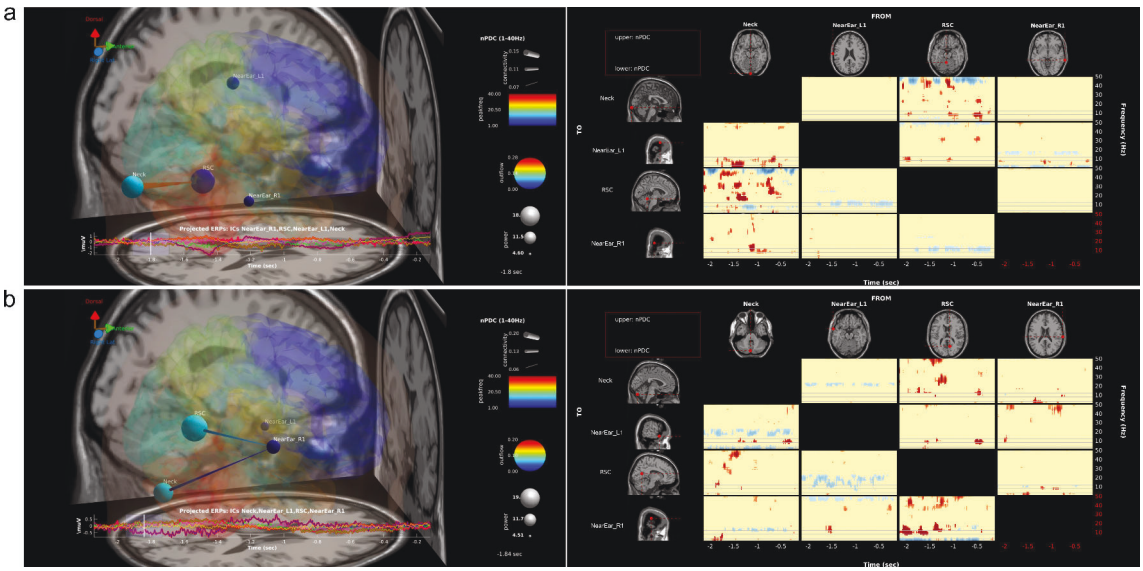

Figure 5.6 : Effective brain connectivity. The estimated effective connectivity of the four clusters (the RSC, neck, near the ear on the left side, and near the ear on the right side) in one participant in the (a) allocentric and (b) egocentric strategy groups. The results indicate that theta activity in the neck cluster has no effect on the RSC.

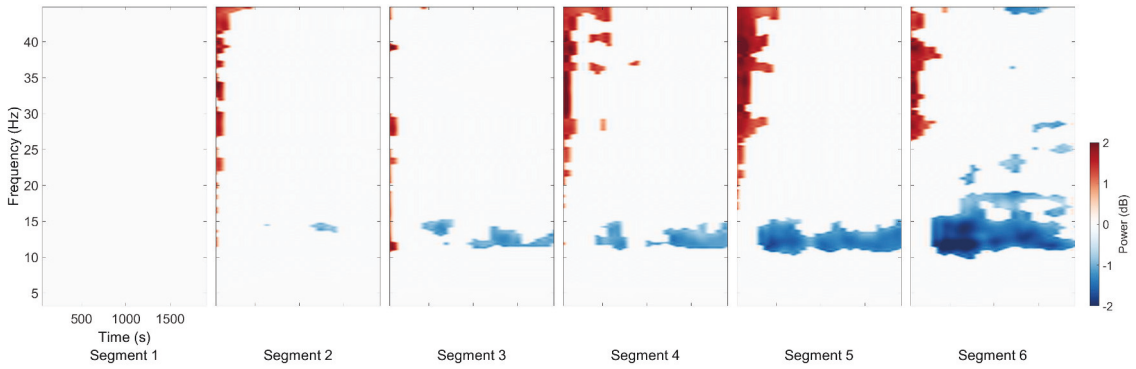

Figure 5.7 : The permutation test (n=2000, FDR-correlated) of the RSC ERSP for 6 segments in comparison to segment 1.

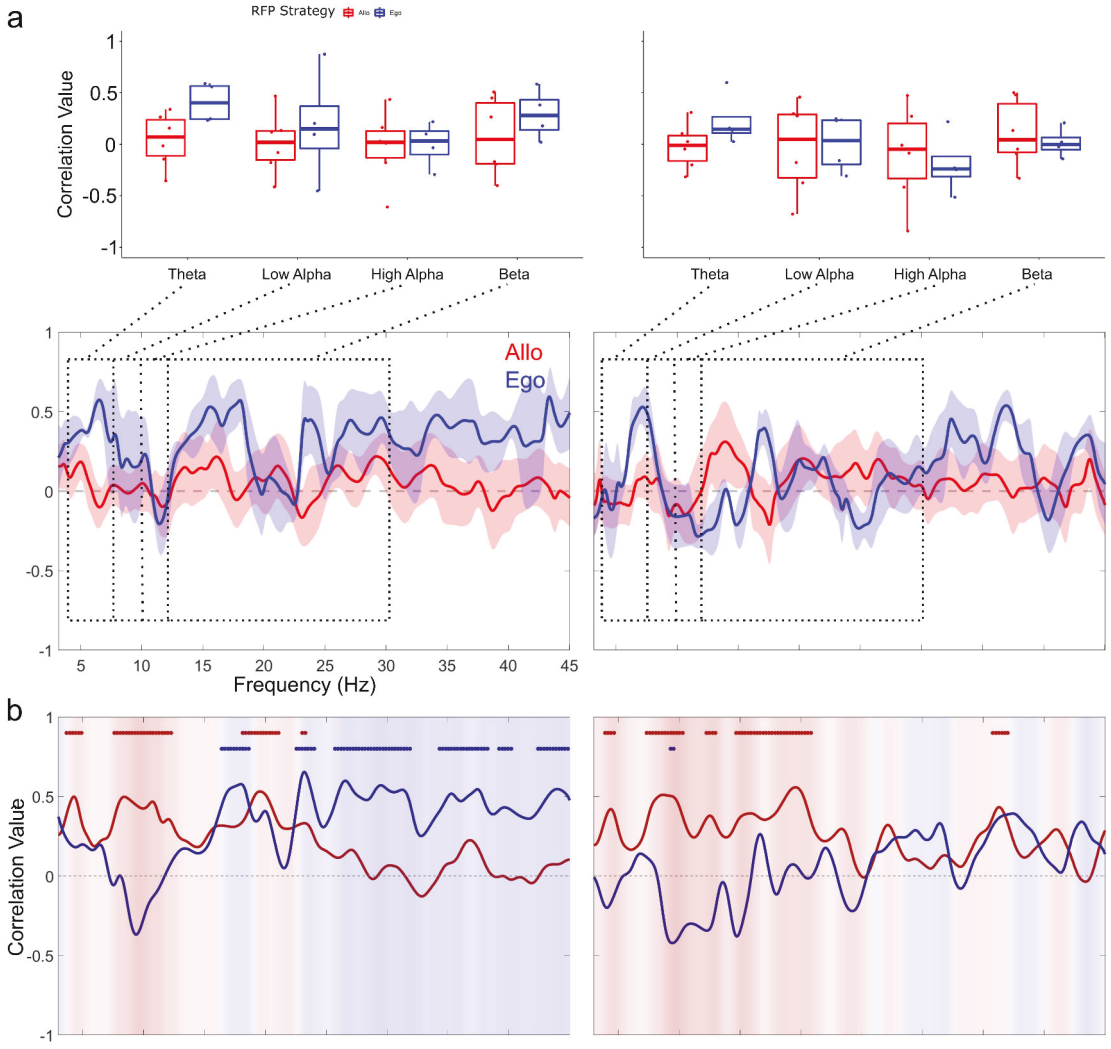

Figure 5.8 : Correlation between landmark pointing error and ERSP at participant level. These are correlation coefficients between performance and the RSC ERSP in the continuous frequency (3-45 Hz) in the first ten percent (left column) and middle ten percent (right column) of the segment length. The asterisk (*) indicates a significant difference ($p<0.05$) between the allocentric (red) and egocentric strategies (blue).

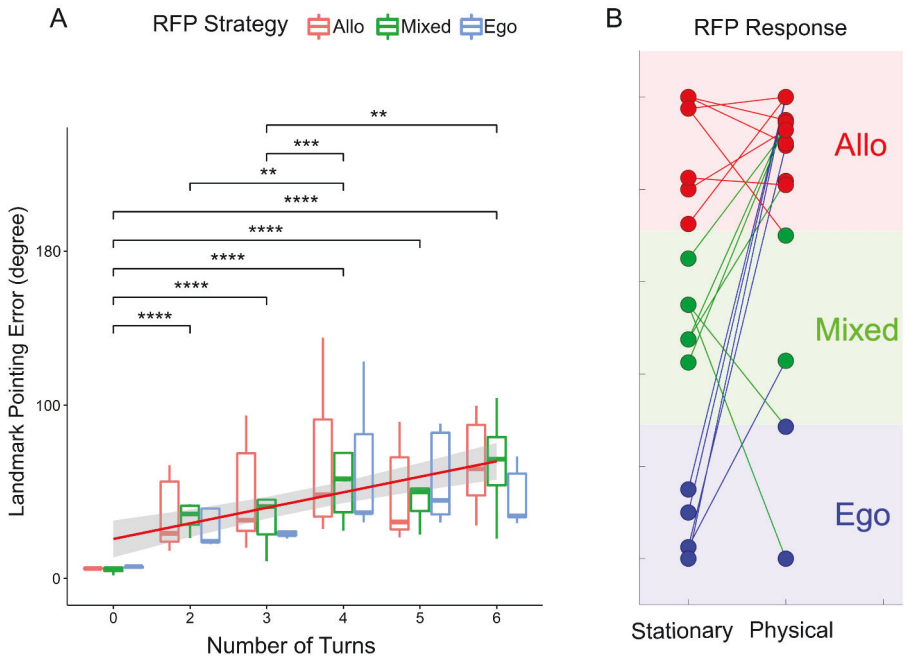

Figure 5.9 : The results of participant behaviour. a. The participant behaviour in the landmark pointing task. The X axis indicated for the number of turn points in the trial, the Y axis indicated for the absolute error of participant when they performed the landmark pointing task (the error was measured by the angular difference between the pointing vector and the participant to landmark vector). The regression was visualized by the red line (*, **, ***, **** indicated for p<.05, p<.01, p<.001, p<.0001 respectively). b. The RFPT results were in both passive condition (stationary test with the tunnel paradigm) and active condition (based on the participant's response at position 12, path 3 in the Figure 1b). Three groups of strategies egocentric, mixed and allocentric were colour coded with green, blue and red, respectively.

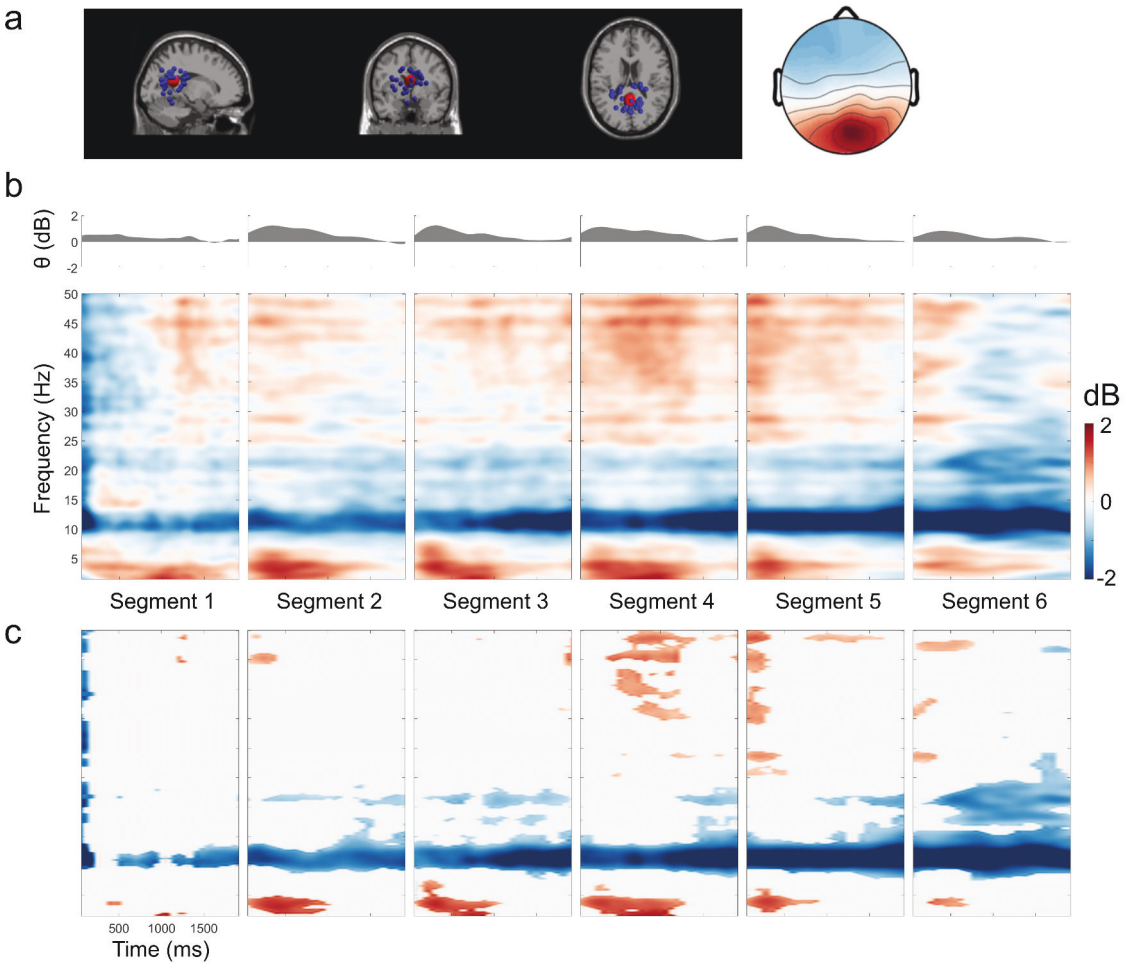

Figure 5.10 : Retrosplenial complex (RSC) event-related spectral perturbation (ERSP). a. Dipole locations of independent component (in or near retrosplenial complex (RSC) cluster at the sagittal, coronal, and top view respectively and the corresponding mean of scalp map. b. The RSC ERSP with respect to segment of turns from 1 to 6 turns. **c.** The permutation test (n=2000, FDR-correlated) of the RSC ERSP in 6 segments.

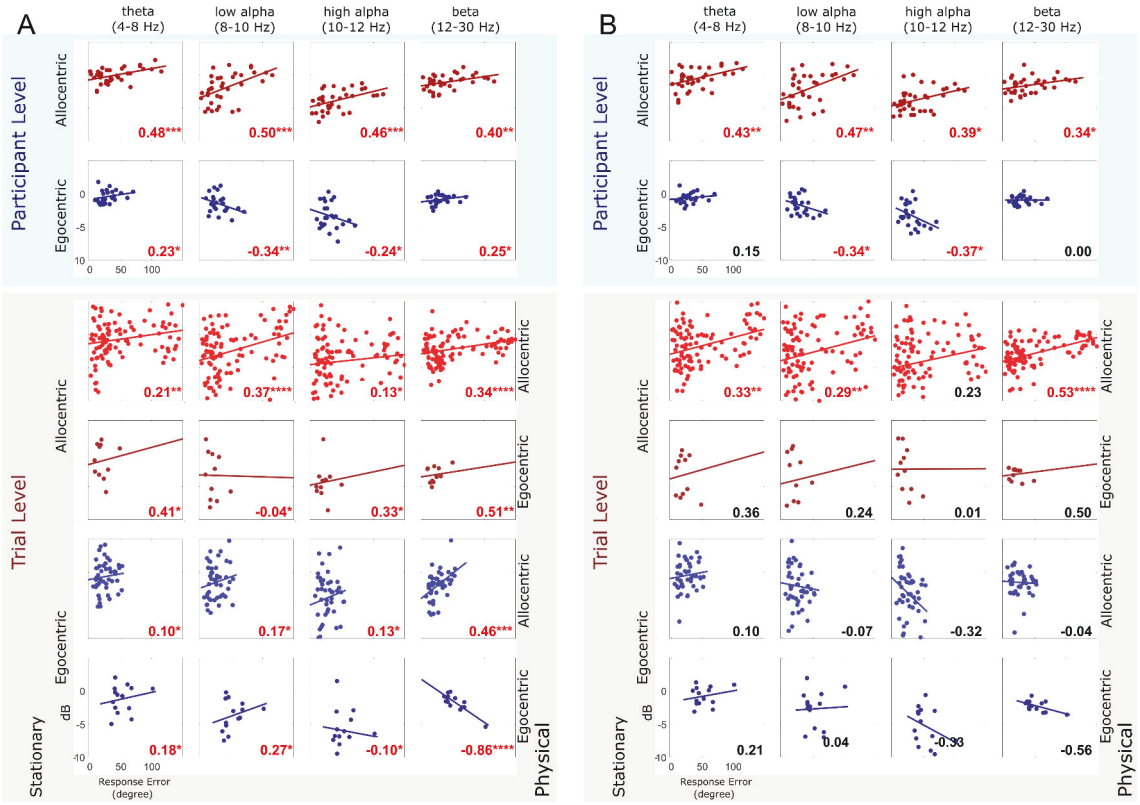

Figure 5.11 : RSC ERSP correlated with participant performance in the first 10 percent (a) and mid 10 percent (b) of the segment length in both participant and trial level respectively. The top figure showed the correlation coefficients computed (the number on the bottom right corner, red color indicated for statistical significance; *, **, ***, **** indicated for p<.05, p<.01, p<.001, p<.0001 respectively) between individual performance and RSC ERSP at participant level in different frequency band at theta (4-8 Hz), low Alpha (8-10 Hz), high Alpha (10-12 Hz), and beta (12-30 Hz). The row indicated for the RFP strategy in the passive RFPT response: the red colour indicates for allocentric, and blue indicates for egocentric strategy. The bottom figure showed the correlation coefficients computed between individual performance and RSC ERSP in the trial level at same the range of frequency as top figure. The color-coded indicated for RFP strategy; the lighter color in the same RFP strategy group indicated for active allocentric response, while the darker color indicated for active egocentric trial response.

Chapter 6

Local information processing in RSC under different navigation load conditions

This chapter investigates the local information processed via RSC in different navigation load conditions in a physical navigation experiment. Chin-Teng Lin conceived this work. Tien-Thong Nguyen Do performed data collection and analysis. All the authors discussed and wrote the manuscript (J-5) (Do et al. 2020a).

6.1 Abstract

Spatial navigation is a complex cognitive process based on vestibular, proprioception, and visual cues that are integrated and processed by an extensive network of brain areas. The retrosplenial complex (RSC) is an integral part of coordination and translation between spatial reference frames. Previous works have demonstrated that the RSC is active during a spatial navigation task. The specifics of RSC activity under different navigation loads, however, are still not characterized. This study investigated the local information processed by the RSC under different navigation load conditions manipulated by the number of turns in the physical navigation setup. The results showed that the local information processed via the RSC, which was reflected by the segregation network, was higher when the number of turns increased, suggesting that RSC activity is associated with the navigation task load. The present findings shed light on how the brain processes spatial information in a physical navigation task.

6.2 Introduction

Spatial navigation is an essential human skill. Without it, we would be lost—literally. However, in comparison to other areas of the brain, relatively little is known about

how our sense of direction works. We know that several regions of the brain (Doeller et al. 2010; Ekstrom et al. 2003) are involved in integrating and translating our movements (McNaughton et al. 2006), visual cues, proprioceptive information, and other sensory inputs into a mental representation of space (Cullen and Taube 2017). One of these brain regions is the retrosplenial complex (RSC) (Epstein 2008), which is a central hub between the areas of the brain that govern visual processing, associations, learning, and memory and is indirectly linked to planning and decision-making. The RSC is thought (but not confirmed) to act as a bridge between perception and memory and may be involved in imagining future events or processing scenes. Studies have also shown that the RSC plays an important role in helping us switch between spatial reference frames (Gramann et al. 2010; Lin et al. 2017): egocentric (self-centered) navigation, where we view the world around us in relation to ourselves, and allocentric (world-centered) navigation, where we reference one object to another (Vann et al. 2009).

However, only a few studies have explored brain dynamics in spatial navigation in full-body movement due to the limitation of brain imaging hardware. A stationary experiment involved participants laying still in a fMRI machine (Doeller et al. 2010); therefore, the experiments were not designed to explore the neural mechanisms that contribute to navigation in real-world environments. Other studies did involve freely moving participants, but the participants were clinical subjects suffering from severe epilepsy (Bohbot et al. 2017).

Moreover, cognitive function depends on sufficient configuration among brain regions (Shine 2019). Thus, examining brain network properties could help us better understand the underlying mechanism of cognitive function. There is clear evidence of the relationship between cognitive performance, network segregation and network integration, which are essential attributes of the brain network. Notably, a decline in network segregation leads to lower cognitive performance (Cassady et al. 2019; Chan et al. 2014; King et al. 2018; Ng et al. 2016).

Nevertheless, many functional connectivity (FC) studies have investigated the larger-scale brain network, which may not reflect the involvement of each region in

task execution. Those studies performed analysis at the global level and considered all the nodes of the brain to have the same roles, as opposed to scrutinizing specific brain regions related to the experimental task. Furthermore, brain network segregation and integration are not generalized for all tasks and rely on the cognitive demand of specific tasks (Cohen and D'Esposito 2016). For instance, at the global level, in the N-back experiment, the 2-back showed a higher integration than the 0-back (Cohen and D'Esposito 2016; Fransson et al. 2018; Shine et al. 2016a). Moreover, trial accuracy was positively related to network integration (Cohen and D'Esposito 2016). However, this feature is not the same for all subnetworks in the brain and even contradicts findings in the frontoparietal network (Fransson et al. 2018).

A few studies have investigated specific brain regions related to experimental tasks. A study on sensorimotor performance demonstrated that reduced sensorimotor network segregation leads to poorer behavioral performance (Cassady et al. 2019). The same relationship between sensorimotor network segregation and performance has been found at the whole-brain level (King et al. 2018). Moreover, increased network segregation reflects the greater autonomy of task-related networks and saves resources for other cognitive demands (Bassett et al. 2015). Thus, there might be a mechanism to segregate brain tasks related to processing cognitive tasks.

Furthermore, investigating brain activity across a network under a specific frequency might rigorously reflect their attributions. Theta frequency has been revealed as an important mechanism of head direction (HD) cell activity in physical navigation (Brandon et al. 2011; Koenig et al. 2011; Winter et al. 2015). In addition, theta frequency was modulated and correlated with the mental workload and was reflected in the frontal midline region (Onton et al. 2005). Therefore, examining the network properties under a specific frequency in a distinct brain region related to an experimental task may reflect a precise mechanism of the brain network in a specific task-related brain region (Mohan et al. 2016). In short, studying a large-scale brain network may reflect the whole cognitive stage of the brain but might not fully reveal the specific mechanism of the task-related brain region. It is necessary to investigate

the segregation and integration of specific brain regions related to the experimental task.

This study investigated the brain network dynamics of healthy human participants during active navigation under different workload conditions. To overcome the movement restrictions associated with standard brain imaging modalities, such as fMRI, we adapted a mobile brain/body imaging (MoBI) system (Gramann et al. 2014b, 2011; Makeig et al. 2009), to give participants the freedom to move naturally. We equipped participants with a high-density EEG cap synchronized to a head-mounted virtual reality (VR) display and then asked them to walk paths that included several turns and straight segments while we recorded EEG signals. At various intervals, participants were also asked to point in the direction in which a landmark they had previously seen might be (see Fig. 6.1). These physical navigation tasks required the participants to track their location and orientation through motor efferences and self-motion cues from their visual, vestibular, proprioception, and kinesthetic systems. Hence, the data we gathered allowed us to assess the network segregation and integration in the RSC and frontal regions of each walking segment during actual navigation. The results showed that the segregation of the RSC region increased with a higher number of turning points (NT) during physical navigation, reflecting that the navigation load modulated RSC segregation. In this thesis, the terms number of turns, and number of segments are used interchangeably to mean the navigation load.

6.3 Materials and Methods

6.3.1 Experimental Design

Refer to the Chapter 5, section 5.3.

6.3.2 EEG analysis

All the preprocessing steps were performed in EEGLAB (version 14.2.0) (Delorme and Makeig 2004; Delorme et al. 2011). The EEG data were first bandpass filtered (1-100 Hz) and then downsampled to 250 Hz. Next, all idle segments with

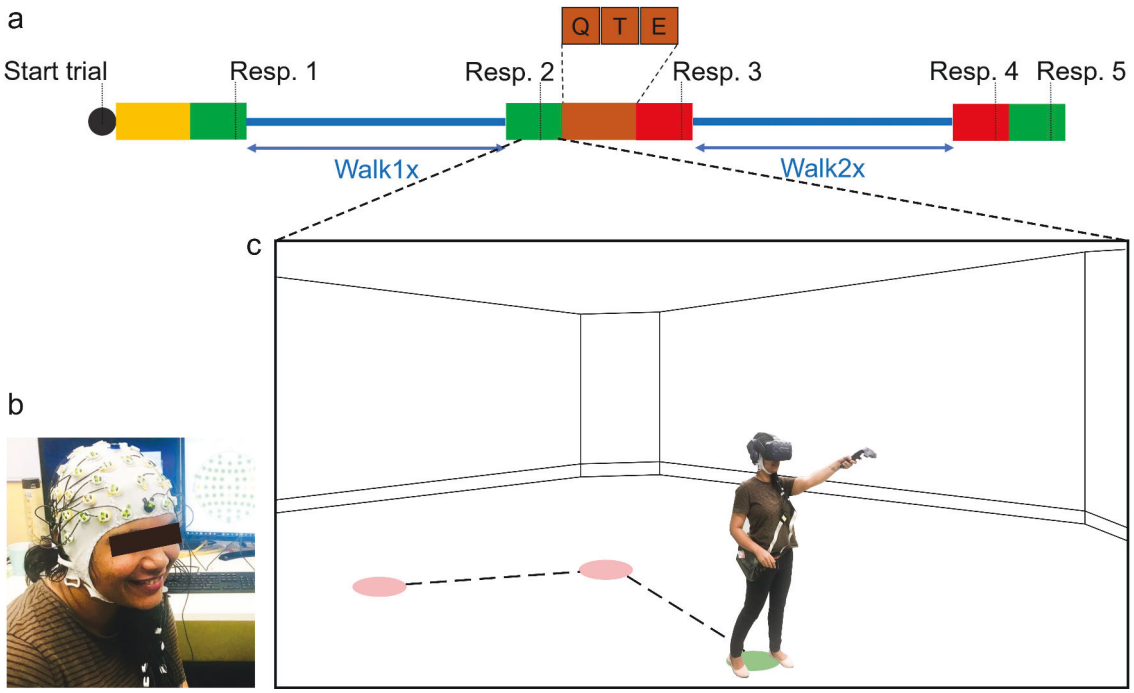

Figure 6.1 : The experimental design. (a) Trial representation. At the beginning of the trial, participants had 4 seconds to remember a landmark, which was presented approximately 200 meters in front of them. Then, the landmark disappeared (in the rest of the trial), and participants answered the question: "Where is the landmark position?" (Resp. 1, green square). Next, participants freely walked in a predefined path with the number of turns points being randomly chosen as 2 or 3 (walk 1x). Subsequently, participants were asked to recall the landmark position (Resp. 2, green square). Next, participants encoded a set of letters (3, 5, or 7 letters) (orange square) and then performed the letter-retrieval task (Resp. 3, red square). Then, participants started the second walk (2x) with 2 or 3 turn points. After finishing the walk, participants performed the letter-retrieval task (Resp. 4, red square) and spatial-retrieval task (Resp. 5, green square). (b) EEG cap set up. (c) The participant responded to a landmark position.

zero values in the raw data (continuous data) were removed (threshold = 3 seconds). Then, an automatic cleaning segment was run to remove the noise in the data. Next, the bad channels were identified and removed, and the missing channels were interpolated by applying the sphere method. Next, the high-power segments

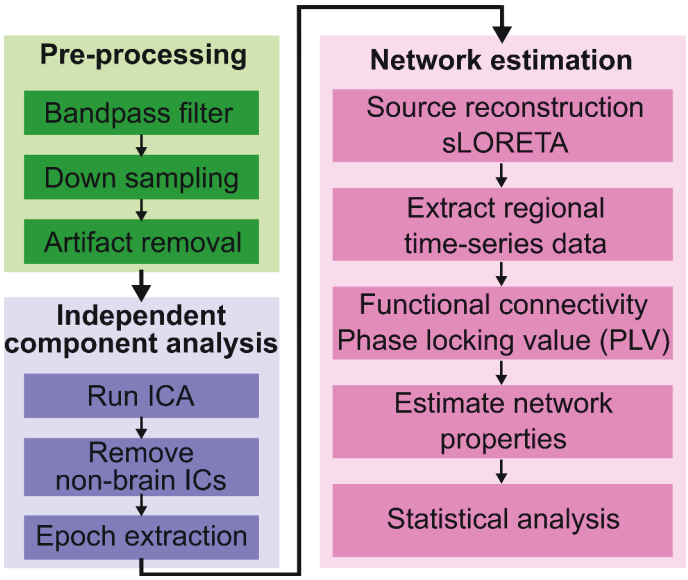

Figure 6.2 : pipeline for brain network segregation and integration analysis.

in the continuous data were identified and removed before rereferencing to the average. Subsequently, adaptive mixed independence component analysis (AMICA) was applied to the rereferenced data to decompose them into maximally independent components (ICs). Then, the dipole-fitting routine (Oostenveld and Oostendorp 2002) was applied to identify the locations of the ICs. Next, the AMICA solution was copied back to the rereferenced dataset. The nonbrain components were identified and removed by using the IClabel toolbox (Pion-Tonachini et al. 2019) (with a confident threshold $> 95\%$) before extracting data from six walking navigation segments with respect to the NT during navigation. Then, the bad epochs were identified and removed by checking the raw value (threshold = 100 μV).

6.3.3 Functional connectivity

Distributed source localization was used to address the inverse problem. The dipole brain source localization activity was estimated from cleaned epoched data, and then the brain FC was estimated from the source activity by using the Brainstorm toolbox (version 02-Jun-2020) (Tadel et al. 2011).The epoched data were first coregistered with the MRI template ("ICBM152" template (Fonov et al. 2009)) and EEG sensor locations (same template for all participants) in the same anatomical

landmarks. Next, the lead field of cortical mesh (15,002 vertices, 29984 faces) was estimated by using openMEEG (Gramfort et al. 2010; Kybic et al. 2005). The noise covariance matrix was calculated using the idle period during the experiment. Then, a standardized low-resolution brain electromagnetic tomography (sLORETA) method (Pascual-Marqui et al. 2002) was used to reconstruct the regional time series from the 68 brain regions (Desikan-Killiany (Desikan et al. 2006), FreeSurfer (Fischl 2012)). Finally, the FC among regions was estimated by the phase-locking value (PLV) (eq. 6.1) (Lachaux et al. 1999) in four different frequency bands: delta (1–4 Hz), theta (4–8 Hz), alpha (8–12 Hz), and beta (12–30 Hz). Then, the highest 10% (of the highest PLV values) were kept for further estimating the network properties (Rizkallah et al. 2019), and the remaining PLV values were set to zero.
Phase locking value:

$$PLV(\tau) = |\frac{1}{\delta}\int_{\tau+\frac{\delta}{2}}^{\tau-\frac{\delta}{2}} e^{j(\phi_y(\tau)-\phi_x(\tau)}d\tau| \tag{6.1}$$

where $\phi_y(\tau)$ and $\phi_x(\tau)$ indicate the phases of the time series signals x and y at time τ, respectively, and δ indicates the size of the window. PLV values ranged between 0 (no phase-locking) and 1 (full synchrony).

6.3.4 Network properties

The network properties (segregation and integration) were calculated from the PLV connectivity matrix at each frequency of each walking segment. The network segregation indicated the local information processing at each node (each cortical region) related to the experimental task, while network integration indicated the global information exchanged at each node (each cortical region) related to the experimental task. The network properties were calculated for all walking segments of each participant. Then, a statistical test was conducted to check the impact of the walking sequence on the network properties. In this study, we used the clustering coefficient (eq. 6.2),which reflected local information processing in each region, for measuring segregation, and the participation coefficient (eq. 6.3), which reflected local information processing in each region, for measuring integration. Both

measurements were calculated using the Brain Connectivity Toolbox (Rubinov and Sporns 2010).

Network segregation:

$$C_i = \frac{2t_i}{k_i(k_i-1)'} \tag{6.2}$$

where t_i represents the number of triangles around node i and k_i indicates the number of edges connected to node i. The clustering coefficient is the portion of links among a node's neighbors divided by the number of connections that could exist between them, which is 0 if no connections exist and 1 if all neighbors are connected.

Network integration:

$$P_i = 1 - \sum_{N_m}^{s=1} (\frac{k_{is}}{k_i})^2 \tag{6.3}$$

where N_m indicates the number of modules, k_{is} represents the number of edges between node i and other nodes in module s, and k_i is the total degree of node i. The participation coefficient of a node is close to 1 if its links are uniformly distributed among all the modules and 0 if all of its links are within its own module.

6.4 Results

6.4.1 Behavioral performance

Linear regression was conducted to determine whether the NT affected participants' pointing errors. The landmark-pointing error (in degrees) was significantly different under different NTs using the Friedman test, $\chi^2(5) = 53.34$, p<.0001. A significant regression equation was found (F(5,96) = 9.18, p<.0001), with an R^2 of 0.32. Then, the Wilcoxon sign-rank test was used to check the significant difference in participants' pointing landmark errors between different NTs (table 6.1).

6.4.2 Functional connectivity

The group average FC was estimated across six walking segments (Fig. 6.3, visualized by using the BrainNet Viewer (Xia et al. 2013)). Then, the Fried-man test was recruited to measure the significant difference of the network properties (segregation was measured by the clustering coefficient, and integration was mea-

Number of turning points (NT)		p-adjust value
0	2	0.000046****
0	3	0.000046****
0	4	0.000046****
0	5	0.000046****
0	6	0.000046****
2	3	1
2	4	0.007**
2	5	0.1
2	6	0.075
3	4	0.000114***
3	5	0.1
3	6	0.003**
4	5	0.1
4	6	0.876
5	6	0.114

Table 6.1 : Error in the landmark pointing task. The first and second columns indicate the number of turning points, the third column contains the p-values (FDR-adjusted) of the Wilcoxon signed-rank tests (the *, **, ***, and **** indicate for p<.05, p<.01, p<.001, and p<.0001, respectively.

sured by the participation coefficient) across walking segments, followed by the post hoc pairwise Wilcoxon signed-rank test (FDR-corrected). For network segregation, the Friedman test showed significant differences in the frontal delta band ($\chi^2(5) = 23.18$, p=.00031), frontal theta band ($\chi^2(5) = 12.93$, p=.024), frontal alpha band ($\chi^2(5) = 14.61$, p=.012), and RSC theta band ($\chi^2(5) = 17.44$, p=.0037). For the network integration, the Fried-man test showed there was a statistical difference in frontal theta band ($\chi^2(5) = 18.68$, p=.0022). Post hoc pairwise Wilcoxon signed-rank (FDR-corrected) results showed that there was a significant difference

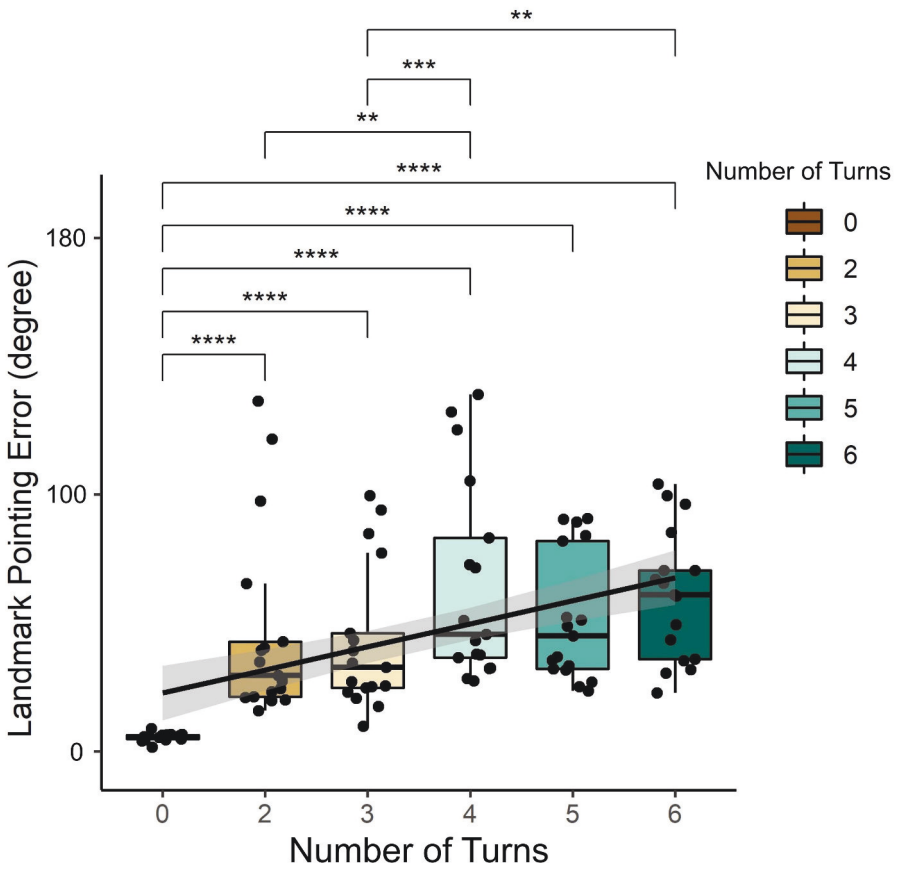

Figure 6.3 : The landmark-pointing response error (absolute) across walking segments with a distinct NT during the navigation trial. The Wilcoxon signed-rank tests were used to check for significant differences between behavior performance (*, **, ***, and **** indicate $p<0.05$, $p<0.01$, $p<0.001$, and $p<0.0001$, respectively)

in the clustering coefficient in the frontal theta (segment 1 and segment 5, p=.042; segment 2 and segment 5, p=.042); frontal alpha (segment 1 and segment 4, p=.049; segment 1 and segment 6, p=.025; segment 3 and segment 4, p=.027; segment 3 and segment 6, p=.025), and RSC theta (segment 2 and segment 6, p=.011; segment 3 and segment 6, p=.018; segment 4 and segment 6, p=.007; segment 5 and segment 6, p=.046) values.

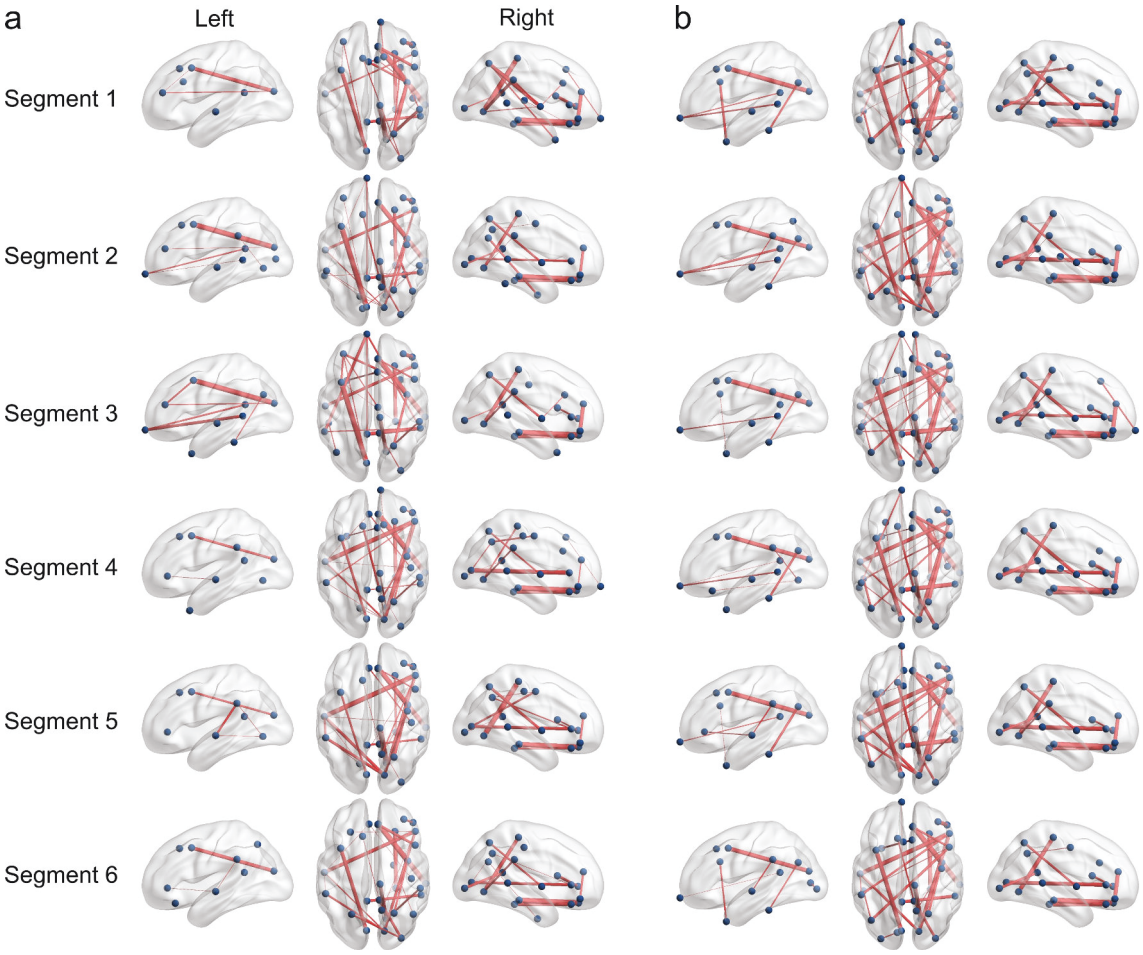

Figure 6.4 : Functional connectivity of the brain network across six walking segments in the (a) theta band and (b) alpha band. The nodes indicate brain regions (based on 68 Desikan-Killiany atlas). The edges indicate a significant connection between nodes; the edge size indicates the strength of the connection.

6.5 Discussion

Spatial navigation is a vital aspect of many daily activities that require updating position and orientation information as well as computing a homing trajectory. The present study addressed these processes in an active navigation task under different mental workload conditions by manipulating the NT that allowed navigators to move through a large virtual space. We recorded and analyzed the brain activities from navigating participants using the MoBI approach (Gramann et al. 2011, 2014b; Makeig et al. 2009; Jungnickel et al. 2019). We found that participant performance

measured by landmark-pointing errors increased as the navigation load increased, which was manipulated by the NT during the navigation. In addition, we found that this navigation load covaried with RSC segregation. When the NT increased, RSC segregation increased in the theta band measured by the PLV connectivity matrix.

First, we analyzed participants' behavior in the landmark point task to check the effect of turning points on navigation performance. As expected, landmark-pointing errors increased as the NT increased (Fig. 6.3). In other words, the behavioral results revealed that an increasing NT led to greater difficulty in navigation. Therefore, the NT in this experimental design manipulated the navigation load. The possible explanation for this decline in path integration performance could be biased velocity estimation (Lakshminarasimhan et al. 2018) or leaky integration (Lappe et al. 2007).However, in the present study, participants actively ambulated from a location to several other locations; thus, the brain can receive rich information from motor efference, visual, proprioception, vestibular, and kinesthetic systems. Therefore, the main corruption factor for this decline in landmark-pointing performance could be explained by the Stangl et al. (2020) model. The accumulating noise in the traveled distance increased with the NT, which led to an increased error in the pointing task.

Spatial navigation involves several brain regions that communicate and exchange information via the brain network. The synchronization of cortical oscillations has been believed to be a mechanism for this communication and computation (Nadasdy 2010). Through a specific frequency, a subpopulation of the neuronal population will likely be coactivated, interact with other regions, and exchange information. Therefore, the synchronization among brain regions reflects both the segregation of the cortical population for processing incoming information and integration among regions for transferring information (Cavanagh and Frank 2014). Thus, we further investigated the brain dynamics in each walking segment under specific frequencies, which may reflect processing during active navigation. There is a growing body of evidence demonstrating that theta-band oscillation plays a role in memory encoding (Onton et al. 2005), retrieval (Mitchell et al. 2008), and heading computation activity (Winter et al. 2015). The theta phase has been reported as a plausible mechanism

for neuronal computation and communication (Cassady et al. 2019). In addition, theta oscillation was reported as an important mechanism for HD cell activities (Winter et al. 2015). Therefore, investigating the brain network properties that were analyzed in the theta band might reflect the underlying mechanism of the brain regions subserving cognitive navigation processing. The results of the network segregation further showed that navigation pointing errors seems to correspond to frontal segregation (Fig. 6.5a). A higher NT led to poorer behavioral performance and a decrease in frontal segregation in the theta band.

Remarkably, in the present work, we found that RSC segregation increased with an increased NT. This result revealed that RSC activity was modulated by the navigation load (NT). The RSC coordinates with the parietal and occipital regions to translate different spatial reference frames (Vann et al. 2009). In addition, the RSC communicates with the hippocampus to update the spatial information of the cognitive map, which is in the form of an allocentric framework (Epstein et al. 2017; Vann et al. 2009). Furthermore, HD cells are present in several regions in the brain, including the RSC (Epstein 2008). HD cells exchange information across the network via theta oscillation to modulate grid cell formation in the parahippocampus (Winter et al. 2015). As a result, considering the brain as a complex system, the RSC plays a role as a hub in the brain network to coordinate the in and out spatial information. In previous studies (Gramann et al. 2010; Lin et al. 2015), the experimental setup was performed in the stationary condition with only an optical flow visual information stimulus, and the head direction activity, which obtains input from the vestibular system, might be attenuated. In the current study, participants could freely navigate and receive richer sensory information via their movements. Thus, the activity of the RSC might depend on the amount of spatial information that needed to be processed. Therefore, when the navigation load increased, the local information processed in the RSC was higher, which was measured by the clustering coefficient. These study results provide the first evidence that RSC activity covaries with spatial information processing.

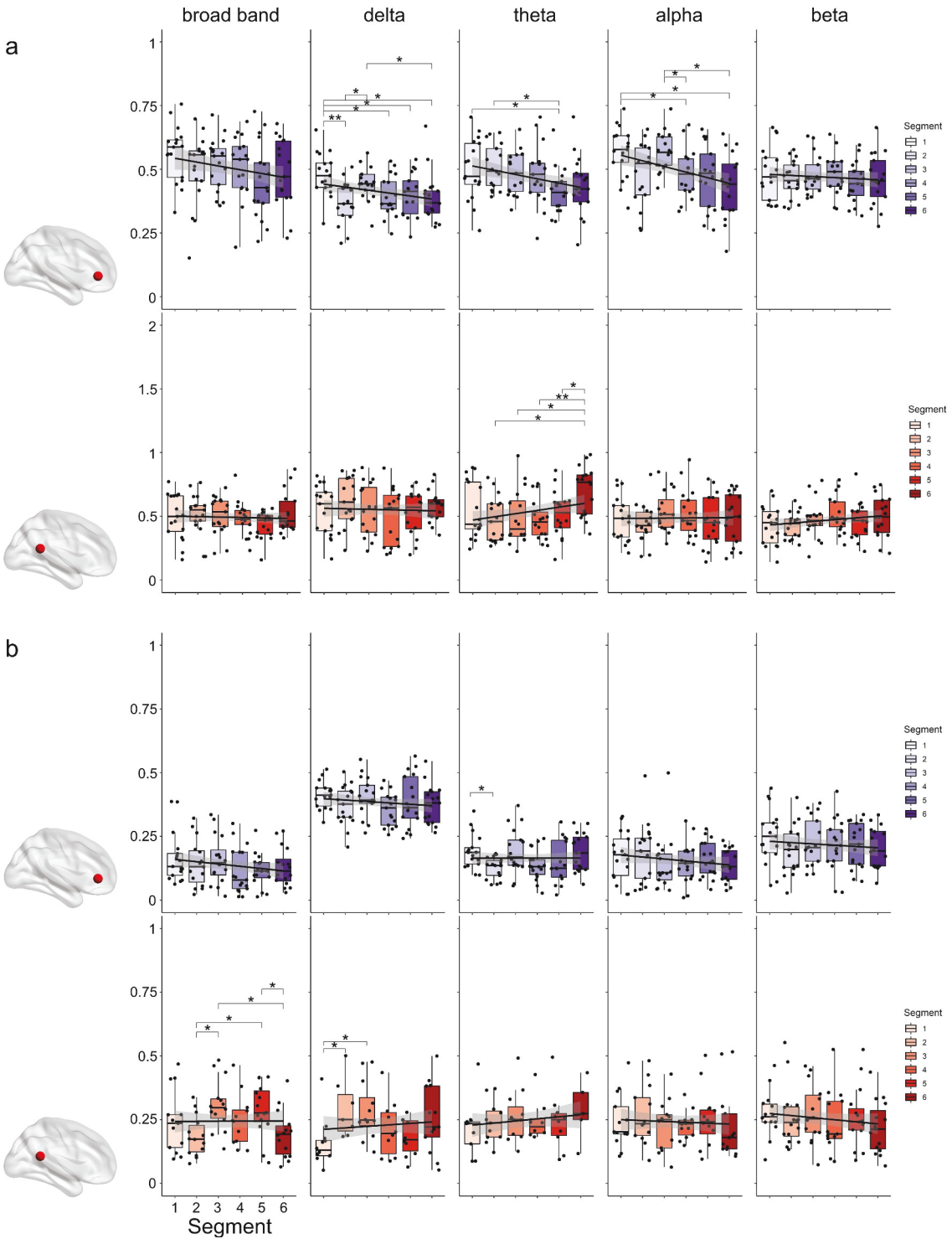

Figure 6.5 : Graph properties at the frontal and retrosplenial complex (RSC): (a) Clustering coefficient (a) and (b) participation coefficient across six walking segments in various frequency ranges. Pairwise post hoc Wilcoxon signed-rank tests (FDR-corrected) were used to check for significant differences between walking segments (* and ** indicate $p<0.05$ and $p<0.01$, respectively).

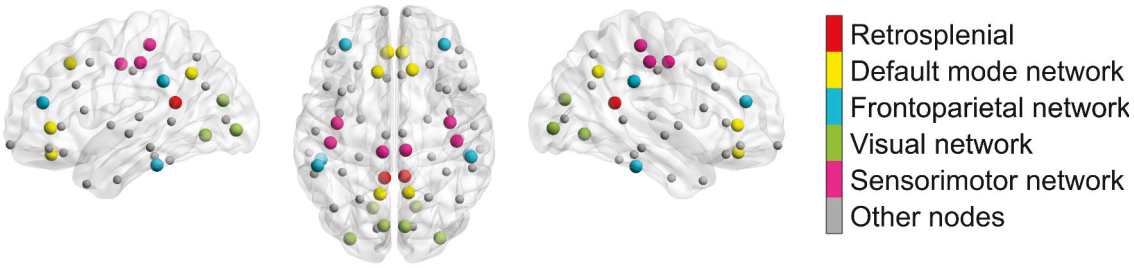

Figure 6.6 : Network atlas.

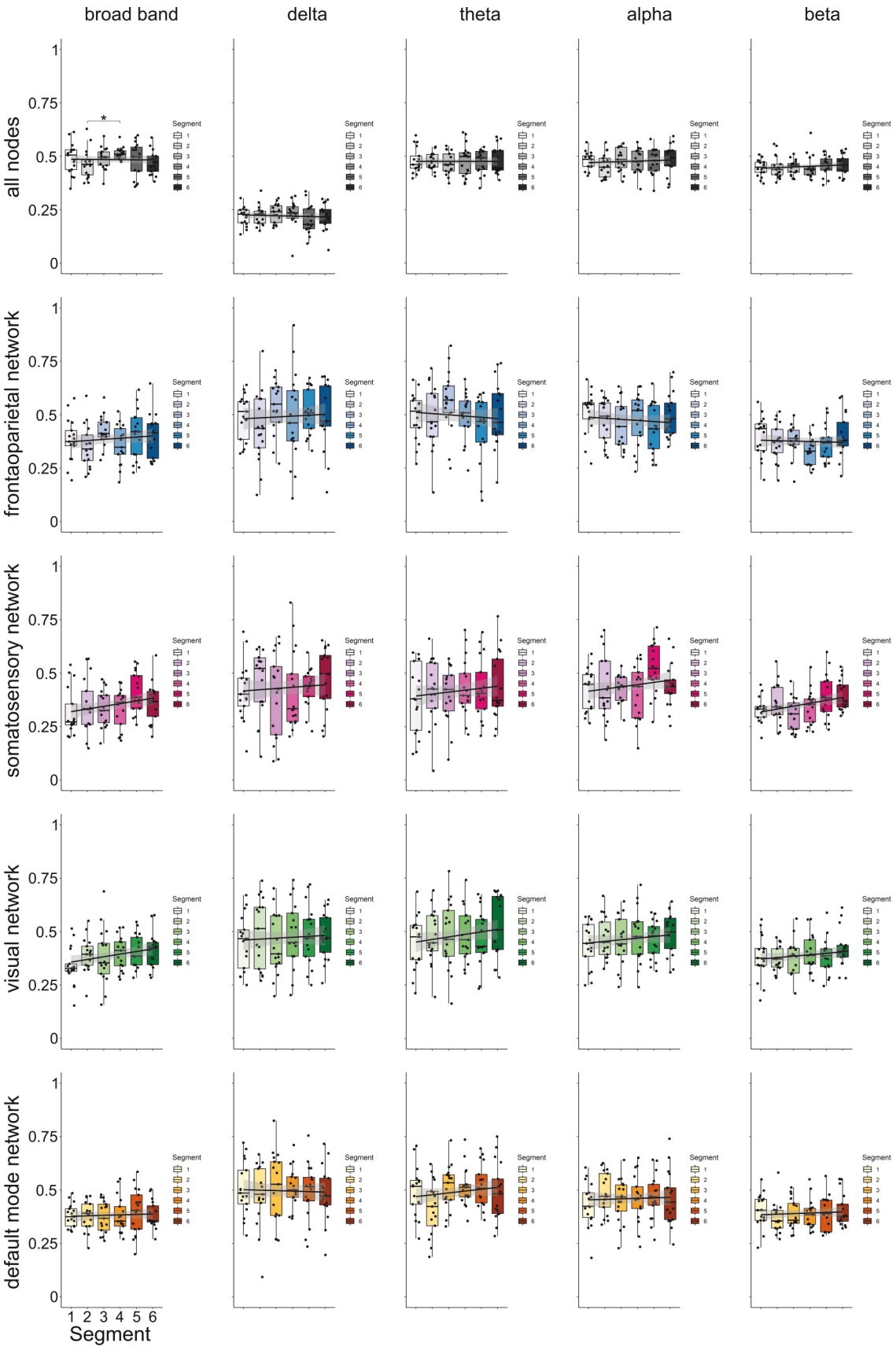

Figure 6.7 : Clustering coefficient among different brain networks, including the whole-brain network, frontoparietal network, somatosensory network, visual network, and default mode network across walking segments under various frequencies.

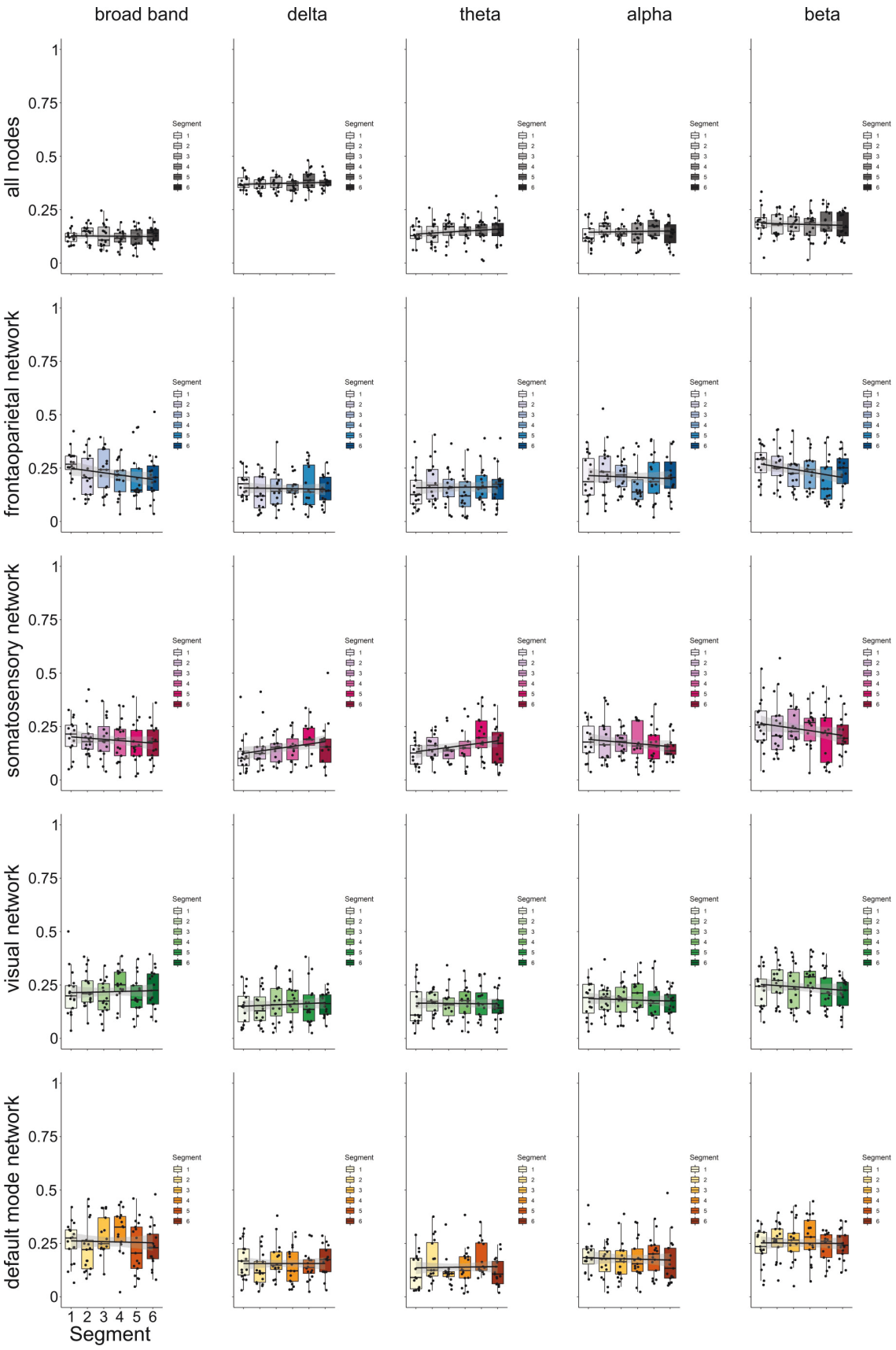

Figure 6.8 : Participation coefficients among different brain networks, including the whole-brain network, frontoparietal network, somatosensory network, visual network, and default mode network, across walking segments under various frequencies.

Chapter 7

Conclusion and Future Work

This thesis systematically unpacked the brain dynamics involved in multitasking in active navigation. We first designed two experiments that mimicked our daily navigation tasks: driving and walking. Due to the sensitivity of the measured EEG data, the tasks were designed to be from semi-active in the driving experiment, where participants could use their hands to control the car, to active navigation, where participants could use their full-body movement to perform the task. The simulated driving was mostly related to investigating brain dynamics in concurrent tasks, while the free ambulatory walking experiment demonstrated the neural activity in RSC in physical navigation.

The concurrent multitasking driving systematically exploring the executive control system that governs coordination and allocation of attention across multiple tasks. This study obtained evidence of the comodulatory activities that govern the allocation of attention across different stimulus modalities in dual-task experiments (Chapter 3). The IMA was applied to the spectra of temporally independent EEG components obtained from sessions using different stimulus modalities to contrast the differences of the resulting comodulators. For each experimental case, we found spectral fluctuations in distinct cortical areas that were mediated by the IM. The results demonstrated synchronized spectral fluctuations between distinct components. Furthermore, the results showed that the activation of the IM was related to continuous, dynamic allocation of attentional brain resources. Though the attentional resources were limited, the components had different spectral projection weights under different stimulus modalities engaged by the dual tasks. Regarding the effect of distractions on the brain-behavior relationship, the attentional resource allocation showed that the frontal component was allocated more attentional resources

for cognitive processing. In the occipital component, the region was associated with sensory processing or stimulus selection. Thus, more attentional resources were allocated while performing in dual-task conditions. Taken together, it was shown that secondary stimuli significantly affect brain-behavior relationships. Such findings could have major implications for understanding the underlying brain mechanisms that mediate synchronization across brain regions and govern the allocation of attention in distracted driving. The results of this simulated driving study could be a useful feature that can be adapted in the realistic driving experience to detect distracted driving based on the brain-behavior relationship.

Then, we further examined dynamic EEG changes in ECs across different fatigue states during the performance of single and dual tasks in the same simulated driving experiment (Chapter 4). Overall, increased EC was evident across the entire brain network during the dual tasks, which involved several brain regions. The EEG EC in the high-risk fatigue group was lower across all brain regions except the frontal region, which showed increased EC in the concurrent dual tasks compared to that in the single task. These brain network dynamics may have implications for understanding the complex neurophysiology of relationships between real-world fatigue and task conditions.

Furthermore, we analyzed some of the behaviors and neural dynamics associated with physical navigation (Chapter 5). We found that theta oscillations originating from the RSC are present during human navigation, more prominent while computing direction changes, and consistently synchronized irrespective of the length of the total path walked. In addition, retrieving spatial information is associated with alpha modulations in the RSC. As the first evidence of how our sense of direction works in healthy moving humans, these findings demonstrate that, for some, brain dynamics are not the same when thinking about navigating through space as opposed to actually moving through space.

Lastly, we investigated the behavior and neural dynamics in active spatial navigation under different workload conditions (Chapter 6). The behavior showed the increased error in the landmark pointing task when the number of turnings was

higher. We further investigated neural activity to find the underlying mechanism for this phenomenon. We found that the RSC local information processing via RSC increased when the number of turn points increased, reflecting that the RSC plays an important role in coordinate and process information in active navigation. In addition, we found that the decline in frontal segregation might reflect spatial navigation performance. These findings demonstrate that human brain dynamics systematically vary in stationary and physical navigation experiments. The change in RSC segregation could be an important feature for monitoring navigation workload in actively exploring space.

The results from studies on simulated driving and physical navigation provide some useful features that can be applied in real-life applications. Chapter 3 revealed that the frontal and parietal power correlated with the task-load. Chapter 4 further showed that there was an increase in brain connectivity when the task-load was higher. However, this brain pattern is different in the high fatigue group, which was measured based on sleep-related fatigue. Despite the driving simulation providing meaningful features for mental workload, the experimental design was limited to a semi-physical task, where participants still sat in the car. The participants could control the wheel, but their heads still kept looking toward the screen. This arrangement might eliminate other sensory effects that are often involved in real-life situations.

Chapter 5 continued to leverage the complexity of the experimental design. The participants could move freely in different locations inside the virtual environment. In this experimental design, the participant could receive richer information from motor efference, visual, proprioception, vestibular, and kinesthetic systems. However, the data in this active navigation experiment contained more noise than in the stationary experiment. The work in Chapters 5 and 6 overcame this issue by systematic analysis of the data using repeated k-mean for localizing the brain source of activation and effective connectivity to estimate the information flow between brain source and muscle cluster (Chapter 5) and distributed-source approach (Chapter 6). Thus, we believe that the findings in this experiment are reliable and non-sensitive

to noise from complex movement actions. Chapter 5 further provided information on the activity of the head direction cells network in active ambulation. This feature has been found in active movement experiments in rodents but not in healthy human participants. Chapter 6 demonstrated that the local information processed in the RSC is correlated with navigation load.

Frontal theta might reflect mental workload in multiple tasks. The RSC theta indicates heading computation in active navigation, and the RSC clustering coefficient might indicate navigation load with physical movement. Thus, the findings can provide useful features for supportive navigation hardware in the future.

There are various possibilities for further work. This EEG analysis pipeline has been evaluated in other work with different experimental designs, ensuring that it can be replicated and that it cleans the EEG data. Although this technique is solid in the current work, it could be improved by minimizing the error in source localization. In this work, we used the same MRI template for all participants; thus, the solution for inverse problem in dipole fitting and distributed source remains the error. In future work, we might need an individual MRI template of a participant to address this issue.

At the moment, EEG seems to be appropriate brain imaging hardware to investigate ambulatory spatial navigation. However, the features found by EEG in this work need to be confirmed with other brain imaging methods, such as MEG and fMRI. With rapid developments in technology, active navigation studies might be benefit from mobile MEG or even mobile fMRI hardware. However, that scenario may not happen within a decade.

This work is a step forward in bringing research from the laboratory to real-life applications. Although participants could perform the task with their full-body rotation and translation, the experimental design is still not sufficient to control co-founding factors. Thus, future work might involve more components to mimic dynamics and complexity from real-life situations.

And finally, the completed system of navigation assistance should be built to

evaluate the consistency of those human brain features. Intuitively, this system can assist navigators in navigating efficiently by adaptive presentation information in the head-mounted display based on their cognitive stages. Moreover, this completed system can be useful in many ways, like preventing lost, reducing mental workload. However, this evaluation will require a tremendous effort to be a success.

Bibliography

Adcock, R. A., Constable, R. T., Gore, J. C. & Goldman-Rakic, P. S., 2000, 'Functional neuroanatomy of executive processes involved in dual-task performance', *Proceedings of the National Academy of Sciences*, vol. 97, no. 7, pp. 3567–3572.

Aguirre, G. K., Detre, J. A., Alsop, D. C. & D'Esposito, M., 1996, 'The parahippocampus subserves topographical learning in man', *Cerebral cortex*, vol. 6, no. 6, pp. 823–829.

Akimoto, H., Yamaguchi, N., Okabe, K., Nakagawa, T., Nakamura, I., Abe, R., Torii, H. & Masahashi, K., 1956, 'On the sleep induced througb electrical stimulation on dog thalamus.', *Psychiatry and Clinical Neurosciences*, vol. 10, no. 2, pp. 117–146.

Al-Shargie, F., Tariq, U., Hassanin, O., Mir, H., Babiloni, F. & Al-Nashash, H., 2019, 'Brain connectivity analysis under semantic vigilance and enhanced mental states', *Brain Sciences*, vol. 9, no. 12, p. 363.

Anguera, J. A., Boccanfuso, J., Rintoul, J. L., Al-Hashimi, O., Faraji, F., Janowich, J., Kong, E., Larraburo, Y., Rolle, C. & Johnston, E., 2013, 'Video game training enhances cognitive control in older adults', *Nature*, vol. 501, no. 7465, p. 97.

Arora, A., Weiss, B., Schurz, M., Aichhorn, M., Wieshofer, R. C. & Perner, J., 2015, 'Left inferior-parietal lobe activity in perspective tasks: identity statements', *Frontiers in human neuroscience*, vol. 9, p. 360.

Arranz, M. A., 2005, 'Portmanteau test statistics in time series', *Time Orientated Language*, pp. 1–8.

Artoni, F., Fanciullacci, C., Bertolucci, F., Panarese, A., Makeig, S., Micera, S. & Chisari, C., 2017, 'Unidirectional brain to muscle connectivity reveals motor

cortex control of leg muscles during stereotyped walking', *NeuroImage*, vol. 159, pp. 403–416.

Banaei, M., Hatami, J., Yazdanfar, A. & Gramann, K., 2017, 'Walking through architectural spaces: The impact of interior forms on human brain dynamics', *Frontiers in Human Neuroscience*, vol. 11, p. 477.

Banino, A., Barry, C., Uria, B., Blundell, C., Lillicrap, T., Mirowski, P., Pritzel, A., Chadwick, M. J., Degris, T. & Modayil, J., 2018, 'Vector-based navigation using grid-like representations in artificial agents', *Nature*, p. 1.

Bardo, M. T., 1998, 'Neuropharmacological mechanisms of drug reward: beyond dopamine in the nucleus accumbens', *Critical Reviews™ in Neurobiology*, vol. 12, no. 1-2.

Barry, C., Hayman, R., Burgess, N. & Jeffery, K. J., 2007, 'Experience-dependent rescaling of entorhinal grids', *Nature neuroscience*, vol. 10, no. 6, p. 682.

Bassett, D. S., Yang, M., Wymbs, N. F. & Grafton, S. T., 2015, 'Learning-induced autonomy of sensorimotor systems', *Nature neuroscience*, vol. 18, no. 5, pp. 744–751.

Bassett, J. P., Zugaro, M. B., Muir, G. M., Golob, E. J., Muller, R. U. & Taube, J. S., 2005, 'Passive movements of the head do not abolish anticipatory firing properties of head direction cells', *Journal of neurophysiology*, vol. 93, no. 3, pp. 1304–1316.

Baumann, O. & Mattingley, J. B., 2010, 'Medial parietal cortex encodes perceived heading direction in humans', *Journal of Neuroscience*, vol. 30, no. 39, pp. 12897–12901.

Becker, W., Nasios, G., Raab, S. & Jürgens, R., 2002, 'Fusion of vestibular and podokinesthetic information during self-turning towards instructed targets', *Experimental brain research*, vol. 144, no. 4, pp. 458–474.

Bell, A. J. & Sejnowski, T. J., 1995, 'An information-maximization approach to blind separation and blind deconvolution', *Neural computation*, vol. 7, no. 6, pp. 1129–1159.

Bellmund, J. L., Deuker, L., Schröder, T. N. & Doeller, C. F., 2016, 'Grid-cell representations in mental simulation', *Elife*, vol. 5, p. e17089.

Bertram, E. H., 2010, 'Exploring the thalamus and its role in cortical function', *Journal of Neuro-Ophthalmology*, vol. 30, no. 1, pp. 110–111.

Betti, V., Della Penna, S., de Pasquale, F., Mantini, D., Marzetti, L., Romani, G. L. & Corbetta, M., 2013, 'Natural scenes viewing alters the dynamics of functional connectivity in the human brain', *Neuron*, vol. 79, no. 4, pp. 782–797.

Bird, C. M., Capponi, C., King, J. A., Doeller, C. F. & Burgess, N., 2010, 'Establishing the boundaries: the hippocampal contribution to imagining scenes', *Journal of Neuroscience*, vol. 30, no. 35, pp. 11688–11695.

Blumenfeld, H., Rivera, M., McNally, K., Davis, K., Spencer, D. & Spencer, S., 2004, 'Ictal neocortical slowing in temporal lobe epilepsy', *Neurology*, vol. 63, no. 6, pp. 1015–1021.

Boccara, C. N., Sargolini, F., Thoresen, V. H., Solstad, T., Witter, M. P., Moser, E. I. & Moser, M.-B., 2010, 'Grid cells in pre-and parasubiculum', *Nature neuroscience*, vol. 13, no. 8, p. 987.

Bohbot, V. D., Copara, M. S., Gotman, J. & Ekstrom, A. D., 2017, 'Low-frequency theta oscillations in the human hippocampus during real-world and virtual navigation', *Nature Communications*, vol. 8, p. 14415.

Borragán, G., Guerrero-Mosquera, C., Guillaume, C., Slama, H. & Peigneux, P., 2019, 'Decreased prefrontal connectivity parallels cognitive fatigue-related performance decline after sleep deprivation. an optical imaging study', *Biological Psychology*.

Brandon, M. P., Bogaard, A. R., Libby, C. P., Connerney, M. A., Gupta, K. & Hasselmo, M. E., 2011, 'Reduction of theta rhythm dissociates grid cell spatial periodicity from directional tuning', *Science*, vol. 332, no. 6029, pp. 595–599.

Bullmore, E. & Sporns, O., 2009, 'Complex brain networks: graph theoretical analysis of structural and functional systems', *Nature Reviews Neuroscience*, vol. 10, no. 3, pp. 186–198.

Burgess, N., Maguire, E. A., Spiers, H. J. & O'Keefe, J., 2001, 'A temporoparietal and prefrontal network for retrieving the spatial context of lifelike events', *Neuroimage*, vol. 14, no. 2, pp. 439–453.

Byrne, P., Becker, S. & Burgess, N., 2007, 'Remembering the past and imagining the future: a neural model of spatial memory and imagery.', *Psychological review*, vol. 114, no. 2, p. 340.

Cassady, K., Gagnon, H., Lalwani, P., Simmonite, M., Foerster, B., Park, D., Peltier, S. J., Petrou, M., Taylor, S. F., Weissman, D. H. et al., 2019, 'Sensorimotor network segregation declines with age and is linked to gaba and to sensorimotor performance', *Neuroimage*, vol. 186, pp. 234–244.

Cavanagh, J. F. & Frank, M. J., 2014, 'Frontal theta as a mechanism for cognitive control', *Trends in cognitive sciences*, vol. 18, no. 8, pp. 414–421.

Chadwick, M. J., Jolly, A. E., Amos, D. P., Hassabis, D. & Spiers, H. J., 2015, 'A goal direction signal in the human entorhinal/subicular region', *Current Biology*, vol. 25, no. 1, pp. 87–92.

Chan, M. Y., Park, D. C., Savalia, N. K., Petersen, S. E. & Wig, G. S., 2014, 'Decreased segregation of brain systems across the healthy adult lifespan', *Proceedings of the National Academy of Sciences*, vol. 111, no. 46, pp. E4997–E5006.

Chen, X., DeAngelis, G. C. & Angelaki, D. E., 2018, 'Flexible egocentric and allocentric representations of heading signals in parietal cortex', *Proceedings of the National Academy of Sciences*, vol. 115, no. 14, pp. E3305–E3312.

Chiu, T.-C., Gramann, K., Ko, L.-W., Duann, J.-R., Jung, T.-P. & Lin, C.-T., 2012, 'Alpha modulation in parietal and retrosplenial cortex correlates with navigation performance', *Psychophysiology*, vol. 49, no. 1, pp. 43–55.

Chuang, S.-W., Chuang, C.-H., Yu, Y.-H., King, J.-T. & Lin, C.-T., 2016, 'EEG alpha and gamma modulators mediate motion sickness-related spectral responses', *International journal of neural systems*, vol. 26, no. 02, p. 1650007.

Chuang, S.-W., Ko, L.-W., Lin, Y.-P., Huang, R.-S., Jung, T.-P. & Lin, C.-T., 2012, 'Co-modulatory spectral changes in independent brain processes are correlated with task performance', *Neuroimage*, vol. 62, no. 3, pp. 1469–1477.

Clark, B. J., Bassett, J. P., Wang, S. S. & Taube, J. S., 2010, 'Impaired head direction cell representation in the anterodorsal thalamus after lesions of the retrosplenial cortex', *Journal of Neuroscience*, vol. 30, no. 15, pp. 5289–5302.

Cohen, J. R. & D'Esposito, M., 2016, 'The segregation and integration of distinct brain networks and their relationship to cognition', *Journal of Neuroscience*, vol. 36, no. 48, pp. 12083–12094.

Cohen, M. X., 2014, *Analyzing neural time series data: theory and practice*, MIT press.

Cole, M. W., Bassett, D. S., Power, J. D., Braver, T. S. & Petersen, S. E., 2014, 'Intrinsic and task-evoked network architectures of the human brain', *Neuron*, vol. 83, no. 1, pp. 238–251.

Committeri, G., Galati, G., Paradis, A.-L., Pizzamiglio, L., Berthoz, A. & LeBihan, D., 2004, 'Reference frames for spatial cognition: different brain areas are involved in viewer-, object-, and landmark-centered judgments about object location', *Journal of Cognitive Neuroscience*, vol. 16, no. 9, pp. 1517–1535.

Cullen, K. E. & Taube, J. S., 2017, 'Our sense of direction: progress, controversies and challenges', *Nature neuroscience*, vol. 20, no. 11, p. 1465.

De Sanctis, P., Butler, J. S., Malcolm, B. R. & Foxe, J. J., 2014, 'Recalibration of inhibitory control systems during walking-related dual-task interference: a mobile brain-body imaging (mobi) study', *Neuroimage*, vol. 94, pp. 55–64.

Delorme, A. & Makeig, S., 2004, 'EEGLAB: an open source toolbox for analysis of single-trial EEG dynamics including independent component analysis', *Journal of neuroscience methods*, vol. 134, no. 1, pp. 9–21.

Delorme, A., Mullen, T., Kothe, C., Acar, Z. A., Bigdely-Shamlo, N., Vankov, A. & Makeig, S., 2011, 'EEGLAB, SIFT, NFT, BCILAB, and ERICA: new tools for advanced EEG processing', *Computational intelligence and neuroscience*, vol. 2011, p. 10.

Delorme, A., Palmer, J., Onton, J., Oostenveld, R. & Makeig, S., 2012, 'Independent EEG sources are dipolar', *PloS one*, vol. 7, no. 2, p. e30135.

DeSalvo, M. N., Douw, L., Takaya, S., Liu, H. & Stufflebeam, S. M., 2014, 'Task-dependent reorganization of functional connectivity networks during visual semantic decision making', *Brain and behavior*, vol. 4, no. 6, pp. 877–885.

Desikan, R. S., Ségonne, F., Fischl, B., Quinn, B. T., Dickerson, B. C., Blacker, D., Buckner, R. L., Dale, A. M., Maguire, R. P., Hyman, B. T. et al., 2006, 'An automated labeling system for subdividing the human cerebral cortex on mri scans into gyral based regions of interest', *Neuroimage*, vol. 31, no. 3, pp. 968–980.

Ding, M., Bressler, S. L., Yang, W. & Liang, H., 2000, 'Short-window spectral analysis of cortical event-related potentials by adaptive multivariate autoregressive modeling: data preprocessing, model validation, and variability assessment', *Biological cybernetics*, vol. 83, no. 1, pp. 35–45.

Do, T.-T. N., Chuang, C.-H., Hsiao, S.-J., Lin, C.-T. & Wang, Y.-K., 2019, 'Neural comodulation of independent brain processes related to multitasking', *IEEE Transactions on Neural Systems and Rehabilitation Engineering*, vol. 27, no. 6, pp. 1160–1169.

Do, T.-T. N., Jung, T.-P. & Lin, C.-T., 2020a, 'Retrosplenial segregation reflects mental workload in physical spatial navigation', .

Do, T.-T. N., Lin, C.-T. & Gramann, K., 2020b, 'Human retrosplenial theta and alpha modulation in active spatial navigation', .

Do, T.-T. N., Wang, Y.-K. & Lin, C.-T., 2020c, 'Increase in brain effective connectivity in multitasking but not in a high-fatigue state', *IEEE Transactions on Cognitive and Developmental Systems*.

Doeller, C. F., Barry, C. & Burgess, N., 2010, 'Evidence for grid cells in a human memory network', *Nature*, vol. 463, no. 7281, pp. 657–661.

Doeller, C. F., King, J. A. & Burgess, N., 2008, 'Parallel striatal and hippocampal systems for landmarks and boundaries in spatial memory', *Proceedings of the National Academy of Sciences*, vol. 105, no. 15, pp. 5915–5920.

Drews, F. A., Pasupathi, M. & Strayer, D. L., 2008, 'Passenger and cell phone conversations in simulated driving', *Journal of Experimental Psychology: Applied*, vol. 14, no. 4, p. 392.

Dux, P. E., Ivanoff, J., Asplund, C. L. & Marois, R., 2006, 'Isolation of a central bottleneck of information processing with time-resolved fmri', *Neuron*, vol. 52, no. 6, pp. 1109–1120.

Dux, P. E., Tombu, M. N., Harrison, S., Rogers, B. P., Tong, F. & Marois, R., 2009, 'Training improves multitasking performance by increasing the speed of information processing in human prefrontal cortex', *Neuron*, vol. 63, no. 1, pp. 127–138.

Ehinger, B. V., Fischer, P., Gert, A. L., Kaufhold, L., Weber, F., Pipa, G. & König, P., 2014, 'Kinesthetic and vestibular information modulate alpha activity during spatial navigation: a mobile EEG study', *Frontiers in human neuroscience*, vol. 8.

Ekstrom, A. D., Kahana, M. J., Caplan, J. B., Fields, T. A., Isham, E. A., Newman,

E. L. & Fried, I., 2003, 'Cellular networks underlying human spatial navigation', *Nature*, vol. 425, no. 6954, p. 184.

Epstein, R. & Kanwisher, N., 1998, 'A cortical representation of the local visual environment', *Nature*, vol. 392, no. 6676, pp. 598–601.

Epstein, R. A., 2008, 'Parahippocampal and retrosplenial contributions to human spatial navigation', *Trends in cognitive sciences*, vol. 12, no. 10, pp. 388–396.

Epstein, R. A., Patai, E. Z., Julian, J. B. & Spiers, H. J., 2017, 'The cognitive map in humans: spatial navigation and beyond', *Nature neuroscience*, vol. 20, no. 11, p. nn. 4656.

Epstein, R. A. & Vass, L. K., 2014, 'Neural systems for landmark-based wayfinding in humans', *Phil. Trans. R. Soc. B*, vol. 369, no. 1635, p. 20120533.

Esposito, M. D., Detre, J. A., Alsop, D. C. & Shin, R. K., 1995, 'The neural basis of the central executive system of working memory', *Nature*, vol. 378, no. 6554, p. 279.

Fernández, T., Harmony, T., Rodríguez, M., Bernal, J., Silva, J., Reyes, A. & Marosi, E., 1995, 'EEG activation patterns during the performance of tasks involving different components of mental calculation', *Electroencephalography and clinical Neurophysiology*, vol. 94, no. 3, pp. 175–182.

Fischl, B., 2012, 'Freesurfer', *Neuroimage*, vol. 62, no. 2, pp. 774–781.

Fonov, V. S., Evans, A. C., McKinstry, R. C., Almli, C. & Collins, D., 2009, 'Unbiased nonlinear average age-appropriate brain templates from birth to adulthood', *NeuroImage*, vol. 54, no. 47, p. S102.

Fonseca, A., Kerick, S., King, J.-T., Lin, C.-T. & Jung, T.-P., 2018, 'Brain network changes in fatigued drivers: a longitudinal study in a real-world environment based on the effective connectivity analysis and actigraphy data', *Frontiers in human neuroscience*, vol. 12, p. 418.

Fransson, P., Schiffler, B. C. & Thompson, W. H., 2018, 'Brain network segregation and integration during an epoch-related working memory fmri experiment', *Neuroimage*, vol. 178, pp. 147–161.

Frissen, I., Campos, J. L., Souman, J. L. & Ernst, M. O., 2011, 'Integration of vestibular and proprioceptive signals for spatial updating', *Experimental brain research*, vol. 212, no. 2, p. 163.

Friston, K. J., 2011, 'Functional and effective connectivity: a review', *Brain connectivity*, vol. 1, no. 1, pp. 13–36.

Gevins, A., Smith, M. E., McEvoy, L. & Yu, D., 1997, 'High-resolution EEG mapping of cortical activation related to working memory: effects of task difficulty, type of processing, and practice', *Cerebral cortex (New York, NY: 1991)*, vol. 7, no. 4, pp. 374–385.

Ghaem, O., Mellet, E., Crivello, F., Tzourio, N., Mazoyer, B., Berthoz, A. & Denis, M., 1997, 'Mental navigation along memorized routes activates the hippocampus, precuneus, and insula', *Neuroreport*, vol. 8, no. 3, pp. 739–744.

Goeke, C., Kornpetpanee, S., Köster, M., Fernández-Revelles, A. B., Gramann, K. & König, P., 2015, 'Cultural background shapes spatial reference frame proclivity', *Scientific reports*, vol. 5, p. 11426.

Gonzalez-Castillo, J. & Bandettini, P. A., 2017, 'Task-based dynamic functional connectivity: Recent findings and open questions', *Neuroimage*.

Gottsdanker, R. & Way, T. C., 1966, 'Varied and constant intersignal intervals in psychological refractoriness', *Journal of Experimental Psychology*, vol. 72, no. 6, p. 792.

Gramann, K., 2013, 'Embodiment of spatial reference frames and individual differences in reference frame proclivity', *Spatial Cognition & Computation*, vol. 13, no. 1, pp. 1–25.

Gramann, K., Ferris, D. P., Gwin, J. & Makeig, S., 2014a, 'Imaging natural cognition in action', *International Journal of Psychophysiology*, vol. 91, no. 1, pp. 22–29.

Gramann, K., Gwin, J. T., Ferris, D. P., Oie, K., Jung, T.-P., Lin, C.-T., Liao, L.-D. & Makeig, S., 2011, 'Cognition in action: imaging brain/body dynamics in mobile humans', *Reviews in the Neurosciences*, vol. 22, no. 6, pp. 593–608.

Gramann, K., Hohlefeld, F. U., Gehrke, L. & Klug, M., 2018, 'Heading computation in the human retrosplenial complex during full-body rotation', *BioRxiv*, p. 417972.

Gramann, K., Jung, T.-P., Ferris, D. P., Lin, C.-T. & Makeig, S., 2014b, 'Toward a new cognitive neuroscience: modeling natural brain dynamics', *Frontiers in human neuroscience*, vol. 8.

Gramann, K., Müller, H., Schönebeck, B. & Debus, G., 2006, 'The neural basis of ego-and allocentric reference frames in spatial navigation: Evidence from spatio-temporal coupled current density reconstruction', *Brain research*, vol. 1118, no. 1, pp. 116–129.

Gramann, K., Müller, H. J., Eick, E.-M. & Schönebeck, B., 2005, 'Evidence of separable spatial representations in a virtual navigation task', *Journal of Experimental Psychology: Human Perception and Performance*, vol. 31, no. 6, p. 1199.

Gramann, K., Onton, J., Riccobon, D., Mueller, H. J., Bardins, S. & Makeig, S., 2010, 'Human brain dynamics accompanying use of egocentric and allocentric reference frames during navigation', *Journal of cognitive neuroscience*, vol. 22, no. 12, pp. 2836–2849.

Gramfort, A., Papadopoulo, T., Olivi, E. & Clerc, M., 2010, 'Openmeeg: open-source software for quasistatic bioelectromagnetics', *Biomedical engineering online*, vol. 9, no. 1, p. 45.

Grandchamp, R. & Delorme, A., 2011, 'Single-trial normalization for event-related spectral decomposition reduces sensitivity to noisy trials', *Frontiers in psychology*, vol. 2, p. 236.

Granger, C. W., 1969, 'Investigating causal relations by econometric models and cross-spectral methods', *Econometrica Journal of the Econometric Society*, pp. 424–438.

Hafting, T., Fyhn, M., Molden, S., Moser, M.-B. & Moser, E. I., 2005, 'Microstructure of a spatial map in the entorhinal cortex', *Nature*, vol. 436, no. 7052, p. 801.

Han, C., Sun, X., Yang, Y., Che, Y. & Qin, Y., 2019, 'Brain complex network characteristic analysis of fatigue during simulated driving based on electroencephalogram signals', *Entropy*, vol. 21, no. 4, p. 353.

Harris, M. A. & Wolbers, T., 2012, 'Ageing effects on path integration and landmark navigation', *Hippocampus*, vol. 22, no. 8, pp. 1770–1780.

Hartley, T., Trinkler, I. & Burgess, N., 2004, 'Geometric determinants of human spatial memory', *Cognition*, vol. 94, no. 1, pp. 39–75.

Herath, P., Klingberg, T., Young, J., Amunts, K. & Roland, P., 2001, 'Neural correlates of dual task interference can be dissociated from those of divided attention: an fmri study', *Cerebral cortex*, vol. 11, no. 9, pp. 796–805.

Herculano-Houzel, S., Munk, M. H., Neuenschwander, S. & Singer, W., 1999, 'Precisely synchronized oscillatory firing patterns require electroencephalographic activation', *Journal of neuroscience*, vol. 19, no. 10, pp. 3992–4010.

Herman, L. M. & Kantowitz, B. H., 1970, 'The psychological refractory period effect: Only half the double-stimulation story?', *Psychological Bulletin*, vol. 73, no. 1, p. 74.

Hick, W. E., 1952, 'On the rate of gain of information', *Quarterly Journal of Experimental Psychology*, vol. 4, no. 1, pp. 11–26.

Hsieh, L.-T. & Ranganath, C., 2014, 'Frontal midline theta oscillations during working memory maintenance and episodic encoding and retrieval', *Neuroimage*, vol. 85, pp. 721–729.

Huang, C.-S., Pal, N. R., Chuang, C.-H. & Lin, C.-T., 2015, 'Identifying changes in EEG information transfer during drowsy driving by transfer entropy', *Frontiers in human neuroscience*, vol. 9.

Huang, K.-C., Huang, T.-Y., Chuang, C.-H., King, J.-T., Wang, Y.-K., Lin, C.-T. & Jung, T.-P., 2016, 'An EEG-based fatigue detection and mitigation system', *International journal of neural systems*, vol. 26, no. 04, p. 1650018.

Huang, L.-Y., She, H.-C., Chou, W.-C., Chuang, M.-H., Duann, J.-R. & Jung, T.-P., 2013, 'Brain oscillation and connectivity during a chemistry visual working memory task', *International Journal of Psychophysiology*, vol. 90, no. 2, pp. 172–179.

Huang, R.-S., Jung, T.-P., Delorme, A. & Makeig, S., 2008, 'Tonic and phasic electroencephalographic dynamics during continuous compensatory tracking', *NeuroImage*, vol. 39, no. 4, pp. 1896–1909.

Huang, R.-S., Jung, T.-P. & Makeig, S., 2009, 'Tonic changes in EEG power spectra during simulated driving', *Foundations of augmented cognition. neuroergonomics and operational neuroscience*, pp. 394–403.

Huang, R.-S., Tsai, L.-L. & Kuo, C. J., 2001, 'Selection of valid and reliable EEG features for predicting auditory and visual alertness levels', *Proceedings-national Science Council Republic of China Part B Life Sciences*, vol. 25, no. 1, pp. 17–25.

Hursh, S. R., Raslear, T. G., Kaye, A. S. & Fanzone Jr, J. F., 2006, 'Validation and calibration of a fatigue assessment tool for railroad work schedules, summary report', Report.

Hursh, S. R., Redmond, D. P., Johnson, M. L., Thorne, D. R., Belenky, G., Balkin, T. J., Storm, W. F., Miller, J. C. & Eddy, D. R., 2004, 'Fatigue models for applied research in warfighting', *Aviation, space, and environmental medicine*, vol. 75, no. 3, pp. A44–A53.

Hyman, R., 1953, 'Stimulus information as a determinant of reaction time', *Journal of experimental psychology*, vol. 45, no. 3, p. 188.

Jaeggi, S. M., Seewer, R., Nirkko, A. C., Eckstein, D., Schroth, G., Groner, R. & Gutbrod, K., 2003, 'Does excessive memory load attenuate activation in the prefrontal cortex? load-dependent processing in single and dual tasks: functional magnetic resonance imaging study', *NeuroImage*, vol. 19, no. 2, pp. 210–225.

Jap, B. T., Lal, S., Fischer, P. & Bekiaris, E., 2009, 'Using EEG spectral components to assess algorithms for detecting fatigue', *Expert Systems with Applications*, vol. 36, no. 2, pp. 2352–2359.

Javadi, A.-H., Emo, B., Howard, L. R., Zisch, F. E., Yu, Y., Knight, R., Silva, J. P. & Spiers, H. J., 2017, 'Hippocampal and prefrontal processing of network topology to simulate the future', *Nature communications*, vol. 8, p. 14652.

Jung, T.-P., Makeig, S., McKeown, M. J., Bell, A. J., Lee, T.-W. & Sejnowski, T. J., 2001, 'Imaging brain dynamics using independent component analysis', *Proceedings of the IEEE*, vol. 89, no. 7, pp. 1107–1122.

Jung, T.-P., Makeig, S., Stensmo, M. & Sejnowski, T. J., 1997, 'Estimating alertness from the EEG power spectrum', *IEEE transactions on biomedical engineering*, vol. 44, no. 1, pp. 60–69.

Jungnickel, E., Gehrke, L., Klug, M. & Gramann, K., 2019, 'Mobi—mobile brain/body imaging', *Neuroergonomics*, Elsevier, pp. 59–63.

Jungnickel, E. & Gramann, K., 2016, 'Mobile brain/body imaging (mobi) of physical interaction with dynamically moving objects', *Frontiers in human neuroscience*, vol. 10.

Jürgens, R. & Becker, W., 2006, 'Perception of angular displacement without landmarks: evidence for bayesian fusion of vestibular, optokinetic, podokinesthetic, and cognitive information', *Experimental Brain Research*, vol. 174, no. 3, pp. 528–543.

Just, M. A., Carpenter, P. A., Keller, T. A., Emery, L., Zajac, H. & Thulborn, K. R., 2001, 'Interdependence of nonoverlapping cortical systems in dual cognitive tasks', *Neuroimage*, vol. 14, no. 2, pp. 417–426.

Just, M. A., Keller, T. A. & Cynkar, J., 2008, 'A decrease in brain activation associated with driving when listening to someone speak', *Brain research*, vol. 1205, pp. 70–80.

Kahana, M. J., 2006, 'The cognitive correlates of human brain oscillations', *Journal of Neuroscience*, vol. 26, no. 6, pp. 1669–1672.

Kahneman, D., 1973, *Attention and effort*, vol. 1063, Prentice-Hall Englewood Cliffs, NJ.

Kane, M. J. & Engle, R. W., 2002, 'The role of prefrontal cortex in working-memory capacity, executive attention, and general fluid intelligence: An individual-differences perspective', *Psychonomic bulletin and review*, vol. 9, no. 4, pp. 637–671.

Kar, K., Kubilius, J., Schmidt, K., Issa, E. B. & DiCarlo, J. J., 2019, 'Evidence that recurrent circuits are critical to the ventral stream's execution of core object recognition behavior', *Nature neuroscience*, vol. 22, no. 6, pp. 974–983.

Kim, M. & Maguire, E. A., 2019, 'Encoding of 3d head direction information in the human brain', *Hippocampus*, vol. 29, no. 7, pp. 619–629.

Kim, N. Y., Wittenberg, E. & Nam, C. S., 2017, 'Behavioral and neural correlates of executive function: Interplay between inhibition and updating processes', *Frontiers in Neuroscience*, vol. 11, p. 14.

King, B., Van Ruitenbeek, P., Leunissen, I., Cuypers, K., Heise, K.-F., Santos Monteiro, T., Hermans, L., Levin, O., Albouy, G., Mantini, D. et al., 2018, 'Age-related declines in motor performance are associated with decreased segregation of large-scale resting state brain networks', *Cerebral Cortex*, vol. 28, no. 12, pp. 4390–4402.

Klatzky, R. L., 1998, 'Allocentric and egocentric spatial representations: Definitions, distinctions, and interconnections', *Spatial cognition*, Springer, pp. 1–17.

Klimesch, W., 1999, 'EEG alpha and theta oscillations reflect cognitive and memory performance: a review and analysis', *Brain research reviews*, vol. 29, no. 2-3, pp. 169–195.

Knierim, J. J., Kudrimoti, H. S. & McNaughton, B. L., 1995, 'Place cells, head direction cells, and the learning of landmark stability', *Journal of Neuroscience*, vol. 15, no. 3, pp. 1648–1659.

Koenig, J., Linder, A. N., Leutgeb, J. K. & Leutgeb, S., 2011, 'The spatial periodicity of grid cells is not sustained during reduced theta oscillations', *Science*, vol. 332, no. 6029, pp. 592–595.

Kothe, C., 2014, 'Lab streaming layer (lsl)', .

Krupic, J., Bauza, M., Burton, S., Barry, C. & O'Keefe, J., 2015, 'Grid cell symmetry is shaped by environmental geometry', *Nature*, vol. 518, no. 7538, p. 232.

Kubilius, J., Schrimpf, M., Kar, K., Hong, H., Majaj, N. J., Rajalingham, R., Issa, E. B., Bashivan, P., Prescott-Roy, J., Schmidt, K. et al., 2019, 'Brain-like object recognition with high-performing shallow recurrent anns', *arXiv preprint arXiv:1909.06161*.

Kwon, S., Watanabe, M., Fischer, E. & Bartels, A., 2017, 'Attention reorganizes connectivity across networks in a frequency specific manner', *NeuroImage*, vol. 144, pp. 217–226.

Kybic, J., Clerc, M., Abboud, T., Faugeras, O., Keriven, R. & Papadopoulo, T., 2005, 'A common formalism for the integral formulations of the forward EEG problem', *IEEE transactions on medical imaging*, vol. 24, no. 1, pp. 12–28.

Lachaux, J.-P., Rodriguez, E., Martinerie, J. & Varela, F. J., 1999, 'Measuring phase synchrony in brain signals', *Human brain mapping*, vol. 8, no. 4, pp. 194–208.

Lakshminarasimhan, K. J., Petsalis, M., Park, H., DeAngelis, G. C., Pitkow, X. & Angelaki, D. E., 2018, 'A dynamic bayesian observer model reveals origins of bias in visual path integration', *Neuron*, vol. 99, no. 1, pp. 194–206.

Lal, S. K. & Craig, A., 2001, 'A critical review of the psychophysiology of driver fatigue', *Biological psychology*, vol. 55, no. 3, pp. 173–194.

Lal, S. K. & Craig, A., 2002, 'Driver fatigue: electroencephalography and psychological assessment', *Psychophysiology*, vol. 39, no. 3, pp. 313–321.

Lal, S. K., Craig, A., Boord, P., Kirkup, L. & Nguyen, H., 2003, 'Development of an algorithm for an EEG-based driver fatigue countermeasure', *Journal of safety Research*, vol. 34, no. 3, pp. 321–328.

Lappe, M., Jenkin, M. & Harris, L. R., 2007, 'Travel distance estimation from visual motion by leaky path integration', *Experimental brain research*, vol. 180, no. 1, pp. 35–48.

Lin, C.-T., Chen, S.-A., Chiu, T.-T., Lin, H.-Z. & Ko, L.-W., 2011, 'Spatial and temporal EEG dynamics of dual-task driving performance', *Journal of neuroengineering and rehabilitation*, vol. 8, no. 1, p. 11.

Lin, C.-T., Chiu, T.-C. & Gramann, K., 2015, 'EEG correlates of spatial orientation in the human retrosplenial complex', *NeuroImage*, vol. 120, pp. 123–132.

Lin, C.-T., Chiu, T.-C., Wang, Y.-K., Chuang, C.-H. & Gramann, K., 2017, 'Granger causal connectivity dissociates navigation networks that subserve allocentric and egocentric path integration', *Brain Research*.

Lin, C.-T., Chuang, C.-H., Kerick, S., Mullen, T., Jung, T.-P., Ko, L.-W., Chen, S.-A., King, J.-T. & McDowell, K., 2016, 'Mind-wandering tends to occur under low perceptual demands during driving', *Scientific reports*, vol. 6, p. 21353.

Lin, C.-T., Huang, K.-C., Chuang, C.-H., Ko, L.-W. & Jung, T.-P., 2013, 'Can arousing feedback rectify lapses in driving? prediction from EEG power spectra', *Journal of neural engineering*, vol. 10, no. 5, p. 056024.

Lin, C.-T., Nascimben, M., King, J.-T. & Wang, Y.-K., 2018, 'Task-related EEG and HRV entropy factors under different real-world fatigue scenarios', *Neurocomputing*, vol. 311, pp. 24–31.

Lisman, J., Buzsáki, G., Eichenbaum, H., Nadel, L., Rangananth, C. & Redish, A. D., 2017, 'Viewpoints: how the hippocampus contributes to memory, navigation and cognition', *Nature*, vol. 20, p. 1.

Lord, S. A. G. & Marsh, G. R., 1975, 'Age differences in the speed of a spatial cognitive process', *Journal of Gerontology*, vol. 30, no. 6, pp. 674–678.

Lütkepohl, H., 2005, *New introduction to multiple time series analysis*, Springer Science and Business Media.

Luu, T. P., Brantley, J. A., Nakagome, S., Zhu, F. & Contreras-Vidal, J. L., 2017, 'Electrocortical correlates of human level-ground, slope, and stair walking', *PloS one*, vol. 12, no. 11, p. e0188500.

Maguire, E. A., Burgess, N., Donnett, J. G., Frackowiak, R. S., Frith, C. D. & O'keefe, J., 1998, 'Knowing where and getting there: a human navigation network', *Science*, vol. 280, no. 5365, pp. 921–924.

Maguire, E. A., Nannery, R. & Spiers, H. J., 2006, 'Navigation around london by a taxi driver with bilateral hippocampal lesions', *Brain*, vol. 129, no. 11, pp. 2894–2907.

Maidenbaum, S., Miller, J., Stein, J. M. & Jacobs, J., 2018, 'Grid-like hexadirectional modulation of human entorhinal theta oscillations', *Proceedings of the National Academy of Sciences*, vol. 115, no. 42, pp. 10798–10803.

Makeig, S., Bell, A. J., Jung, T.-P. & Sejnowski, T. J., 1996, 'Independent component analysis of electroencephalographic data', *Advances in neural information processing systems*, pp. 145–151.

Makeig, S., Gramann, K., Jung, T.-P., Sejnowski, T. J. & Poizner, H., 2009, 'Linking brain, mind and behavior', *International Journal of Psychophysiology*, vol. 73, no. 2, pp. 95–100.

Makeig, S. & Jung, T.-P., 1996, 'Tonic, phasic, and transient EEG correlates of

auditory awareness in drowsiness', *Cognitive Brain Research*, vol. 4, no. 1, pp. 15–25.

Makeig, S., Jung, T.-P. & Sejnowski, T. J., 2000, 'Awareness during drowsiness: Dynamics and electrophysiological correlates', *Canadian Journal of Experimental Psychology/Revue canadienne de psychologie expérimentale*, vol. 54, no. 4, p. 266.

Malcolm, B. R., Foxe, J. J., Butler, J. S. & De Sanctis, P., 2015, 'The aging brain shows less flexible reallocation of cognitive resources during dual-task walking: a mobile brain/body imaging (mobi) study', *Neuroimage*, vol. 117, pp. 230–242.

Marchette, S. A., Vass, L. K., Ryan, J. & Epstein, R. A., 2014, 'Anchoring the neural compass: coding of local spatial reference frames in human medial parietal lobe', *Nature neuroscience*, vol. 17, no. 11, p. 1598.

Masters, M. S. & Sanders, B., 1993, 'Is the gender difference in mental rotation disappearing?', *Behavior genetics*, vol. 23, no. 4, pp. 337–341.

Masuda, T. & Nisbett, R. E., 2001, 'Attending holistically versus analytically: comparing the context sensitivity of japanese and americans', *Journal of personality and social psychology*, vol. 81, no. 5, p. 922.

McCormick, D. A. & Bal, T., 1997, 'Sleep and arousal: thalamocortical mechanisms', *Annual review of neuroscience*, vol. 20, no. 1, pp. 185–215.

McNaughton, B. L., Battaglia, F. P., Jensen, O., Moser, E. I. & Moser, M.-B., 2006, 'Path integration and the neural basis of the'cognitive map", *Nature Reviews Neuroscience*, vol. 7, no. 8, p. 663.

Michel, C. M. & Brunet, D., 2019, 'EEG source imaging: a practical review of the analysis steps', *Frontiers in neurology*, vol. 10, p. 325.

Miller, E. K. & Cohen, J. D., 2001, 'An integrative theory of prefrontal cortex function', *Annual review of neuroscience*, vol. 24, no. 1, pp. 167–202.

Mitchell, D. J., McNaughton, N., Flanagan, D. & Kirk, I. J., 2008, 'Frontal-midline theta from the perspective of hippocampal "theta"', *Progress in neurobiology*, vol. 86, no. 3, pp. 156–185.

Moffat, S. D., Hampson, E. & Hatzipantelis, M., 1998, 'Navigation in a "virtual" maze: Sex differences and correlation with psychometric measures of spatial ability in humans', *Evolution and Human Behavior*, vol. 19, no. 2, pp. 73–87.

Moffat, S. D., Zonderman, A. B. & Resnick, S. M., 2001, 'Age differences in spatial memory in a virtual environment navigation task', *Neurobiology of aging*, vol. 22, no. 5, pp. 787–796.

Mohan, A., De Ridder, D. & Vanneste, S., 2016, 'Graph theoretical analysis of brain connectivity in phantom sound perception', *Scientific reports*, vol. 6.

Morgan, L. K., MacEvoy, S. P., Aguirre, G. K. & Epstein, R. A., 2011, 'Distances between real-world locations are represented in the human hippocampus', *Journal of Neuroscience*, vol. 31, no. 4, pp. 1238–1245.

Muir, G. M., Brown, J. E., Carey, J. P., Hirvonen, T. P., Della Santina, C. C., Minor, L. B. & Taube, J. S., 2009, 'Disruption of the head direction cell signal after occlusion of the semicircular canals in the freely moving chinchilla', *Journal of Neuroscience*, vol. 29, no. 46, pp. 14521–14533.

Muller, R. U., Kubie, J. L. & Ranck, J. B., 1987, 'Spatial firing patterns of hippocampal complex-spike cells in a fixed environment', *Journal of Neuroscience*, vol. 7, no. 7, pp. 1935–1950.

Muñoz-Gutiérrez, P. A., Giraldo, E., Bueno-López, M. & Molinas, M., 2018, 'Localization of active brain sources from EEG signals using empirical mode decomposition: A comparative study', *Frontiers in Integrative Neuroscience*, vol. 12, p. 55.

Murray, S. O. & Wojciulik, E., 2004, 'Attention increases neural selectivity in the human lateral occipital complex', *Nature neuroscience*, vol. 7, no. 1, p. 70.

Nadasdy, Z., 2010, 'Binding by asynchrony: the neuronal phase code', *Frontiers in Neuroscience*, vol. 4, p. 51.

Nasr, S., Liu, N., Devaney, K. J., Yue, X., Rajimehr, R., Ungerleider, L. G. & Tootell, R. B., 2011, 'Scene-selective cortical regions in human and nonhuman primates', *Journal of Neuroscience*, vol. 31, no. 39, pp. 13771–13785.

National Academies of Sciences, E. & Medicine, 2016, *Commercial Motor Vehicle Driver Fatigue, Long-Term Health, and Highway Safety: Research Needs*, National Academies Press.

Newhouse, P., Newhouse, C. & Astur, R. S., 2007, 'Sex differences in visual-spatial learning using a virtual water maze in pre-pubertal children', *Behavioural brain research*, vol. 183, no. 1, pp. 1–7.

Ng, K. K., Lo, J. C., Lim, J. K., Chee, M. W. & Zhou, J., 2016, 'Reduced functional segregation between the default mode network and the executive control network in healthy older adults: a longitudinal study', *Neuroimage*, vol. 133, pp. 321–330.

Nielson, D. M., Smith, T. A., Sreekumar, V., Dennis, S. & Sederberg, P. B., 2015, 'Human hippocampus represents space and time during retrieval of real-world memories', *Proceedings of the National Academy of Sciences*, vol. 112, no. 35, pp. 11078–11083.

Nijboer, M., Borst, J., van Rijn, H. & Taatgen, N., 2014, 'Single-task fmri overlap predicts concurrent multitasking interference', *NeuroImage*, vol. 100, pp. 60–74.

Näätänen, R., 1992, *Attention and brain function*, Psychology Press.

O'Keefe, J. & Dostrovsky, J., 1971, 'The hippocampus as a spatial map: Preliminary evidence from unit activity in the freely-moving rat', *Brain research*.

O'Keefe, J. & Nadel, L., 1978, *The hippocampus as a cognitive map*, Oxford: Clarendon Press.

Oken, B., Salinsky, M. & Elsas, S., 2006, 'Vigilance, alertness, or sustained attention: physiological basis and measurement', *Clinical neurophysiology*, vol. 117, no. 9, pp. 1885–1901.

Onton, J., Delorme, A. & Makeig, S., 2005, 'Frontal midline EEG dynamics during working memory', *Neuroimage*, vol. 27, no. 2, pp. 341–356.

Onton, J. A. & Makeig, S., 2009, 'High-frequency broadband modulation of electroencephalographic spectra', *Frontiers in human neuroscience*, vol. 3, p. 61.

Oostenveld, R. & Oostendorp, T. F., 2002, 'Validating the boundary element method for forward and inverse EEG computations in the presence of a hole in the skull', *Human brain mapping*, vol. 17, no. 3, pp. 179–192.

Oviedo-Trespalacios, O., 2018, 'Getting away with texting: Behavioural adaptation of drivers engaging in visual-manual tasks while driving', *Transportation Research Part A: Policy and Practice*, vol. 116, pp. 112–121.

Oviedo-Trespalacios, O., Haque, M. M., King, M. & Demmel, S., 2018, 'Driving behaviour while self-regulating mobile phone interactions: A human-machine system approach', *Accident Analysis and Prevention*, vol. 118, pp. 253–262.

Oviedo-Trespalacios, O., Haque, M. M., King, M. & Washington, S., 2017a, 'Effects of road infrastructure and traffic complexity in speed adaptation behaviour of distracted drivers', *Accident Analysis and Prevention*, vol. 101, pp. 67–77.

Oviedo-Trespalacios, O., Haque, M. M., King, M. & Washington, S., 2017b, 'Self-regulation of driving speed among distracted drivers: An application of driver behavioral adaptation theory', *Traffic injury prevention*, vol. 18, no. 6, pp. 599–605.

Oviedo-Trespalacios, O., King, M., Haque, M. M. & Washington, S., 2017c, 'Risk factors of mobile phone use while driving in queensland: Prevalence, attitudes, crash risk perception, and task-management strategies', *PLoS one*, vol. 12, no. 9, p. e0183361.

Oviedo-Trespalacios, O., Nandavar, S., Newton, J. D. A., Demant, D. & James, G. P., 2019a, 'Problematic use of mobile phones in australia... is it getting worse?', *Frontiers in Psychiatry*, vol. 10, pp. Article number–105.

Oviedo-Trespalacios, O., Truelove, V., Watson, B. & Hinton, J. A., 2019b, 'The impact of road advertising signs on driver behaviour and implications for road safety: A critical systematic review', *Transportation research part A: policy and practice*, vol. 122, pp. 85–98.

Palmer, J. A., Kreutz-Delgado, K. & Makeig, S., 2006, 'Super-gaussian mixture source model for ica', *International Conference on Independent Component Analysis and Signal Separation*, Springer, pp. 854–861.

Pascual-Marqui, R. D. et al., 2002, 'Standardized low-resolution brain electromagnetic tomography (sloreta): technical details', *Methods Find Exp Clin Pharmacol*, vol. 24, no. Suppl D, pp. 5–12.

Pashler, H., 1994, 'Dual-task interference in simple tasks: data and theory', *Psychological bulletin*, vol. 116, no. 2, p. 220.

Peltier, S. J., LaConte, S. M., Niyazov, D. M., Liu, J. Z., Sahgal, V., Yue, G. H. & Hu, X. P., 2005, 'Reductions in interhemispheric motor cortex functional connectivity after muscle fatigue', *Brain research*, vol. 1057, no. 1-2, pp. 10–16.

Peltier, S. J. & Shah, Y., 2011, 'Biophysical modulations of functional connectivity', *Brain connectivity*, vol. 1, no. 4, pp. 267–277.

Perlmutter, M., Metzger, R., Nezworski, T. & Miller, K., 1981, 'Spatial and temporal memory in 20 and 60 year olds', *Journal of Gerontology*, vol. 36, no. 1, pp. 59–65.

Pion-Tonachini, L., Kreutz-Delgado, K. & Makeig, S., 2019, 'Iclabel: An automated electroencephalographic independent component classifier, dataset, and website', *NeuroImage*, vol. 198, pp. 181–197.

Pizzamiglio, S., Naeem, U., Abdalla, H. & Turner, D. L., 2017, 'Neural correlates of

single-and dual-task walking in the real world', *Frontiers in human neuroscience*, vol. 11, p. 460.

Plank, M., Müller, H. J., Onton, J., Makeig, S. & Gramann, K., 2010, 'Human EEG correlates of spatial navigation within egocentric and allocentric reference frames', *International Conference on Spatial Cognition*, Springer, pp. 191–206.

Popov, T., Popova, P., Harkotte, M., Awiszus, B., Rockstroh, B. & Miller, G. A., 2018, 'Cross-frequency interactions between frontal theta and posterior alpha control mechanisms foster working memory', *NeuroImage*, vol. 181, pp. 728–733.

Proskovec, A. L., Heinrichs-Graham, E. & Wilson, T. W., 2019, 'Load modulates the alpha and beta oscillatory dynamics serving verbal working memory', *NeuroImage*, vol. 184, pp. 256–265.

Rizkallah, J., Annen, J., Modolo, J., Gosseries, O., Benquet, P., Mortaheb, S., Amoud, H., Cassol, H., Mheich, A., Thibaut, A. et al., 2019, 'Decreased integration of EEG source-space networks in disorders of consciousness', *NeuroImage: Clinical*, vol. 23, p. 101841.

Robbins, T. W., 1997, 'Arousal systems and attentional processes', *Biological psychology*, vol. 45, no. 1-3, pp. 57–71.

Rubinov, M. & Sporns, O., 2010, 'Complex network measures of brain connectivity: uses and interpretations', *Neuroimage*, vol. 52, no. 3, pp. 1059–1069.

Ruthruff, E., Johnston, J. C. & Van Selst, M., 2001, 'Why practice reduces dual-task interference.', *Journal of Experimental Psychology: Human Perception and Performance*, vol. 27, no. 1, p. 3.

Ruthruff, E., Johnston, J. C., Van Selst, M., Whitsell, S. & Remington, R., 2003, 'Vanishing dual-task interference after practice: Has the bottleneck been eliminated or is it merely latent?', *Journal of Experimental Psychology: Human Perception and Performance*, vol. 29, no. 2, p. 280.

Saalmann, Y. B., 2014, 'Intralaminar and medial thalamic influence on cortical synchrony, information transmission and cognition', *Frontiers in systems neuroscience*, vol. 8, p. 83.

Salthouse, T. A., Mitchell, D. R., Skovronek, E. & Babcock, R. L., 1989, 'Effects of adult age and working memory on reasoning and spatial abilities', *Journal of Experimental Psychology: Learning, Memory, and Cognition*, vol. 15, no. 3, p. 507.

Sammer, G., Blecker, C., Gebhardt, H., Bischoff, M., Stark, R., Morgen, K. & Vaitl, D., 2007, 'Relationship between regional hemodynamic activity and simultaneously recorded EEG–theta associated with mental arithmetic–induced workload', *Human brain mapping*, vol. 28, no. 8, pp. 793–803.

Sauseng, P., Klimesch, W., Schabus, M. & Doppelmayr, M., 2005, 'Fronto-parietal EEG coherence in theta and upper alpha reflect central executive functions of working memory', *International Journal of Psychophysiology*, vol. 57, no. 2, pp. 97–103.

Schier, M. A., 2000, 'Changes in EEG alpha power during simulated driving: a demonstration', *International Journal of Psychophysiology*, vol. 37, no. 2, pp. 155–162.

Schroeder, P., Wilbur, M., Pena, R. & Abt, S., 2018, 'National survey on distracted driving attitudes and behaviors-2015', Report, United States. National Highway Traffic Safety Administration.

Schubert, T., Fischer, R. & Stelzel, C., 2008, 'Response activation in overlapping tasks and the response-selection bottleneck', *Journal of Experimental Psychology: Human Perception and Performance*, vol. 34, no. 2, p. 376.

Schubert, T. & Szameitat, A. J., 2003, 'Functional neuroanatomy of interference in overlapping dual tasks: an fmri study', *Cognitive Brain Research*, vol. 17, no. 3, pp. 733–746.

Seeber, M., Cantonas, L.-M., Hoevels, M., Sesia, T., Visser-Vandewalle, V. & Michel, C. M., 2019, 'Subcortical electrophysiological activity is detectable with high-density EEG source imaging', *Nature communications*, vol. 10, no. 1, pp. 1–7.

Serrien, D. J., 2009, 'Verbal–manual interactions during dual task performance: An EEG study', *Neuropsychologia*, vol. 47, no. 1, pp. 139–144.

Sherrill, K. R., Erdem, U. M., Ross, R. S., Brown, T. I., Hasselmo, M. E. & Stern, C. E., 2013, 'Hippocampus and retrosplenial cortex combine path integration signals for successful navigation', *Journal of Neuroscience*, vol. 33, no. 49, pp. 19304–19313.

Shine, J. M., 2019, 'Neuromodulatory influences on integration and segregation in the brain', *Trends in cognitive sciences*, vol. 23, no. 7, pp. 572–583.

Shine, J. M., Bissett, P. G., Bell, P. T., Koyejo, O., Balsters, J. H., Gorgolewski, K. J., Moodie, C. A. & Poldrack, R. A., 2016a, 'The dynamics of functional brain networks: integrated network states during cognitive task performance', *Neuron*, vol. 92, no. 2, pp. 544–554.

Shine, J. P., Valdés-Herrera, J. P., Hegarty, M. & Wolbers, T., 2016b, 'The human retrosplenial cortex and thalamus code head direction in a global reference frame', *Journal of Neuroscience*, vol. 36, no. 24, pp. 6371–6381.

Sievertsen, H. H., Gino, F. & Piovesan, M., 2016, 'Cognitive fatigue influences students' performance on standardized tests', *Proceedings of the National Academy of Sciences*, vol. 113, no. 10, pp. 2621–2624.

Simon, M., Schmidt, E. A., Kincses, W. E., Fritzsche, M., Bruns, A., Aufmuth, C., Bogdan, M., Rosenstiel, W. & Schrauf, M., 2011, 'EEG alpha spindle measures as indicators of driver fatigue under real traffic conditions', *Clinical Neurophysiology*, vol. 122, no. 6, pp. 1168–1178.

Spadone, S., Della Penna, S., Sestieri, C., Betti, V., Tosoni, A., Perrucci, M. G., Romani, G. L. & Corbetta, M., 2015, 'Dynamic reorganization of human resting-state

networks during visuospatial attention', *Proceedings of the National Academy of Sciences*, vol. 112, no. 26, pp. 8112–8117.

Spiers, H. J. & Gilbert, S. J., 2015, 'Solving the detour problem in navigation: a model of prefrontal and hippocampal interactions', *Frontiers in human neuroscience*, vol. 9, p. 125.

Spiers, H. J. & Maguire, E. A., 2006, 'Thoughts, behaviour, and brain dynamics during navigation in the real world', *Neuroimage*, vol. 31, no. 4, pp. 1826–1840.

Sporns, O., 2014, 'Contributions and challenges for network models in cognitive neuroscience', *Nature neuroscience*, vol. 17, no. 5, pp. 652–660.

Stackman, R. W., Golob, E. J., Bassett, J. P. & Taube, J. S., 2003, 'Passive transport disrupts directional path integration by rat head direction cells', *Journal of neurophysiology*, vol. 90, no. 5, pp. 2862–2874.

Staines, W. R., Graham, S. J., Black, S. E. & McIlroy, W. E., 2002, 'Task-relevant modulation of contralateral and ipsilateral primary somatosensory cortex and the role of a prefrontal-cortical sensory gating system', *Neuroimage*, vol. 15, no. 1, pp. 190–199.

Stangl, M., Kanitscheider, I., Riemer, M., Fiete, I. & Wolbers, T., 2020, 'Sources of path integration error in young and aging humans', *Nature communications*, vol. 11, no. 1, pp. 1–15.

Stelzel, C., Schumacher, E. H., Schubert, T. & Mark, D., 2006, 'The neural effect of stimulus-response modality compatibility on dual-task performance: an fmri study', *Psychological Research*, vol. 70, no. 6, pp. 514–525.

Suthana, N. A., Ekstrom, A. D., Moshirvaziri, S., Knowlton, B. & Bookheimer, S. Y., 2009, 'Human hippocampal ca1 involvement during allocentric encoding of spatial information', *Journal of Neuroscience*, vol. 29, no. 34, pp. 10512–10519.

Swick, D., Pineda, J., Schacher, S. & Foote, S., 1994, 'Locus coeruleus neuronal activity in awake monkeys: relationship to auditory P300-like potentials and spontaneous EEG', *Experimental Brain Research*, vol. 101, no. 1, pp. 86–92.

Szameitat, A. J., Schubert, T. & Müller, H. J., 2011, 'How to test for dual-task-specific effects in brain imaging studies—an evaluation of potential analysis methods', *Neuroimage*, vol. 54, no. 3, pp. 1765–1773.

Tadel, F., Baillet, S., Mosher, J. C., Pantazis, D. & Leahy, R. M., 2011, 'Brainstorm: a user-friendly application for MEG/EEG analysis', *Computational intelligence and neuroscience*, vol. 2011.

Taube, J. S., 1995, 'Head direction cells recorded in the anterior thalamic nuclei of freely moving rats', *Journal of Neuroscience*, vol. 15, no. 1, pp. 70–86.

Taube, J. S., 2007, 'The head direction signal: origins and sensory-motor integration', *Annu. Rev. Neurosci.*, vol. 30, pp. 181–207.

Tefft, B. C., 2014, *Prevalence of motor vehicle crashes involving drowsy drivers, United States, 2009-2013*, Citeseer.

Telford, L., Howard, I. P. & Ohmi, M., 1995, 'Heading judgments during active and passive self-motion', *Experimental Brain Research*, vol. 104, no. 3, pp. 502–510.

Tellinghuisen, D. J. & Nowak, E. J., 2003, 'The inability to ignore auditory distractors as a function of visual task perceptual load', *Perception and psychophysics*, vol. 65, no. 5, pp. 817–828.

Teng, E. & Squire, L. R., 1999, 'Memory for places learned long ago is intact after hippocampal damage', *Nature*, vol. 400, no. 6745, p. 675.

Theofilatos, A., Ziakopoulos, A., Papadimitriou, E. & Yannis, G., 2018, 'How many crashes are caused by driver interaction with passengers? a meta-analysis approach', *Journal of safety research*, vol. 65, pp. 11–20.

Tolman, E. C., 1948, 'Cognitive maps in rats and men', *Psychological review*, vol. 55, no. 4, p. 189.

Tombini, M., Zappasodi, F., Zollo, L., Pellegrino, G., Cavallo, G., Tecchio, F., Guglielmelli, E. & Rossini, P. M., 2009, 'Brain activity preceding a 2D manual catching task', *Neuroimage*, vol. 47, no. 4, pp. 1735–1746.

Vann, S. D., Aggleton, J. P. & Maguire, E. A., 2009, 'What does the retrosplenial cortex do?', *Nature Reviews Neuroscience*, vol. 10, no. 11, pp. 792–802.

Vass, L. K. & Epstein, R. A., 2017, 'Common neural representations for visually guided reorientation and spatial imagery', *Cerebral cortex*, vol. 27, no. 2, pp. 1457–1471.

Vukovic, N. & Shtyrov, Y., 2017a, 'Cortical networks for reference-frame processing are shared by language and spatial navigation systems', *NeuroImage*, vol. 161, pp. 120–133.

Vukovic, N. & Shtyrov, Y., 2017b, 'Cortical networks for reference-frame processing are shared by language and spatial navigation systems', *NeuroImage*, vol. 161, pp. 120–133.

Wang, C., Trongnetrpunya, A., Samuel, I. B. H., Ding, M. & Kluger, B. M., 2016, 'Compensatory neural activity in response to cognitive fatigue', *Journal of neuroscience*, vol. 36, no. 14, pp. 3919–3924.

Wang, H., Zhang, C., Shi, T., Wang, F. & Ma, S., 2015, 'Real-time EEG-based detection of fatigue driving danger for accident prediction', *International journal of neural systems*, vol. 25, no. 02, p. 1550002.

Wang, Y.-K., Chen, S.-A. & Lin, C.-T., 2014a, 'An EEG-based brain–computer interface for dual task driving detection', *Neurocomputing*, vol. 129, pp. 85–93.

Wang, Y.-K., Jung, T.-P. & Lin, C.-T., 2018, 'Theta and alpha oscillations in attentional interaction during distracted driving', *Frontiers in behavioral neuroscience*, vol. 12, p. 3.

Wang, Y.-T., Huang, K.-C., Wei, C.-S., Huang, T.-Y., Ko, L.-W., Lin, C.-T., Cheng,

C.-K. & Jung, T.-P., 2014b, 'Developing an EEG-based on-line closed-loop lapse detection and mitigation system', *Frontiers in neuroscience*, vol. 8.

Welford, A. T., 1952, 'The psychological refractory periodand the timing of high-speed performance—a review and a theory', *British Journal of Psychology*, vol. 43, no. 1, pp. 2–19.

WHO, W. H. O., 2018, 'Global status report on road safety', .

Wickens, C. D., 2002, 'Multiple resources and performance prediction', *Theoretical issues in ergonomics science*, vol. 3, no. 2, pp. 159–177.

Winter, S. S., Clark, B. J. & Taube, J. S., 2015, 'Disruption of the head direction cell network impairs the parahippocampal grid cell signal', *Science*, vol. 347, no. 6224, pp. 870–874.

Wolbers, T., Wiener, J. M., Mallot, H. A. & Büchel, C., 2007, 'Differential recruitment of the hippocampus, medial prefrontal cortex, and the human motion complex during path integration in humans', *Journal of Neuroscience*, vol. 27, no. 35, pp. 9408–9416.

Woollett, K. & Maguire, E. A., 2011, 'Acquiring "the knowledge" of london's layout drives structural brain changes', *Current biology*, vol. 21, no. 24, pp. 2109–2114.

Woolley, D. G., Vermaercke, B., de Beeck, H. O., Wagemans, J., Gantois, I., D'Hooge, R., Swinnen, S. P. & Wenderoth, N., 2010, 'Sex differences in human virtual water maze performance: Novel measures reveal the relative contribution of directional responding and spatial knowledge', *Behavioural brain research*, vol. 208, no. 2, pp. 408–414.

Xia, M., Wang, J. & He, Y., 2013, 'Brainnet viewer: a network visualization tool for human brain connectomics', *PloS one*, vol. 8, no. 7, p. e68910.

Xu, L., Wang, B., Xu, G., Wang, W., Liu, Z. & Li, Z., 2017, 'Functional connectivity analysis using fnirs in healthy subjects during prolonged simulated driving', *Neuroscience letters*, vol. 640, pp. 21–28.

Young, K., Regan, M. & Hammer, M., 2007, 'Driver distraction: A review of the literature', *Distracted driving*, pp. 379–405.

Zanto, T. P., Rubens, M. T., Thangavel, A. & Gazzaley, A., 2011, 'Causal role of the prefrontal cortex in top-down modulation of visual processing and working memory', *Nature neuroscience*, vol. 14, no. 5, pp. 656–661.

Zugaro, M. B., Tabuchi, E., Fouquier, C., Berthoz, A. & Wiener, S. I., 2001, 'Active locomotion increases peak firing rates of anterodorsal thalamic head direction cells', *Journal of neurophysiology*, vol. 86, no. 2, pp. 692–702.